University of Stavanger

FACULTY OF SCIENCE AND TECHNOLOGY

MASTER'S THESIS

Study programme/specialization: Petroleum Engineering/ Reservoir Technology	Spring/Autumn semester, 2017 Open/~~Confidential~~
Author: Nathan Amuri Bahati	…….. (Signature of author)
Programme coordinator: Supervisor(s): Mesfin Belayneh.	
Title of master's thesis: Heat Recovery Mechanism for Non Condensable Geothermal Fractured Reservoirs by CO_2 injection and Well Heat Insulating.	
Credits: 30	
Keywords: Multi Interacting Continuum (MINC). CO_2 sequestration (sCO_2). Enhanced geothermal reservoir (EGS)	Number of pages: ……76…… + Supplemental material/other: 23……. Stavanger, …… Date/year

Acknowledgements

I would first like to thank my thesis supervisor Mesfin Belayneh Agonafir of department of faculty of science and technology (petroleum engineering) at University of Stavanger. The door to Mesfin Belayneh was always open whenever I ran into trouble situation or had question concerning my research. He consistently allowed this thesis to be my own work, his discipline and high work ethics steered me in the right direction whenever he though I needed it.

Secondly, I wish to thank my loving and supportive wife, Cecilia Chomba, and my two wonderful children, Nathan Junior Amuri & Bahati Amuri, who provides unending inspiration and motivation.

Abstract

In this thesis we analyzed the potential use of operating geothermal plants with water and CO_2 as working fluids using a geothermal simulator TOUGH2 module EOS1 and EOS2, respectively. We also studied the sensitivities of different parameters on heat extraction. In addition, we also analyzed the heat preserving possibilities in the wellbore by varying both the thermal conductivity and thickness of the insulators.

The results showed that CO_2 was a far better working fluid than water, and could be used as an enhanced working together in non-condensable gas reservoir. We also observed that optimization of fracture porosity and flow rate had more positive impacts on heat extracted than fracture permeability and fracture spacing in such system. In addition parameter such as porosity and fracture spacing had direct impact on the time for which the system attained the steady state, which in turn contributed to the amount extracted.

Concerning heat insulating in the well, the result showed that there was a need of using low thermal conductive cement when the production tube was not insulated. On contrary when the tubing was insulated with insulator of specific thickness, for which thicker was better and thermal conductivity, for which lower conductivity was better, then the cement played a minor a role as an insulating material in this regard.

Table of content

List of figures

List of tables

Nomenclature

a	local fracture aperture
A_{nm}	area interface in volume elements n & m, L^2
F_{nm}	mass flux from volume element m into n, m/m^2s
C_p	Specific heat J/kg °C
c	Pore compressibility Pa^{-1}
d_{nm}	distance between nodal points n an m, m
G_{nm}	energy flux from volume element into n, m/s^3
C_R	Heat capacity of the rock, J/kg K
g	Acceleration of gravity vector, m/s^2
F	Mass or energy flux vector kg m2 $/s^2$

h Specific enthalpy, J/Kg

h_f Liquid film convective heat transfer coefficient inside tube, BTU/hr-sq ft ^oF

h_c Natural convective heat transfer coefficient, BTU/hr-sq ft ^oF

hr Radiative heat transfer coefficient BTU/hr-sq ft ^oF

k Permeability, m^2

k Thermal conductivity in pipe simulations, BTU/hr-ft oF

k Components index

kr Relative permeability

K_f Fracture permeability, m^2

k_t Conductivity of tubing material BTU/hr-ft ^oF

kc Conductivity of casing material BTU/hr ^oF

k_{cem} Conductivity of settled cement BTU/hr-ft ^oF

k_{ins} Thermal conductivity of insulator, BTU/hr-ft ^oF

m_{vg} Van Genuchten (1980) papramter

$\dot{m}$ Mass flow rate of flid, kg/s

P Pressiure, Pa

P_G Pressure of gas, Pa

P_L Pressure of liquid, Pa

Q Injection/Production rate kg/s

Q_h heat transfer, BTU/hr-ft

r_{to} Tubing outside radius, in

r_{ci} Casing inside radius, in

r_{ti} Tubing inside radius, in

r_{co} Casing outside radius, in

r_{ins} Insulation radius, in

r_{wb} Wellbore radius, in

S Liquid saturation []

T Thickness, m

T_s Temperature of heat source °C

T Temperature °C

T_∞ Temperature of surrounding fluid °C

t time, s

u Darcy velocity, m/s

U(e) Internal energy, J/kg

$V_{p,}$ total pore volume, m^3

V_b bulk volume of the rock, m^3

X mass fraction w/phase subscript and component superscript

$\propto$ Thermal expansion

β Phase (β = l: liquid; β= g: gas)

ρ Rock grain density kg/m^3

dΓ surface segment, m^2

Γ_n closed surface bounding volume element n, m^2

β Thermal compression coefficient

Ø porosity

λ Rock thermal conductivity $wm^{-1}K^{-1}$

List of abbreviation

FS Fracture spacing

CO2 Carbon di oxide

EOS1 Equation of state 1

EOS2 Equation of state 2

NCG non-condensable gases

EGS Enhanced geothermal system

MINC Multi-Interacting Continua

DFN Discrete fracture network

ECM effective continuum method

DKM dual porosity/ permeability

1 Introduction

Currently and the years to come, the two most worldwide issues are problems related to global warming and energy shortage. CO_2 is one of the main greenhouse gases, which raise the temperature of the earth. Due to population growth, the energy demands also increasing, environmental-friendly and reliable energy source becomes more attractive. As illustrated in figure 1.1.1, several agencies and energy companies indicated the growing interest of the bioenergy projects to be as dominant energy source(IEA, 2015). In addition other renewable energy sources include geothermal, solar, wind and bioenergy with low-carbon energy sources plays a prominent role both for energy shortage and climate change related problems.

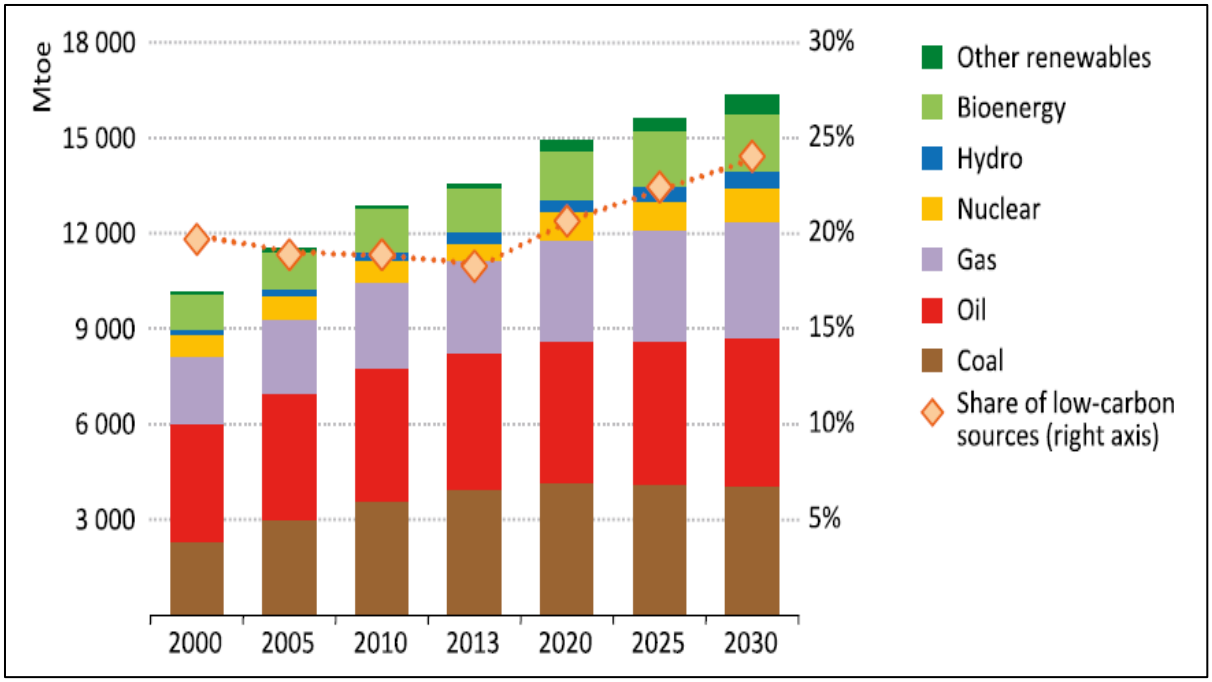

Figure 1.1.1 – Worldwide primary energy consumption by fuel type in million ton of oil equivalent (IEA, 2015)

In literature, among others water and CO_2 are documented as working fluid in a traditional and non-condensable geothermal reservoir, respectively. This thesis deals with simulation studies of geothermal resource by considering water and CO_2 as working fluids. Operational and reservoir parametric sensitivity study on energy recovery is assessed. Finally, heat transfer phenomenon and preserving energy in the wellbore with the objective of extracting more energy to the power plant is also modeled and simulated.

1.1 Background and motivation of the research

Despite promising potential of geothermal energy as one of green energy source, communities and governments globally have only tapped 6 – 7 % of the actual potential for geothermal power based on current geologic and technology (G.E.A, 2016). Most of the resources remain unexploited, which is one of the factors that raise research interests in this field. If it means these untapped resources were explored, it could supply vast amount of energy to the globe, however natural disasters, strict government policies and lack of financial support still hamper the geothermal power development globally. Despite all these challenges, the Geothermal Energy Agency (GEA) reported that 18 new geothermal power were established in 2015, adding about 313 MW of new capacity to electricity grids globally (G.E.A, 2016). Currently, the global market is almost 13.3 GW, distributed across 24 countries, estimated to reach almost 18.4 GW and 32 GW by 2021 and 2030 respectively (G.E.A, 2016). However, this shows high global investment in geothermal energy in the years to come.

Equivalently, global non-condensable gas (NCG) production values from geothermal power plant was 122 gCO_2/kWh in 2001, according to the survey, this amount constitutes more than 50% of overall installed potential worldwide. The average value in the U.S was 106 gCO2/KWh (in 2002), and for New Zealand, Iceland and Italy were 123 gCO_2/KWh (in 2012), 34 gCO_2 /KWh and 330 gCO_2/KWh (in 2013) respectively. Turkey leads the race with reported value of 900 to 1,300 gCO_2/KWh same year (ESMAP, 2006). These represent a vast amount of energy, which met a good fraction of world energy demand, however, this should raise concern and commitment on geothermal energy.

The primarily geothermal activity in Norway is the use of geothermal heat pumps, which are mainly uses for energy in the households. Norway has a vast amount of geothermal energy stored along with reserved hydrocarbon in the North Sea. The heat can be mined by the method called “Co-Production”, for which the heat is produced alongside the oil & gas, and use to develop a geothermal power plant. The power generate by a plant, can be in turn use to run the oil and gas operations.

Non-condensable geothermal gas reservoir possesses different quantities of non-condensable gases (NCG), CO_2 and H_2S being the main gases, and small amount of other

gases (for example; CH_4, N_2 and NH_3). Depending on the fluid source, the NCG content of geothermal steam varies over the world from almost 0 % to greater than 25 % by weight of the total fluid in the reservoir (Ozcan, April 2010). For example at Ohaaki in New Zealand, the amount of CO_2 in the discharges is 6 % of the wet (Grant, 1977). It is mentioned that, CO_2 is the main gas and covers almost 90 % of the total NCGs by volume (Bertani, 2002) , while H_2S almost 2 to 3 %, the rest gases occupies the remaining volume. Proceeding chapters presents the simulation well-reservoir setup. The theory behind the analysis tool and the simulation results are presented in chapter 3 and 4 respectively.

1.2 Objective

The research aimed at the analysis of potential use of operating geothermal plants with water and CO_2 as working fluids by injecting in aquifers and hard rock geothermal reservoirs. In addition, the thesis will analysis the heat transfer phenomenon in wellbore.

1.3 Problem formulation

As mentioned earlier the main focus of this thesis is to simulate the working fluids in geothermal reservoir and exploit as much energy to drive the power plant at surface. For this, the research issues to be addressed in this thesis are related with the reservoir and pipe insulation such as

- ✓ The performance of water as a heat transmission fluid in fractured reservoirs from injection to production well.
- ✓ The performance of CO_2 as an enhanced heat transmission fluid in fractured non-condensable gas reservoir from production well point view.
- ✓ The effect of different reservoir parameters and flow rates on the reservoir pressure, temperature and produced enthalpy as water / CO_2 migrates from injection to production well.
- ✓ How is the overall heat transfer and heat loss possibly in a typical petroleum or geothermal well? Heat conductivity and loss across the well? How can heat be preserved when fluid flowing through the well in order to extract more energy to surface?

1.4 Thesis Structure

In order to meet the desire of the objective and answer the research question addressed above, the research program designed and implemented as illustrated on Figure 1.1.2. The activities basically are divided into two parts, namely literature study and simulation works. The simulation study part deals with the heat transfer phenomenon in the reservoir and through the wellbore. The literature study part deals with the basics of the theory behind the simulators and geothermal related issues.

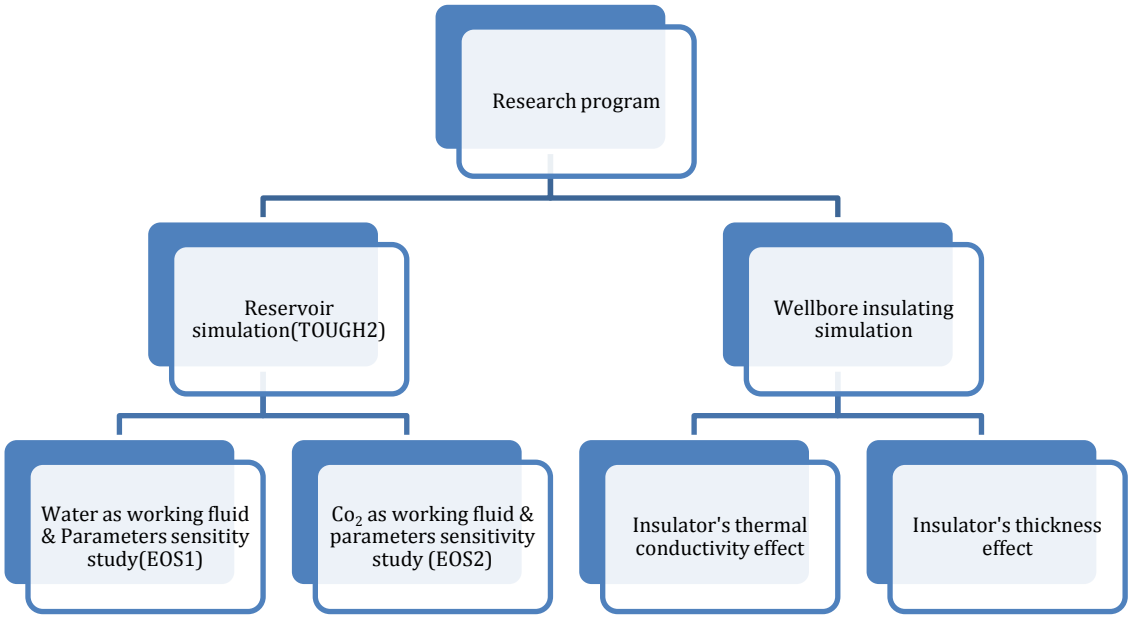

Figure 1.1.2 Research methodology structure

2 Literature study

This chapter gives a short introduction about geothermal energy, and descriptions of different research done most importantly on working fluid. We have also highlighted TOUGH 2 architecture, including fluid and rock characteristics that are the input data for the software.

2.1 Geothermal energy concept

Most power plants whether fueled by coal, gas, nuclear power or geothermal energy have one feature in common: they convert heat to electricity. The term "energy conversion" in the field of geothermal energy refers to the power plant technology that converts the hot geothermal fluids into electric power.

Geothermal Energy is among the most fast growing renewable energies, which exploits energy rocks below ground. The two sources of geothermal energy are (Singh., 2015):

1) Hydrothermal resources mainly found at shallower depth and the reservoir is characterized by porous/permeable formation that contains hot water, steam, or a combination of the two.
2) Hot Dry Rock resources are normally found in a deeper formation and the reservoir contain little or no steam or water, and are not very permeable.

In general, geothermal power generation has the following positive features (Singh., 2015) :

- Lower emission of CO_2, which is a main source of global warming
- Higher availability
- Use of more sustainable energy

The hydrothermal energy resource uses the reservoir fluids to generate electricity. In geothermal energy, electricity is generated by pumping fluid down a borehole (injection well) into the hot rock or an aquifer. As illustrated in Figure 2.1.1, the water flows through fractures in the rock, capturing the heat of the rock transporting to the surface through

the second production borehole. The hydrothermal fluids will then be converted into electricity using either a steam turbine or a binary power plant system. The water will be re-injected back into the ground to heat up again and produce back. If geothermal plant uses a closed-loop binary cycle to generate electricity, none of the fluids vent to the atmosphere. The plant will therefore have no negative impact for the environment.

As the heated water is being transported through the production wells, the heat can be exhausted over time by flowing from well to the surrounding. Advanced techniques are required to preserve/reduce heat loss as fluid flows from reservoir to the surface and also from injection well to the surrounding reservoir until reaching to production well. This can be done by appropriate wellbore design and will be evaluated later in chapter 4. There is also a technology called enhanced geothermal system (EGS), which enhances conductivity of the natural reservoirs by fracturing the rock sufficiently to enable a water to flow between the wells.

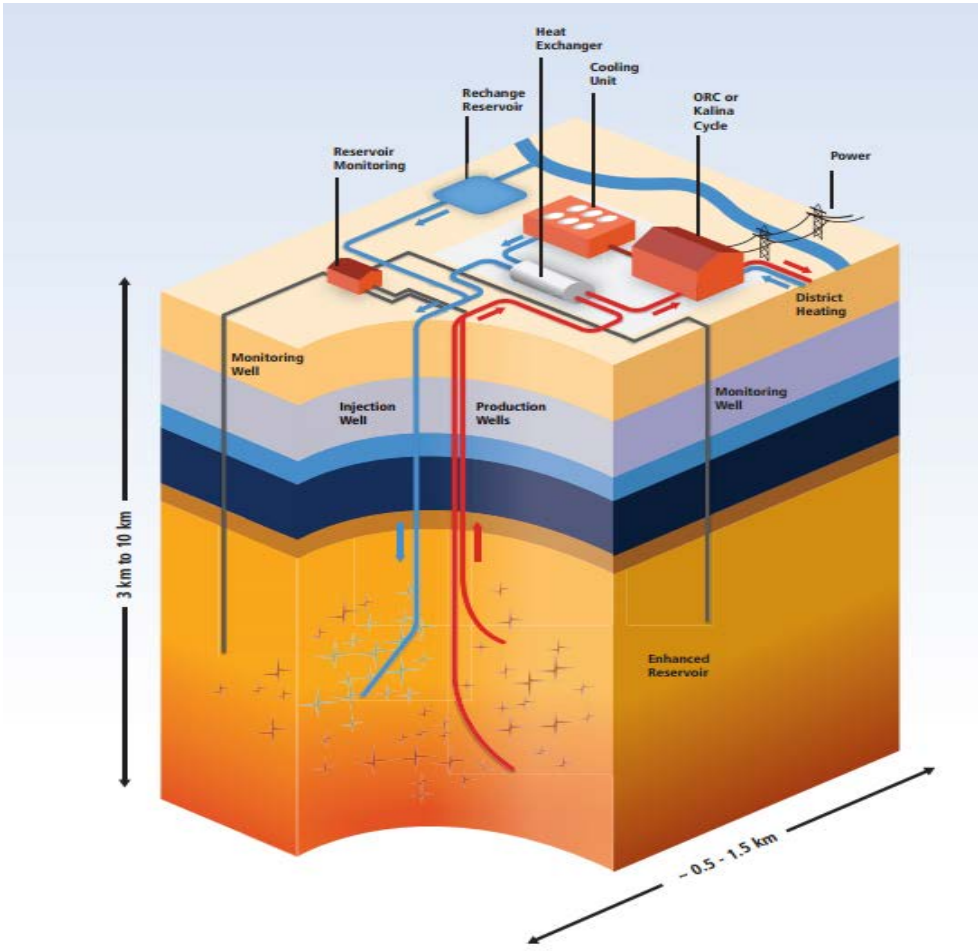

Figure 2.1.1 Geothermal well injection-production and power plant-electricity generation (IPCC, 2012)

The exploitation and development of geothermal fluid depends mainly on the fluids thermodynamic state as its reaches to the power plant. Several authors have classified geothermal fluids different based on temperatures and enthalpy. Enthalpy is the most commonly used criterion to categorize the geothermal resources (Dickson, 2004) . In this thesis, Chapter 4, several sensitivity studies were carried to analyze the degree of enthalpy and temperature variation in a considered reservoir.

2.2 Geothermal working fluids

2.2.1 Water

Fluid temperature and pressure determine the properties of the fluid by what is known as equation of states (EOS). However, at a given temperature and pressure, the fluid can exist in different phases. As shown in figure 2.2.1, water exist as liquid at standard room temperature and pressure, reaching critical point at temperature and pressure of 374 °C and 225 atm respectively. Water is a primarily fluid use for heat extraction in geothermal reservoir. Injection of water into a geothermal reservoir with the objective of extracting is regarded as a traditional way of heat extraction from geothermal system.

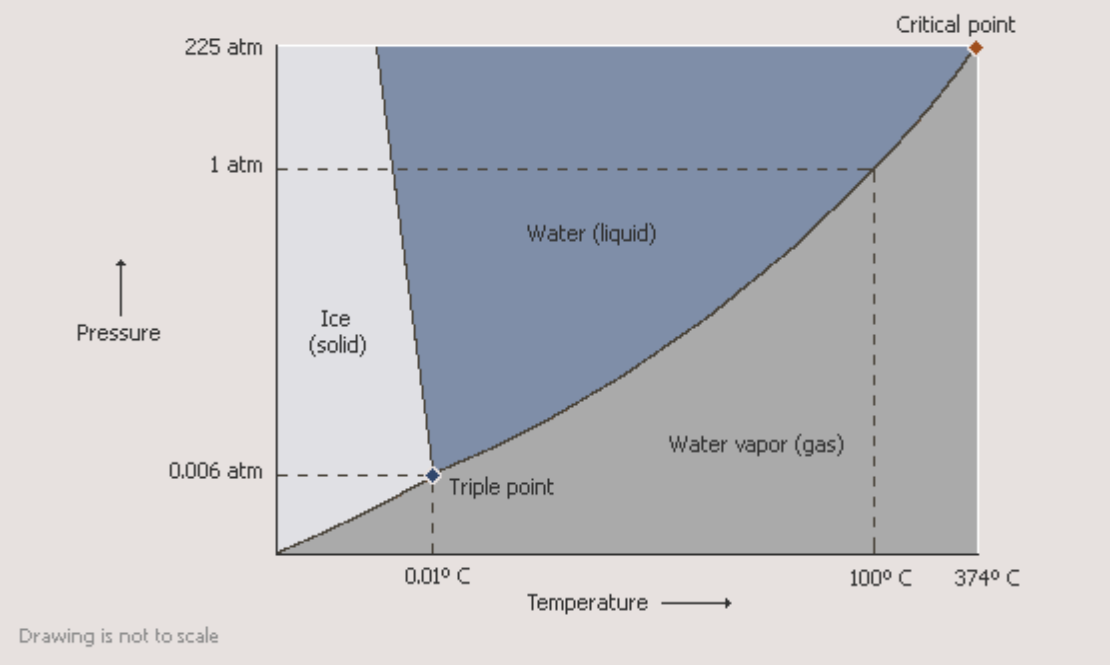

Figure 2.2.1 Phase transition diagram for water (Sciencedirect)

2.2.2 CO_2

CO_2 is another working fluid, which has gained more attention as an enhanced geothermal recovery working fluid. The implementation of CO_2 as working fluid in a geothermal system requires a good understanding of its chemical and thermodynamic properties as shown in figure 2.2.2. CO_2 is at supercritical beyond the temperature of 31 °C and pressure of 72.9 atm, while at standard temperature and pressure CO_2 is in gas form. At it's supercritical state CO_2 acquires both gas and liquid properties. Most important, at supercritical state it has density nearly that of a liquid, meanwhile viscosity and diffusivity similar to that of gas state (Biagi et al., 2015). Fig 2.2.2 illustrates the three phase transition diagram of CO_2.

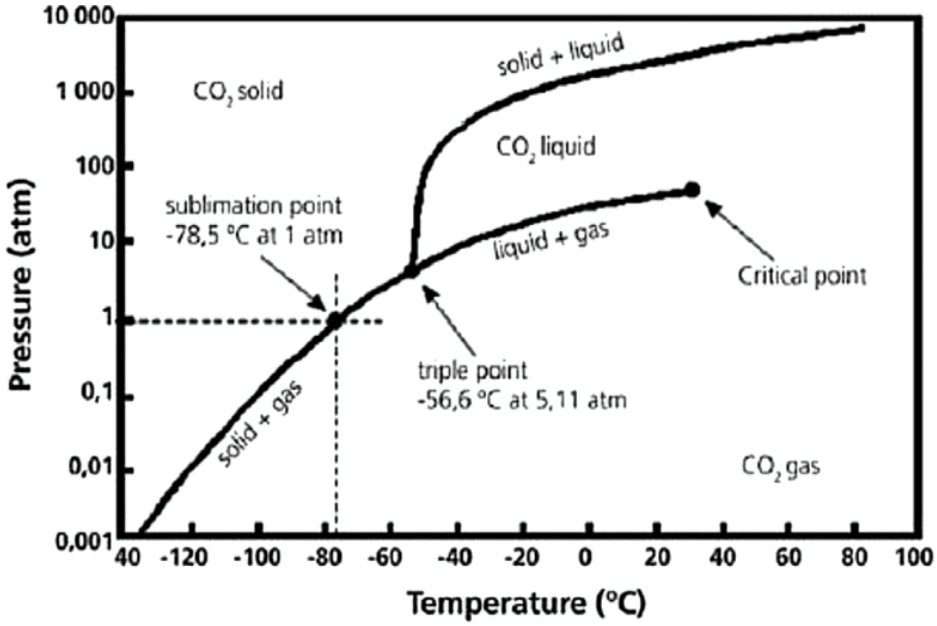

Fig 2.2.2 Phase transition diagram for CO_2 (Biagi et al., 2015)

2.2.3 Fluid density

Fluid density can is defined as mass of the fluid per unit volume it occupies. The change in density is a function of the change in temperature and pressure multiply by thermal expansion and compression coefficient, respectively. This is represented in equation 2.1 below:

$$\frac{\partial \rho}{\partial t} = \rho \left(-\alpha \frac{\partial T}{\partial t} + \beta \frac{(\partial P)}{\partial t}\right) \qquad (2.1)$$

Where $\propto$ and β represent thermal expansion and compression coefficient, respectively. If water is in liquid form, both of these coefficients are small, therefore water can be regarded as incompressible.

2.2.4 Fluid viscosity

Viscosity is defined as the property of fluid to resist continuous deformation on the presence of shear stresses, therefore fluid flow portray a non-stop deformation of fluid when shear stress is applied to it. One another parameter which is use to describe the fluid flow in porous media is the mobility. Mobility is defined as the ratio of effective permeability of the fluid to its viscosity. One of the main reason of preferring CO_2 as working fluid for geothermal system, is that CO_2 has lower viscosity at a given temperature and pressure than water. As result CO_2 possess higher mobility than water at given temperature and pressure (Karsten Pruess, 2006). In addition, the mobility of CO_2 does not vary much with temperature as shown in figure 2.2.3. Its value can still be the same at either high or low temperature. The mobility variation with temperature comes as result of viscosity dependency on temperature.

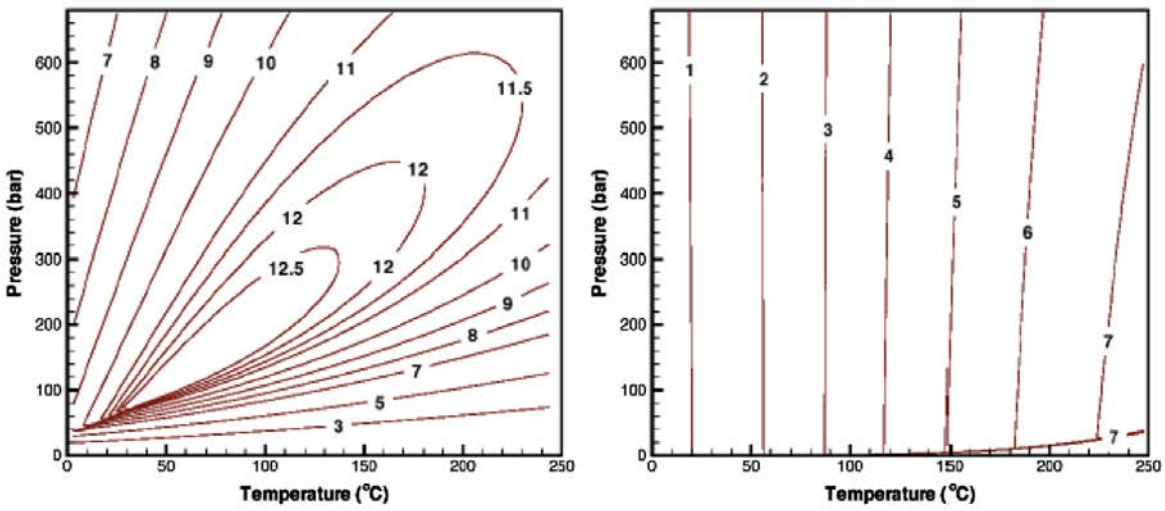

Figure 2.2.3 Mobility of CO_2 (left) and water (right) in units of $10sm^{-2}$ (Karsten Pruess, 2006)

2.2.5 Specific heat, Internal energy and enthalpy

The specific heat capacity is defined as energy needed to increase a unit mass of a certain substance to a given amount. At a constant pressure the specific heat capacity is equivalent to the change of enthalpy per temperature, equivalently at constant volume the heat capacity is equivalent to the change of specific internal energy per temperature.

$$C_p = \left(\frac{\partial h}{\partial T}\right)_p \tag{2.2}$$

$$C_V = \left(\frac{\partial e}{\partial T}\right)_v \tag{2.3}$$

Equation 2.2 and 2.3 denotes specific heat capacity under constant pressure and volume respectively. The difference between these two accounts for thermal expansion coefficient and compressibility coefficient, for liquid water, which is almost incompressible, the compression coefficient is very small; therefore these two heat capacities are nearly the same.

The specific internal energy of a system is the total amount of energy found in a system, and composes of both potential and kinetic energy, excusive of the energy needed to displace the environment and make room for system volume and pressure. The specific enthalpy is the total amount of the internal energy and the energy transferred to the environment by the expansion of the system. Energy mined from a geothermal system is quantified in enthalpy; in addition the input energy at injection well is also quantified in enthalpy.

Figure 2.2.4 show the variation of enthalpy with temperature and pressure for both CO_2 and water. The figure shows that the relative enthalpy of CO_2 varies significantly with changes of both temperature and pressure, whereas the enthalpy of water changes basically with temperature and not significantly with pressure (Karsten Pruess, 2006).

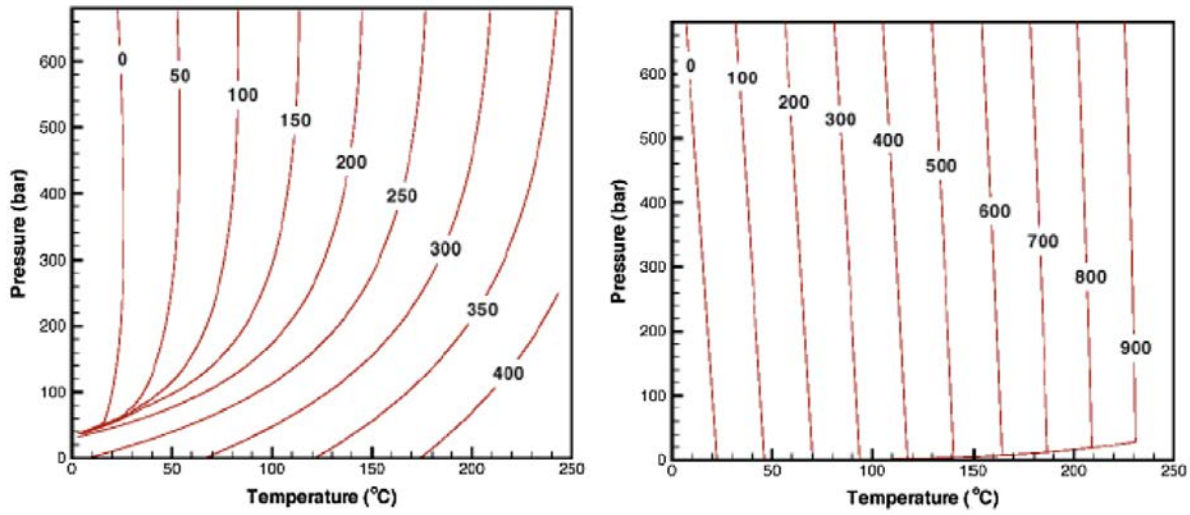

Figure 2.2.4 Enthalpy of CO_2 (left) and water (right) in units of Kj/Kg (Karsten Pruess, 2006).

2.2.6 Published work on working fluids

The interest of promoting renewable energy has been the driving force for implementing CO_2 as working fluid. With the objective of reducing anthropogenic CO_2 emissions to the atmosphere, Brown suggested a novel EGS concept that would implement CO_2 instead of water as a geothermal working fluid (Brown, 2000). The idea was that heat is being extracted during operation; at the same time some CO_2 would geologically stored. The motivation behind Brown's proposals was that, he discovered CO_2 had some chemical and physical properties that would be favorable for the operation of an EGS plant (Brown, 2000). These includes:

- CO_2 being poor solvent compared to water, that it won't interact with most rock minerals.
- CO_2 have higher compressibility and expansivity than water, as result it has a higher natural buoyance and need less pumping power.
- CO_2 has lower viscosity compared to water; therefore it has higher mobility under some thermodynamic conditions.
- Availability of CO_2, than water, which is a scarce resource and always needed in large quantity for this purpose.

His proposals followed by many researchers started researches in this domain, to try to gain more knowledge of which impacts CO_2 injection had one mined and how much CO_2 could be sequestrated in a given geothermal reservoir during operation. In addition, they have been a boost of research based on reservoir rocks properties such as fracture properties, permeability, rock matrix and porosity. For the fluid properties parameters such as injection rate, mobility and buoyance has been studied. One of those researchers is Pruess whose work had the objective of comparing the heat mining potential of water and CO_2. After an intensive work, he came up with the following conclusion concerning CO_2:

> *The advantages of using CO_2 as enhanced energy extraction fluid become more prominent for lower reservoir temperature and pressures. Therefore, using CO_2 as an enhanced recovery fluid was not attractive only for high-temperature thermal resources which are used for electricity generation, but also more beneficial for lower – temperature geothermal resources (Karsten Pruess, 2006).*

Concerning the simulations performed by (Karsten Pruess, 2006), only one fluid (water or CO_2) was implemented in each system as a working fluid. Randolph extended the work done by Pruess and came up with the concept of CO_2 – Plume Geothermal (CPG), for which CO_2 was used as a working fluid, in high permeable and porosity reservoir that was overlain by a low permeability cap rock (Randolph & Saar, 2011a, 2011b). Him too came up with the following conclusion concerning the heat mining, permeability, reservoir temperature and mass flow rate:

> *Heat extraction decreases with time, as the heat is being extracted the reservoir temperature, including production well temperature are depleting with time. Then EGS models with lower permeabilities, which are allowing lower mass flow rate, are cooling slowly than EGS with the same fracture spacing and higher permeability (Randolph & Saar, 2011a, 2011b).*

For simulation conducted by both Pruess and Randolph (Karsten Pruess, 2006; Randolph & Saar, 2011a), it was assumed that the presence of underground CO_2 was naturally existed, and no other fluid existed in the pore spaces. Therefore, there was no consideration of displacement of the native fluid.

Salimi and Wolf (Salimi & Wolf, 2012), came out with another concept of implementing CO_2 in geothermal fields. The method includes co-injection of both CO_2 and water, to prevent drying out and over-pressurized the reservoirs. Additional advantage of this method was related to dissolved phase of CO_2 in water, which would hinder attraction of CO_2 to the upper area of the reservoir, minimizing the chances of potential leakage through the cap rock. During the study, Salimi and Wolf discovered that there was a problem with the model formulation owing to phase transition. However, the developed model results were presented which indicated that; when CO_2 mole fraction was under 0.10, the cumulative heat extraction was as high as 1000 T for 30 years.

Luo (Luo, Xu, & Jiang, 2014) and his fellow researchers assessed the numerical model of fluid flow and heat transfer in a doublet enhanced geothermal system, using carbon dioxide as working. Their study focused mostly on the impact of CO_2 injection rate, the permeability of induced fractures near the wellbores, the injection or production well perforation placement, the working fluid, and finally, the heat flow between the wellbores and the surrounding reservoir. In this case the FLUENT code was used, the code uses the finite volume to solve the Navier-Stokes equations. The following conclusions were made regarding some of mentioned parameters:

> *The thermal breakthrough was inversely proportional to the CO_2 injection rate. Increasing flow rate yield lower exit temperature initially owing to the larger pressure difference in the reservoir with larger injection rates. Concerning the permeability of wellbore fracture, when the well wellbore fracture permeability was increased the pressure difference though the reservoirs decreased also and the net value of these decrement become smaller with additional increment of wellbore fracture permeability (Luo et al., 2014)*

Another study conducted by (Buscheck T, 2012) came up with a hybrid two steps approach to sequester CO_2 and produce geothermal energy in saline and sedimentary formations. With this approach, initially, brine is mined from the reservoir to provide pressure relief for CO_2 injection; thereafter, when injected CO_2 arrives production wells, co-produced treat the brine and CO_2 become the working fluids for heat mining. Three dimensional model results, implementing the NUFT code, for reservoirs temperatures in

the 100 °C range, report heat mining rate applying this approach is as big as 100 MW/m^2 with combined flow rates of almost 280 kg/s.

(Zhang, Ezekiel, Li, Pei, & Ren, 2014) came up with a study, which proved that sCO_2 has good mobility and specific heat, which could be used beside water for heat recovery from geothermal reservoirs. The work performed by (Zhang et al., 2014) different types of geothermal reservoir from China were assessed to find out which reservoirs were appropriate for heat extraction and geological storage by injection of CO_2. The reservoirs were assessed in term of geological properties, development aspects, heat characteristics and storage applicability. A model was designed to analyze heat mining potential and storage efficiency of CO_2 applying explicit calculation method. The result indicated that the recoverable geothermal capacity in china was almost 1.55 x 10^{21} J, using hot dry rock as the main heat source contributor. The corresponding storage potential was almost 3.53 x 10^{14} kg with deep saline playing the main role, contributing for more that 50 % of total storage.

From literature review can we notice that, most of researches in this domain have been focusing on how to improve heat extraction from a geothermal system by CO_2 injection? These have lead to extensive research on for instance, comparing CO_2 and water heat mining potentials and parameters studies, but mostly using traditional reservoir with CO_2 dissolving in water. Among the parameters assessed before are: Mobility, injection rate, wellbore fracture permeability, pressure, and injection methodology and many more. In additional researchers are mostly focused on reservoirs CO_2 storage potentials.

This thesis extends the work presented by Pruess, Randolph and many other geothermal researchers, by modeling water and CO_2 injection into high temperature reservoirs for which one of them is a non- condensable geothermal reservoir. In our case we modeled in first case a traditional reservoir, which is initially saturated with water, and for the second case a non-condensable gas reservoir with almost zero gas at initial condition. Water and CO_2 were chosen as working fluid for both reservoirs respectively. All simulations were accomplished by the use of a multi-phase reservoir simulator TOUGH2 (C. O. Karsten Pruess, George Moridis, 2012) with equation of state module EOS2 and EOS1. The mesh symmetry, fracture and matrix heat exchange were implemented into the

system by the use of the multi-interacting continua method (Botros, Hassan, Reeves, & Pohll, 2008; T. N. N. Karsten Pruess, 1985). The advantages of choosing CO_2 as a working fluid in a geothermal system was analyzed by mapping system temperature, pressure, saturation and phase composition with the heat mined for both water and CO_2 simulations. In addition we assessed the impact of fracture permeability, injection rate, fracture spacing and fracture permeability. The thesis considers only the potential physical processes; chemical, mechanical and biological processes are beyond the scope of this study. The results obtained from both carbon dioxide and water injection were used to determine the optimum heat extraction state of a reservoir and preferable working fluid, which in return could be of great importance for geothermal system designing and field operation.

2.3 Geothermal reservoir characterization

2.3.1 Rock and fracture porosity

The ratio of the total pore volume to the bulk volume of the rock defines the porosity (Ø).

$$\emptyset = \frac{V_p}{V_b} \tag{2.4}$$

Where V_p , and V_b is the pore volume and bulk volume, respectively. Regularly, effective porosity is used in modeling, where the non-connected pores are excluded from the pore volume. Many parameters such as fluid pressure, external stresses form the overburden load and chemical reactions may change the porosity of a media. Fluid component may for example precipitate and narrow or plug pores, or chemically react with the solid to increase the size of the pore space. The dependence of porosity on pressure is accounted by introduction of rock compressibility, which is described in chapter 2.3.2. Porosity varies between reservoirs and even within the same reservoir. For instance In the a geothermal EGS site in Soultz the porosity varies between 0.3% and 10%, depending on the fracture density (Geraud, 2003). In our simulations the fracture porosity is considered as certain percent of the rock porosity. In other word fracture porosity is a part of total porosity.

2.3.3 Rock thermal conductivity

According to Fourier's law heat transfer (Q_h) in a substance is direct proportional to the temperature gradient. The proportional constant ($\boldsymbol{\lambda}$) is what is called the thermal conductivity:

$$Q_h = \boldsymbol{\lambda} \nabla T \qquad (2.5)$$

The thermal conductivity is defined as materials ability to conduct heat. The full description and its impact on heat transfer are studied in chapter 4 of this thesis. Different materials have different heat conductivity capacities as shown in table 1.1

Table 1: Formation and rock minerals heat conductivity

Medium	$\boldsymbol{\lambda}[\,\boldsymbol{W\,m^{-1}K^{-1}}]$
Quartz	6
Granite	2.5 – 3.8
Dry sand	0.4 – 0.8
Wet sand	2.5 – 3.5
Dry clay	0.8 – 2.0
Wet clay	1.2 – 1.7
Sandstone	1.5 – 4.3

(Tough2 micro- courses)

From the table, quartz with its origin as volcanic rock has a highest value, with dry sand having the lowest heat conductivity capacity. In our simulations, the value was 2.51[$wm^{-1}K^{-1}$] which shows that our formation was wet sand.

2.3.4 Rock's fracture permeability

Permeability **(K)** can be defined as rock's ability to transmit fluid. The permeability is related to the porosity and the tortuosity of the pores, since the actual structure of the

pores is not known, the permeability is normally determined experimentally, by well logging and well testing. Permeability exhibits strong heterogeneities; therefore it is best described by a tensor. In our simulation we considered permeability to be homogenous in all directions. Flow in open fractures can be describe by either Navier-Stokes or the Stokes in equation considered the flow is persistent and negligible inertial forces. In addition if the fractures are considered to be parallel planes, like in our simulation, and the normal velocity is neglected and shear forces acting normal to the fracture wall becomes significant, then the fracture permeability is given by local cubic law as follow:

$$K_f = \frac{a^2}{12} \qquad (2.6)$$

Where "a" denotes local fracture aperture and K_f is fracture permeability.

2.4 TOUGH2- Reservoir simulation tool

2.4.1 Introduction to TOUGH2

TOUGH2 is a numerical simulation program for multi-dimensional fluid and heat flows of multiphase, multicomponent fluid mixtures in porous and fractures media (C. O. Karsten Pruess, George Moridis, 2012). The main application domains include; geothermal reservoir engineering, nuclear waste isolation researches, environment assessment and remediation, and finally flow and transport in saturated media and aquifers. Table 2 gives us an overview of the above definition:

Our model is characterized as 3D, nonisothermal, multicomponent (water & CO2) and fracture is implemented by introducing the MINC method. The remaining of this chapter will describe all these areas in details.

Table 2: TOUGH2 definition overview

Model Area	Description
Multi-dimensional	0D, 1D, 2D, 3D
Multiphase	liquid, gas, NAPL
Multicomponent	water, CO2; air, VOC, radionuclides
Nonisothermal	heat
Flow and transport	multiphase Darcy law
Fractured-porous media	DFN, dual-ø, dual –K, MINC, ECM
EOS: Equation **O**f **S**tate	Thermophysical properties

(Tough2 micro- courses)

2.4.2 TOUGH2 Governing equations

The component mass – and energy –balance equations shows in table 3 are implemented in TOUGH2 as governing equations. TOUGH2 uses the integral finite difference (IFD) method to compute the solutions of these equations. During the space discretization with IFD, the system geometry is determined by; the volume of grid block, interface area between grid blocks, nodal distances and the orientation of nodal line to the vertical. The method has a precondition that the line connecting two elements are perpendicular to the interface. IFD does not make reference to a global coordinate system; therefore the introduction of fractures using the secondary does not affect the discretization process. By applying this method, system average volume is represented as follow:

$$\int_{Vn} MdV = V_n M_n \tag{2.7}$$

In such way that M represent the volume – normalized extensive quantity, and M_n represent the average value of M over the volume V_n. The area averages in the system are denoted are as follow:

$$\int_{\Gamma n} \boldsymbol{F^k}.\boldsymbol{n}d\Gamma = \sum_m A_{nm}F_{nm} \tag{2.8}$$

In such way that F_{nm} represent the average value of the component of F over the surface interface between volume elements V_n and V_m(Biagi et al., 2015).For details descriptions about conservation equations and solution method can be found in (C. O. Karsten Pruess, George Moridis, 2012).

Table 3: TOUGH2 governing equations

Description	Equation
Conservation of mass & energy	$\frac{d}{dt}\int_{Vn} M^k \, dV_n = \int_{\Gamma n} \boldsymbol{F}^k . \boldsymbol{n} d\Gamma_n + \int_{Vn} q^k dV_n$
Mass accumulation	$M^k = \emptyset \sum_\beta \ S_\beta \rho_\beta X_\beta^k$
Mass flux	$\boldsymbol{F}^k = \sum_\beta X_\beta^k \boldsymbol{F}_\beta$
Porous medium Energy flux	$\mathbf{F}^k = -\lambda \nabla T + \sum_\beta \ h_\beta \boldsymbol{F}_\beta$
Energy accumulation	$M^k = (1 - \emptyset)\rho_R C_R T + \emptyset \sum_\beta S_\beta \rho_\beta \mathcal{U}_\beta$
Darcy velocity	$\boldsymbol{u}_\beta = -K \frac{K_{r\beta}}{\mu_\beta} (\nabla P_\beta - \rho_\beta \, \mathbf{g})$ Phase Darcy's law, with $P_L - P_G = P_C$

2.4.3 Equation Of State (EOS)

From table 2, we mentioned EOS as a part that introduces the thermodynamic properties to the program. In other word, the nature and properties of a given fluid mixture are introduced into the governing equations (listed in table 3) by means of thermophysical parameters. The user determines the primary parameters as input data, these are the time- independent unknowns, but these values can be determined at initial conditions. Primary variable can be pressure, temperature, gas saturation, or saturated pressure, depending on the equation of state module. Secondary parameters which are fluid and

state – related properties calculated as a function of the system state are provided back from EOS as output, these parameters includes; the density, viscosity, or internal energy. In short the EOS act as a link between primary and secondary parameters. It determines the phase state and phase composition.
As we mentioned earlier, different EOS modules handles different fluids, in our case we used EOS1 for the first simulations and EOS2 for the second simulations. EOS1 handles water as working fluid, while EOS2 handles water and CO_2.

The EOS2 module was originally developed by O'Sullivan (O'Sullivan, 1985) to design gas dominated geothermal systems, which possesses CO_2 mass fractions ranging from a few percent to more than 80 %. The EOS2 describes a non-ideal behavior of gaseous CO_2, and the soluble separated CO_2 into the aqueous phase with heat of solution effects

2.4.4 TOUGH2 Program Structure

A full-summarized TOUGH2's architecture description is shown in figure 2.2.5. The governing equations for multiphase and heat flow described in section 2.4.2 remains the central part for solution computation. In addition, the equations are independent of the nature, number of fluid phases and components present. Therefore, solutions can be computed with different fluid property modules and this give TOUGH2 a wide flexibility to deal with different multicomponent, multiphase flow systems.

The assembling to the governing equations includes the input and initialization data described in section 2.2 for working fluid and 2.3 for reservoir parameters. The input files used for both EOS1 and EOS2 are enclosed in the appendix A. Initialization data consist also of boundary conditions, for which in our case, we considered no heat and fluid flow at the boundaries. In other word a closed system with mass flowing between the source and sinks term conserved. In addition, at initial condition the thermodynamics state was assumed to be in equilibrium for all block elements. The system assembles all the parts, thus the parameters from EOS, Input and initialization and the solution of linear equations combine with simulation time and compute the output. An example of output file for EOS1 base case at 30 years simulation time is enclosed in appendix A.

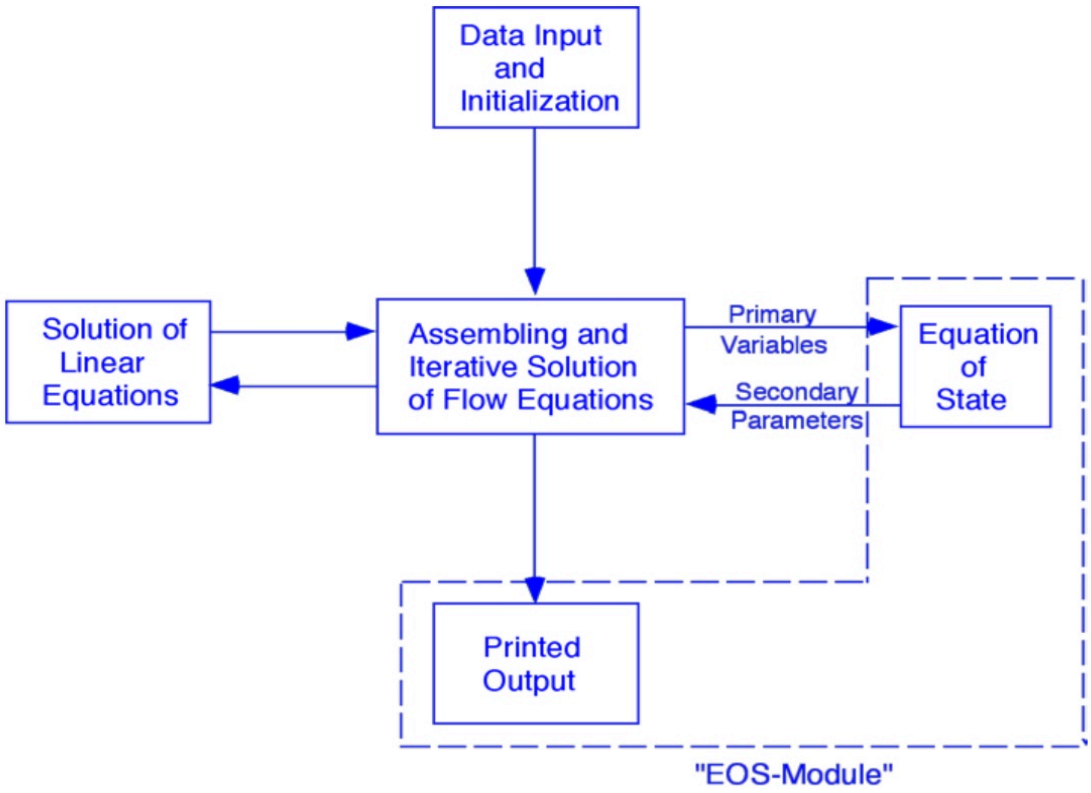

Figure 2.2.5TOUGH2 Architecture (C. O. Karsten Pruess, George Moridis, 2012)

2.4.5 Fracture modeling

Normally, two different methods for modeling flow and transport in fractured media exist, the discrete fracture network and the continuum models. The discrete fracture method account for individual fractures, and allow space for more precise description of fracture network system and corresponding flow movements. Unfortunately, the method is expensive and requires a lot of computer power. In addition it only consider fluid flow and transport within the inter-connected fracture networks and not considering the facture-matrix interactions. Based on the above reasons, this method is not widely used for simulations. Then the most reliable becomes the continuum approaches, among these includes; the effective continuum method (ECM) (Wu, 1999), dual porosity/ permeability (DKM) and the multi – interacting continua (MINC) model (T. N. N. Karsten Pruess, 1985; K. Pruess, 1983) In the MINC which was used for our model, the fracture and matrix systems are handled as separate continua, flow and heat transfer are conceptually

addressed in both matrix and fracture continua. Individual continuum has a complete set of appropriate mass and energy balance equations, then this balance equations are again coupled through a inter-continuum mass and heat transfer (Yue Hao, 2012).

The MINC method is considered as a best used method for numerical simulation of heat and multiphase fluid flow in multidimensional, fractured and porous media (T. N. N. Karsten Pruess, 1985; K. Pruess, 1983). The method is a wider application of the double-porosity method, and gives a far better numerical simulation of matrix-fracture interactions than many other methods. Figure 2.2.6 shows the classical double-porosity model, which is a foundation of the MINC method.

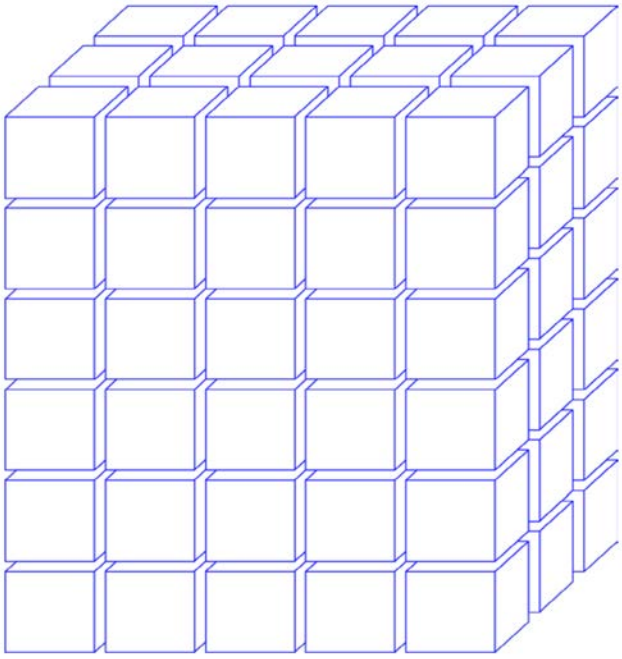

Figure 2.2.6 –Idealized model of a fractured porous medium(C. O. Karsten Pruess, George Moridis, 2012).

The matrix blocks of low permeability lodges in a network of interconnected fractures. The matrix is considered as effective porous continuum, with the global flow-taking place within the matrix blocks only. Heat and fluid flow between the fractures and the rock matrix take place by means of interporosity flow, in such way that the two flows are being driven by temperature and pressure difference between the two continua (matrix and fractures).

Such system will achieve the quasi-steady state at very early time if the pressure diffusivities are very high, in such a way that the pressure changes inters quickly into the

matrix blocks and the flow is isothermal single phase flow, in addition, there will be an acceleration of this effect if the fluid has a very small compressibility (e.g water). However, for the case of multi-phase flow the system will take longer time to reach the steady state. Therefore, in order to have an appropriate description of such flows in this system, it is then important to resolve the driving pressure, temperature, and mass fraction gradients at the two continua interfaces. The resolution process is then introduced by the process of multi– interacting continuum (MINC) (T. N. N. Karsten Pruess, 1985; K. Pruess, 1983), for which the matrix blocks are sub gridded as shown in figure 2.2.7.

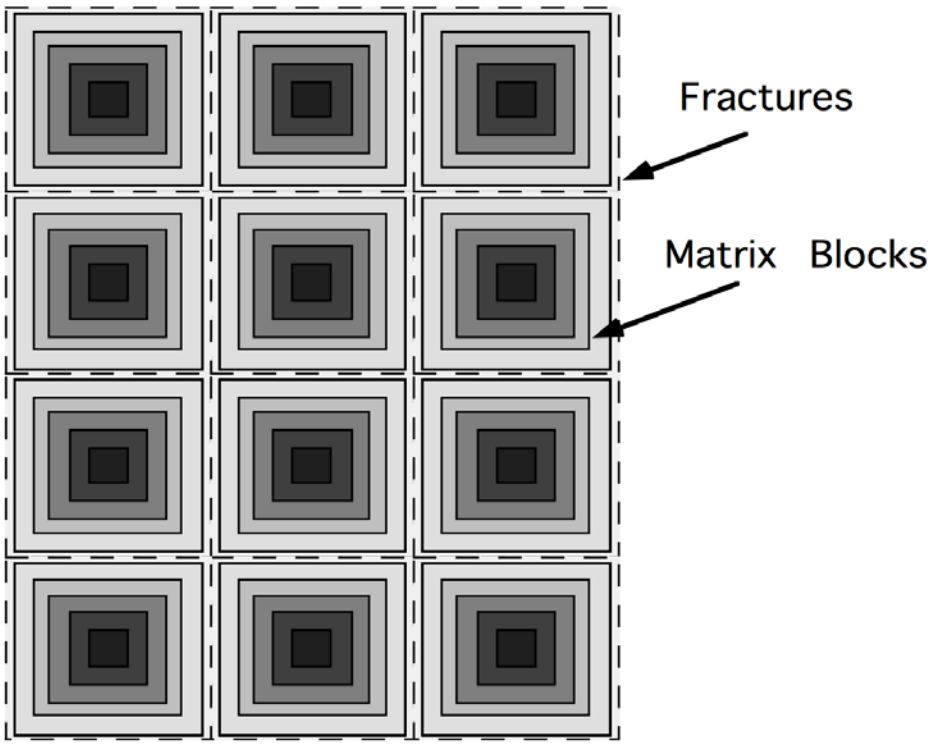

Figure 2.2.7 Subgridding patterns of MINC method (C. O. Karsten Pruess, George Moridis, 2012)

The MINC method is based on the general understanding that changes in fluid pressure; temperature and phase composition develop rapidly through the fracture system at the same time invading the tight matrix blocks slowly(T. N. N. Karsten Pruess, 1985; K. Pruess, 1983). For this reason, the position of the matrix subgrids from the fractures controls the thermodynamics conditions of the block matrix. Interporosity flow (fluid and heat) from fractures into the matrix and vice-versa, can be modeled by the application of one-dimensional strings of nested grid blocks as shown in figure 2.2.7

During the simulation, the MINC-process when implemented operates on the primary mesh data and produces a secondary mesh. In our case, we considered three continua, thus fractures and two matrix continua; the output of the secondary mesh is enclosed in appendix A.

2.5 Heat transfer mechanism

The term heat transfer refers to the transfer of thermal energy due to change in temperature. The heat is transferred from hot to cold region. The heat transfer occurrence can be categorized into various mechanisms, such as conduction, convention and radiation. Heat transfer in general is the phenomenon of thermal energy exchanges between systems, which depends on the thermodynamic states-pressure and temperature.

As fluid flows in a wellbore and in reservoir, the heat transfer is governed by conduction, convection and radiation. The mechanisms are independent of each other and however, they contribute for the overall all heat transferred in the systems.

2.5.1 Conduction

Heat conduction is the transfer of energy (internal energy) from higher internal energy to the neighboring lesser less energetic. Figure 2.2.8 illustrate the Heat transfer through a plane slab. The temperature at one side is higher than the other side. T1 > T2. For one dimensional, the heat transfer flux is proportional to the change in temperature and inversely proportional to the distance between the as showed in equation 2.5

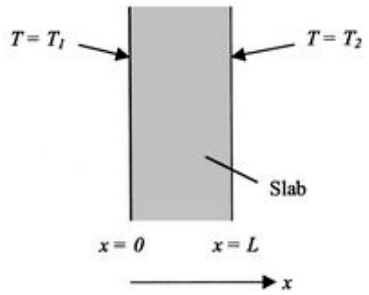

Figure 2.2.8 Temperature boundary conditions for a slab (Fidan, 2011)

In order to emphasize the heat flux proportionality with temperature, the equation 2.5 can be expanded and written in the following form:

$$\dot{Q_{cd}} = -k\frac{dT}{dx} = -k\frac{T_2 - T_1}{L} \qquad (2.9)$$

Where $\dot{Q_{cd}}$ conductive heat flux, T temperature and k thermal conductivity

2.5.2 Convection

Convection is the mode of heat transfer through a liquid or gas medium in motion. This can be from a solid surface to liquid or gas. When the motion of a medium is caused by an external source such as pump or the wind, then the convection is called force convection. In contrast, buoyancy forces cause the so-called natural convection, which is also caused by density differences within the fluid, owing to temperature variation within the fluid.

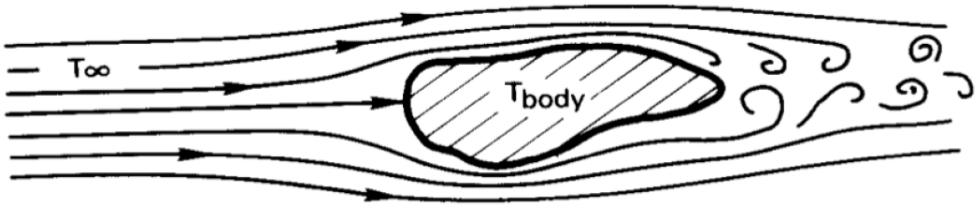

Figure 2.2.9: Convective cooling of heated body (John, 2008)

Newton's law of cooling as shown below represents the convection heat flux:

$$\dot{Q_{cv}} = -kA_s(T_s - T_\infty) \qquad (3.0)$$

Where T_s is the temperature of the heat source and T_∞ is the temperature of the surrounding fluid, $\dot{Q_{cv}}$ convectional heat flux, k thermal conductivity.

2.5.3 Radiation

Radiation is the energy released by an object in the form of electromagnetic waves owing to changes in the electronic distribution of the atoms. The heat emitted by radiation an object depends on many factors, such has hot is an object, object's ability to absorb heat

and the color of an object. Stefan – Boltzman law represents radiation that is achieved at a room temperature:

$$\dot{Q_{rd}} = \sigma A_s T_s^4 \quad (3.1)$$

Where $\dot{Q_{rd}}$ is the radiation heat flux, σ Stefan Boltzman constant, A_s area of radiated surface and T is the absolute temperature.

3 Geothermal reservoir simulations

This chapter introduces the principle behind simulation setup in the reservoir and pipe. Detailed descriptions of how the model was implemented into Tough2 simulator are also highlighted and the results obtained for different parameters are presented.

3.1 SIMULATION FOR WATER RESERVOIR

3.1.1 Simulations setup

The geothermal reservoir we considered in our simulation is an idealized 305 m thick reservoir, with its characteristics shown in table 4.1. We assumed that the reservoir is initially saturated with water, at hydrostatic pressure of 290 Bar and geothermal temperature of 250 °C. These types of reservoirs can be encountered around high geothermal heat flow areas, such as the Texas Gulf Coast (Lehua Pan, 2015). The total area of the five spots well pattern system is 1.0 $x10^6$ m^2. Our simulation considered only 1/8 of the area, which corresponds to a reservoir area of 1.25$x10^5$ m^2 and comprises of one injection and production well pair system as shown in figure 3.1.1. The reservoir has closed boundaries on all its sides, with the top boundary closed for both heat and fluid flow and the bottom permitting only heat flow. Fluid was injected at constant rate, and independent of time, with the amount of mass injected equal to the amount of mass-produced. This satisfies the statement of no fluid flow at the boundaries.

A homogenous single layer reservoir was modeled in three-dimensions (3D), with constant grid block length size of approximately 64 m. The reservoir consists of six grid rows, each containing between one and eleven grid elements, for the overall of thirty-six volume elements.

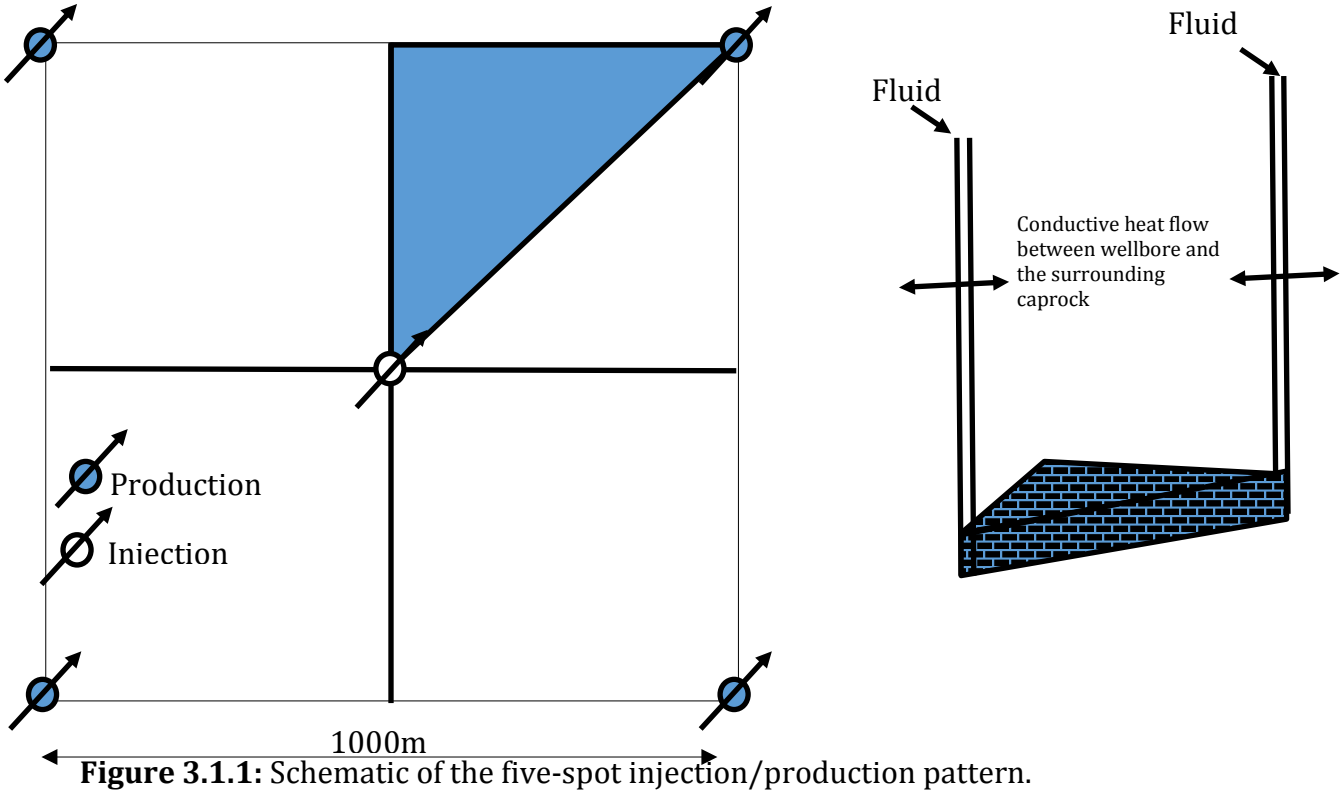

Figure 3.1.1: Schematic of the five-spot injection/production pattern.

Below is the list of the base case reservoir properties data used for the modeling;

Table 4: Reservoir and base case input parameters

Formation	Value
Rock grain density	2600 kg/m3
Specific heat	100 J/kg °C
Heat conductivity	2.51 W/ m °C
Pore compressibility	10^{-10} Pa^{-1}
Matrix porosity	0,254
Permeable volume fraction (fractures)	5 %
Porosity in permeable domain (fractures)	50 %
Cubes with side length (fracture spacing)	60 m
Permeability	1.0x10-13 m^2
Thickness	305 m

Initial Conditions	
Temperatures	250 °C,
Liquid saturation	0.99
Pressure	290 bar
Production/Injection	
Pattern area	1 km2
Distance between producers and injectors	707 m
Production rate	8 kg/s
Injection rate	8kg/s
Injection enthalpy	100 kJ/kg

Table 5: Relative permeability & Capillary pressure data (Lehua Pan, 2015)

Parameter	**value**	**Note**
Parameters for relative permeability		
Residual gas saturation	0.01	Liquid relative permeability K_{rl}
$\mathbf{m_{vg}}$	0.65	given by Van Genutchen- Mualem
Residual liquid saturation	0.05	Model(Van Genuten, 1980)
Saturated liquid saturation	1.0	
Parameters for capillary pressure		
Residual liquid saturation	0.03	Capillary pressure P_c also give by
$\mathbf{m_{vg}}$	0.4118	(Van Genuten, 1980)
Alpha	6.08E-5 Pa^{-1}	
Maximum capillary pressure	6.4x107 Pa	
Saturated liquid saturation	1.0	

As mentioned earlier, the above data were used for simulation of the base case. In order to perform sensitivity studies of different parameters, we varied the input parameters values below and above the base case as shown in table 6. This helps us analyze the

impacts of each parameter on reservoir temperature, pressure distributions and the heat being mined.

Table 6: Variation of water input parameters

Parameters name	Base case value	Lower value	Upper value
Fracture Spacing in all 3D Directions	60 m	10 m	100m
Fracture Porosity	50%	30 %	70%
Flow rate	8 kg /s	4kg/s	12kg/s

3.1.2 Simulation results

On this part, we present the results obtained from the variation of different parameters in the reservoir. We started with temperature distribution after some time of injection, then we continue with pressure distribution interpretation and finally, the amount of heat mined is discussed for a given parameter. Note that the temperature at production remains almost stable for almost all the cases, firstly this is due the fact that, the reservoir possesses high initial temperature and can take long time to deplete than the simulated time presented here. Secondly, as the fluid is being injected, the fluid is being heated as it moves from injection to production by the hot rock, as result it reaches the production block when it temperature has reached quasi-steady state with the rock temperature. Then the temperature at production will remain unchanged for a long production period than any other parts in the reservoir. This trend can be seen from comparing the temperature at injection and production at a specific time, and shows also which important function initial temperature plays on heat extraction. In other words high initial reservoir temperature is a precondition for high and durable energy production as shown in figure 3.1.2. Since our interest has been on which impacts different parameters had on the reservoir pressure, temperature distribution and heat mined, with water as the working fluid, this impacts could only be observed at early time of production.

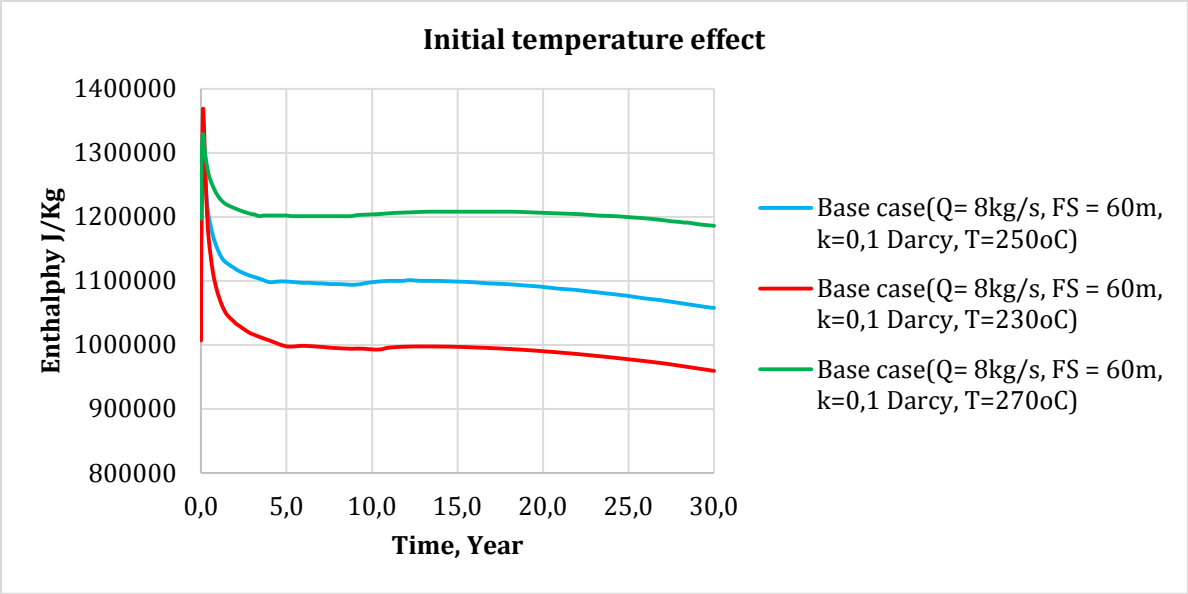

Figure 3.1.2: Effect of initial temperature on enthalpy at production for the first 30years of production.

3.1.2.1 Effect of fracture porosity

The effect of fracture porosity was obtained by maintaining all base parameters constant and varies the fracture size, therefor increasing and decreasing the fracture porosity. The result showed that the temperature of the fluid within the reservoir increased from injection to production well, holding constant at the area near the production as shown in figure 3.1.3.

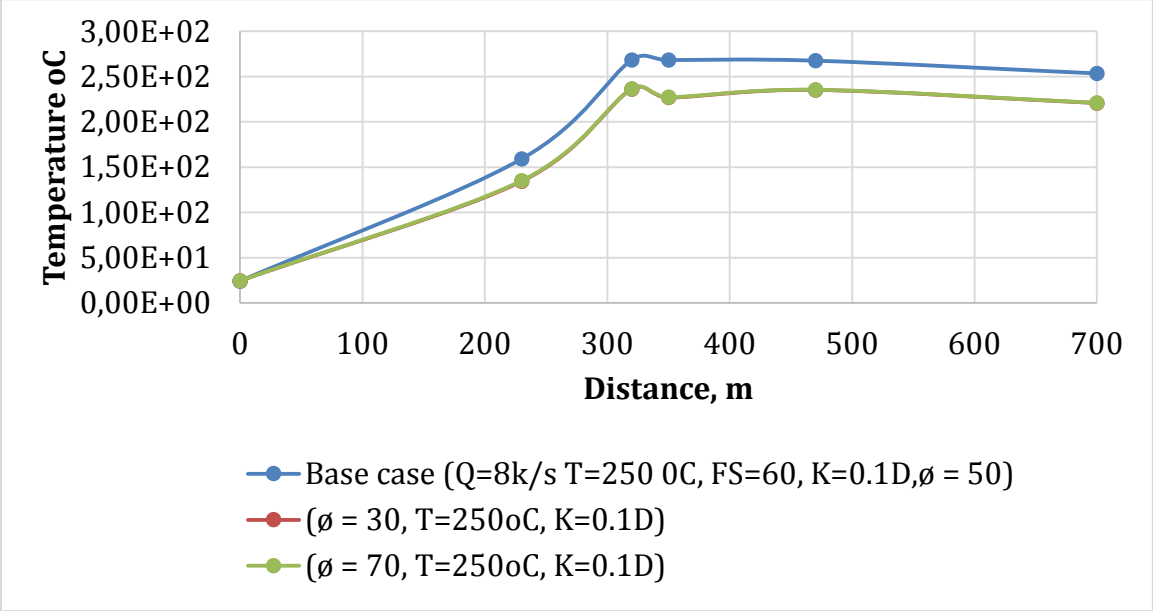

Figure 3.1.3: Effect of fracture porosity on temperature profile along the line from injection and production well at 30 years of production.

The result showed that decrease of temperature distribution of about 13% when the porosity was dropped or increased. The pressures drop between the injection and production well remains constant for all cases, with the same pressure profile within the reservoir. This is shown in figure 3.1.4. In all case the pressure dropped from the initial value of 290 bars, with high value of fracture porosity having most drop from initial value.

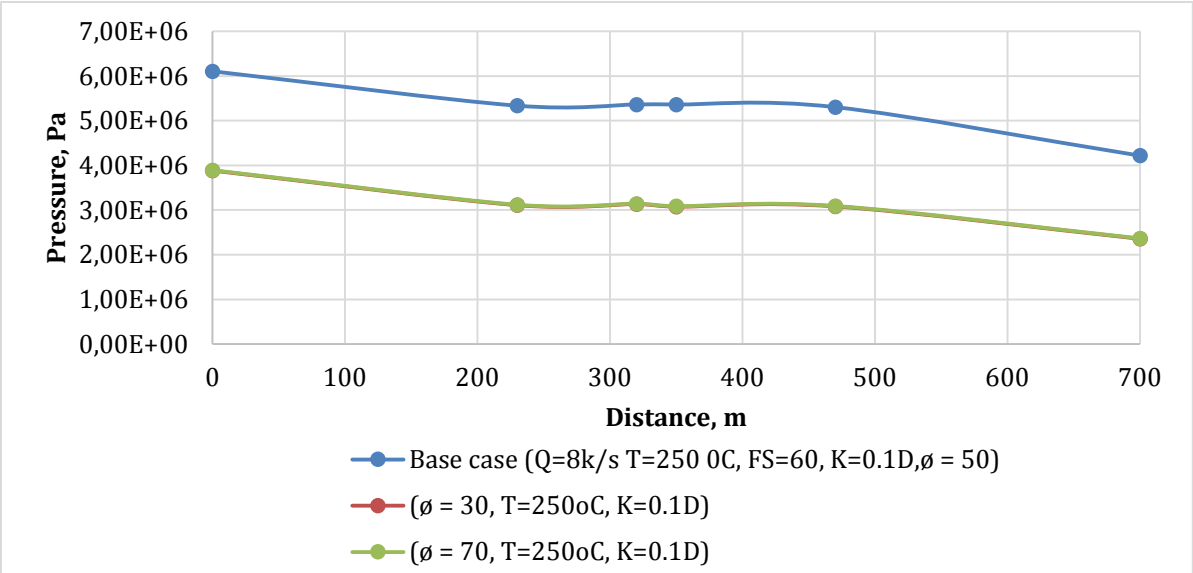

Figure 3.1.4: Effect of fracture porosity on pressure profile along the line injection and production well at 30 years of production.

The pressure and temperature profiles studied are for a given year; our situation is at 30 years of production. Figure 3.1.5 represent the result of the enthalpy at production well, for first five years of production. The result shows highest heat production for lowest fracture porosity at the beginning of production, but the production stabilized at the same level after some time. With increased produced enthalpy of about 7 % when the fracture porosity is reduced by 40%, likewise a reduction enthalpy of about 4 % when the fracture porosity is increased by 40 %.

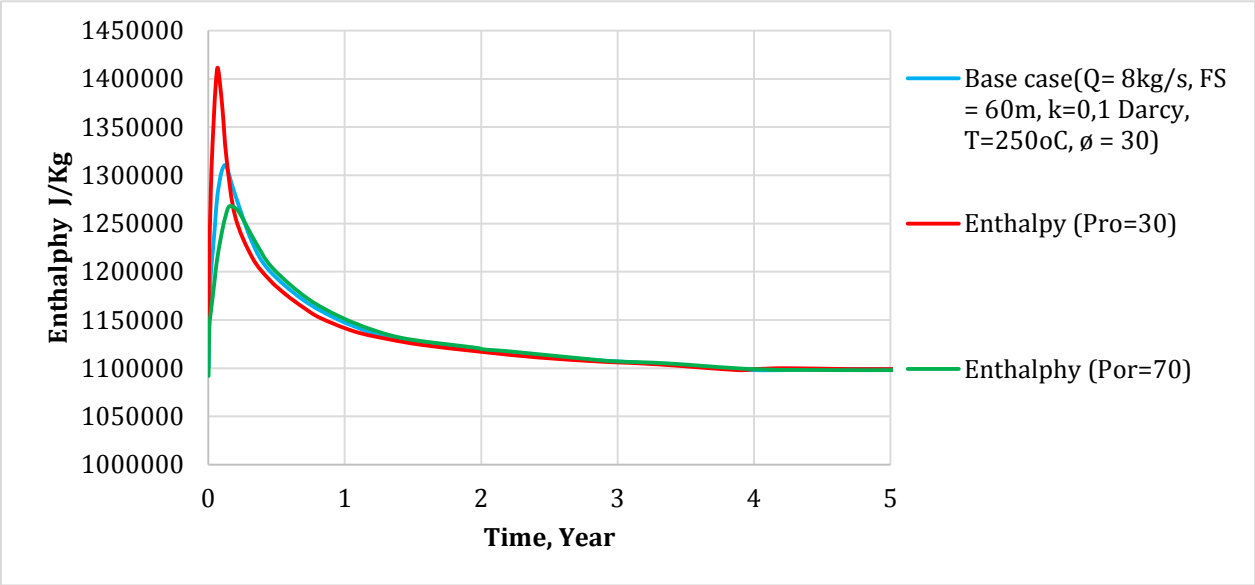

Figure 3.1.5 Effect of fracture porosity on Enthalpy at production for the first 5 years of production

3.1.2.2 Effect of flow rate

Injection and production rate determine how long the injected fluid reside in the reservoir, this in return can have a very big impact on heat carried by the fluid. In our case, the amount of the injected fluid was the amount of the produced at production. Temperature distribution in the reservoir of difference injection rate is plotted in figure 3.1.6, this shows that lowest injection gave highest temperature distribution in the reservoir, therefore the temperature distribution in the reservoir increased with decreasing injection rate. The largest impact for this difference was observed at injection and reduced as the fluid approached the production, this because heat in these areas had more been swept, compared to the area near the production.

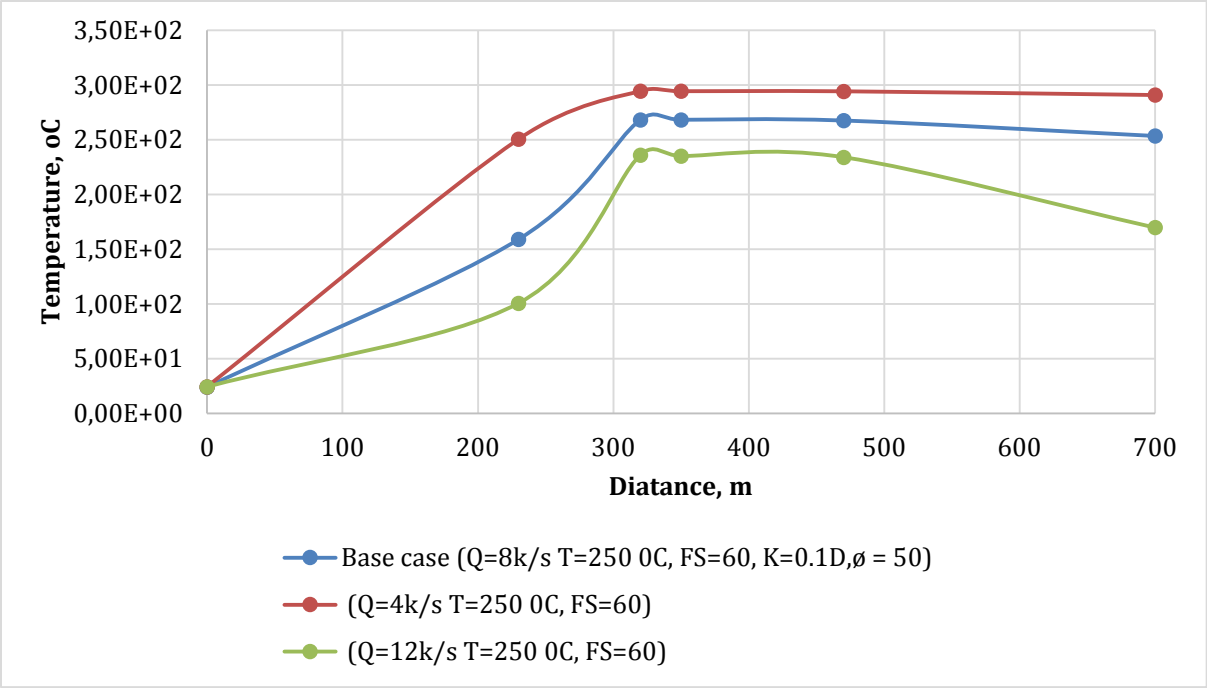

Figure 3.1.6: Effect of injection rate on temperature profiles along the line from injection and production well at 30 years of production.

Pressure profile is a function of flow rate, low flow rate gave low-pressure drop, and when the rate was increased, the pressure drop between the injection and production block increased too. With flow rate of 4 kg/s, 8 kg/s and 12 kg/s giving us the pressure drop of 1.0 KPa/m, 2.7 Kpa /m and 5.0 KPa /m respectively. These results are shown in figure 3.1.7 below, and highest-pressure drop giving us highest heat production.

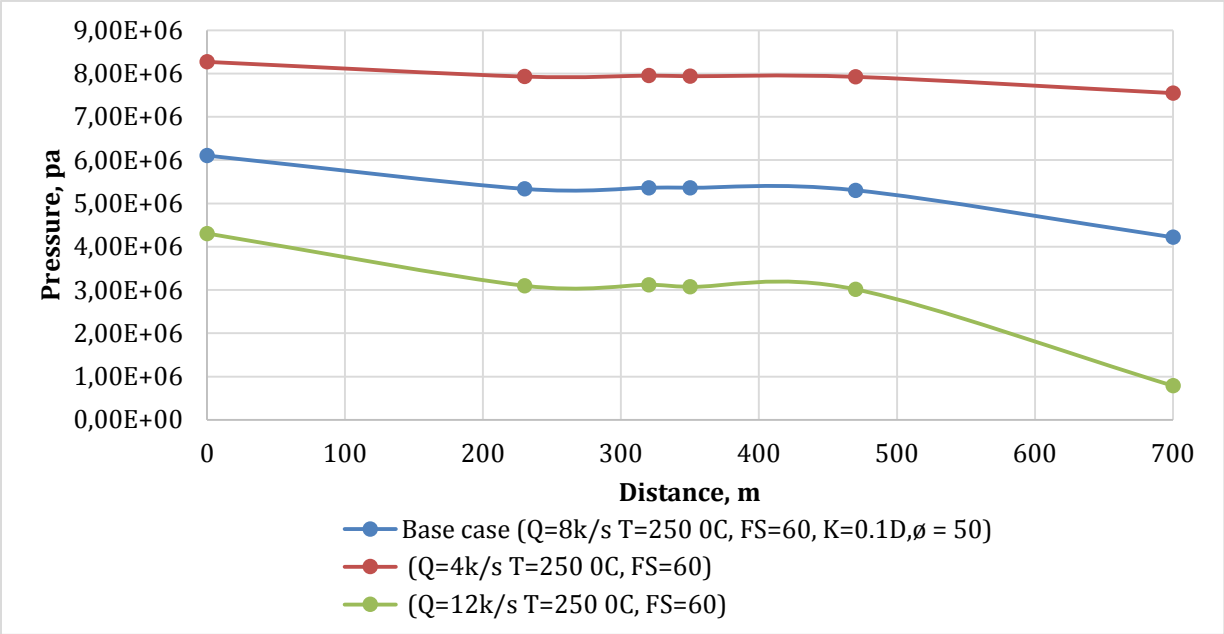

Figure 3.1.7: Effect of injection rate on pressure profiles along the line injection and production well at 30 years of production.

Figure 3.1.8 shows the production enthalpy at different rates, with the highest enthalpy for the rate 12 kg/s within the early year of production. This was an increment of about 5 % from the base case at initial production and when the flow rate decreased to 4 kg/s the production enthalpy dropped by equivalent amount. As production continued, the enthalpy value of the highest production rate began to drop below that for higher flow rate, which was the sign of higher heat sweep efficiency for highest flow rate. This correlate with the temperature distribution in the reservoir where high flow rate result into low temperature distribution at a given time. In overall the difference in energy production was not big.

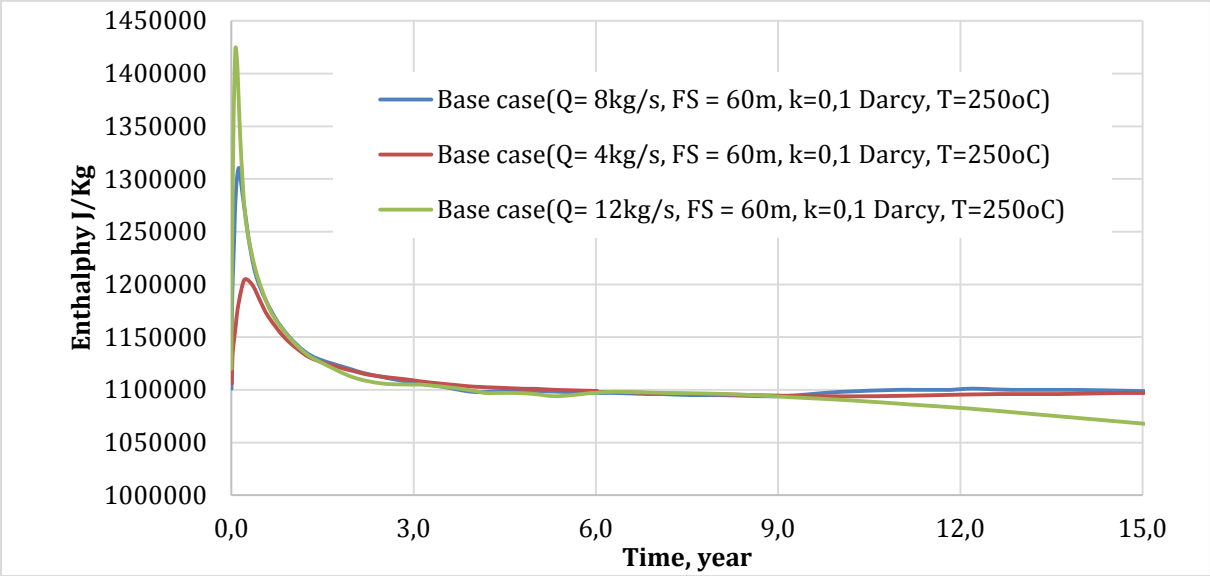

Figure 3.1.8: Effect of injection rate on enthalpy at production for the first 15 years of production.

3.1.2.3 Effect of fracture spacing

Fracture spacing (FS) was another parameter of particular interest to study. This is because it determines the number of fractures and the block matrix size of the reservoir. Figure 3.1.9 shows temperature distribution along the line of injection and production well for different fracture spacing. We could see that the lowest fracture spacing having highest temperature distribution after 30 years of production. From the injection the pressure distribution was almost constant for all three cases and little differences as the fluid approaching the production well.

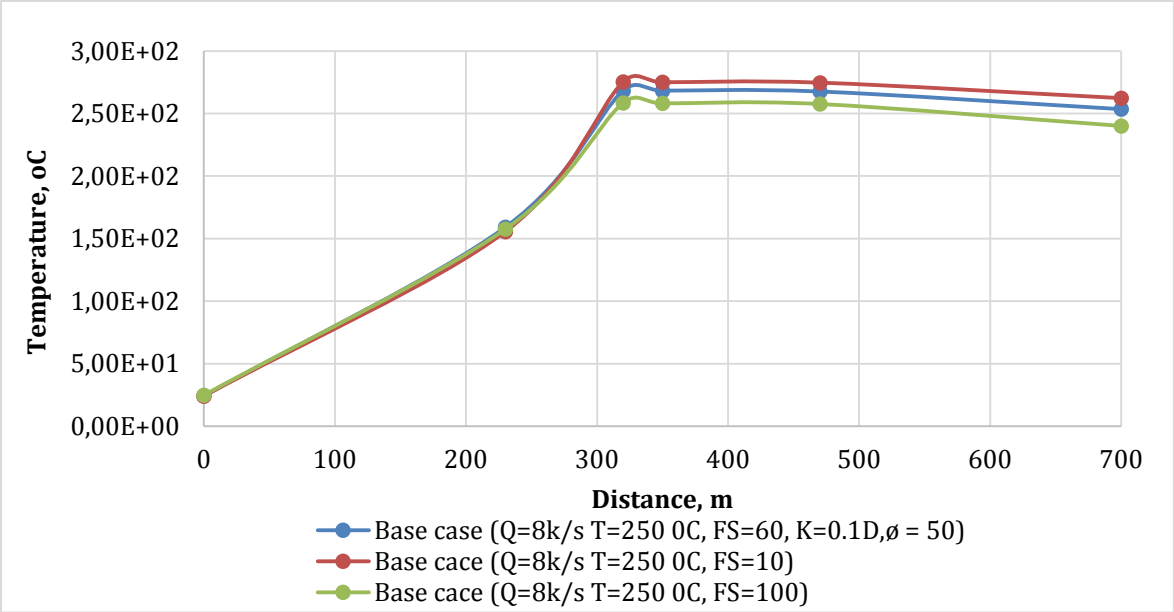

Figure 3.1.9: Effect of fracture spacing on temperature profiles along the line injection and production well at 30 years of production.

The pressure profile follows the same trend of the temperature distribution, with the least fracture spacing on top and the highest on the bottom as shown in figure 3.2.0, which gave us a clear evidence that low fracture spacing result into higher-pressure profile in the reservoir than high fracture spacing. The pressure drop between the production and the injection well remained nearly constant with an average of 2.6KPa/m for all three cases.

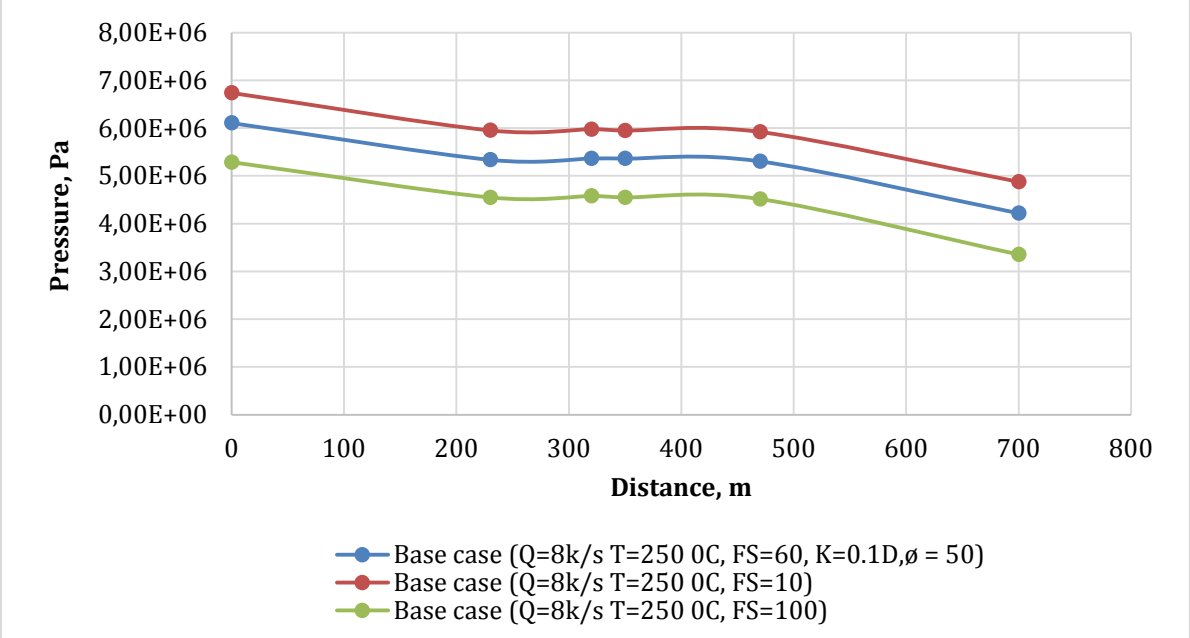

Figure 3.2.0: Effect of fracture spacing on pressure profiles along the line injection and production well at 30 years of production.

Figure 3.2.1 shows the enthalpy produced due the fracture spacing variation, with an increment of produced energy of about 40% when the fracture spacing is reduced by 83% The value stabilized with time to the value of base case. When the fracture spacing (FS) was increased by 67%, the heat production increased by 2% as well. This different results shows which big impact does the small fracture spacing plays on heat production.

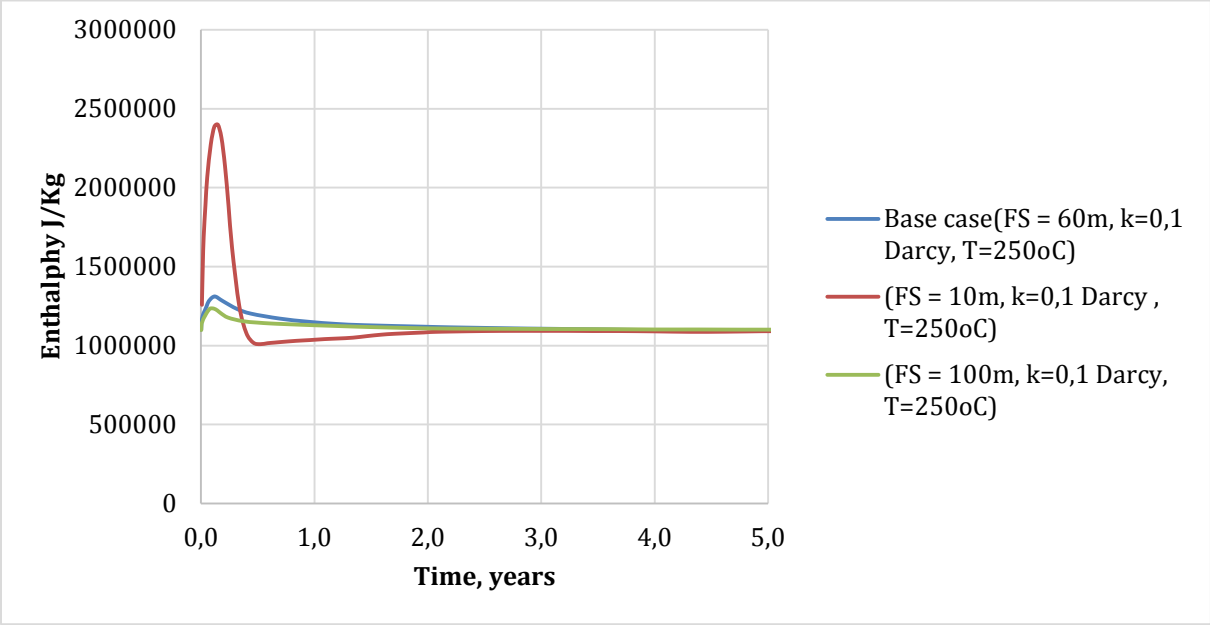

Figure 3.2.1: Effect of fracture spacing on **e**nthalpy at production for the first 5 years of production.

3.2 SIMULATION FOR WATER/CO2 RESERVOIR

3.2.1 Simulation setup

We extended our simulation with CO_2 injection in a non-condensable reservoir. The reservoir characteristics were kept constant, and the thermodynamics properties were changed to match the non-condensable reservoir. The reservoir initial pressure was reset to 90 bars, with saturation temperature at 300 °C. CO_2 partial pressure 0 bars which simply signifies that the reservoir was initially saturated with water. In this case the TOUGH2 module of EOS2 was implemented in order to integrate CO_2 into the system. The boundary conditions were also similar to the one used for water simulation. Different reservoir parameters were also varied as shown in table 6, in order to assess their impacts on flow enthalpy at production, and temperature and pressure distributions within the reservoir.

Table 6: Variation of CO_2 input parameters

Parameters name	Base case value	Lower value	Upper value
Fracture Spacing in all 3D Directions	60 m	10 m	110m
Fracture Porosity	60%	30 %	70%
Fracture Permeability in 3D Directions	0.1 D	0.075 D	0.15D
Flow rate	5kg /s	2.5kg/s	7.kg/s

3.2.2 Simulation results

The results were different from the use of water as working fluid. With CO_2 as a working fluid, the flow enthalpy hold itself constant at its highest value, and starts to decrease immediately CO_2 reaches the production block of the reservoir. This showed that the enthalpy production is direct proportion to the amount of gas in the reservoir. Gas saturation plays a very important role, as CO_2 was injected the gas saturation started to increase, this in turn increased the CO_2 partial pressure and also forcing the reservoir pressure to drop. At the same time the enthalpy production was also following the same trend, it decreased as the gas saturation increased, and attaining it minimum level when the reservoir was fully saturated with CO_2

The base cases are shown below, for which figure 3.2.2 shows that as CO_2 is being injected at injection block, before it reaches the production block, the reservoir pressure increases with increasing gas saturation and CO_2 partial. As the first gas reached the production block, as we mentioned, assumed the reservoir was initially saturated with water and CO_2 in liquid phase at equilibrium state, in such a way that additional CO_2 injected was part of water vapor. By injecting more CO_2, the CO_2 partial pressure kept increasing, until it reached the quasi-steady state, for which the reservoir pressure was equal to the CO_2 partial pressure. Gas saturation within the reservoir followed the same trend as pressure

and partial pressure, with quasi-steady state achieved when gas saturation was equal to one.

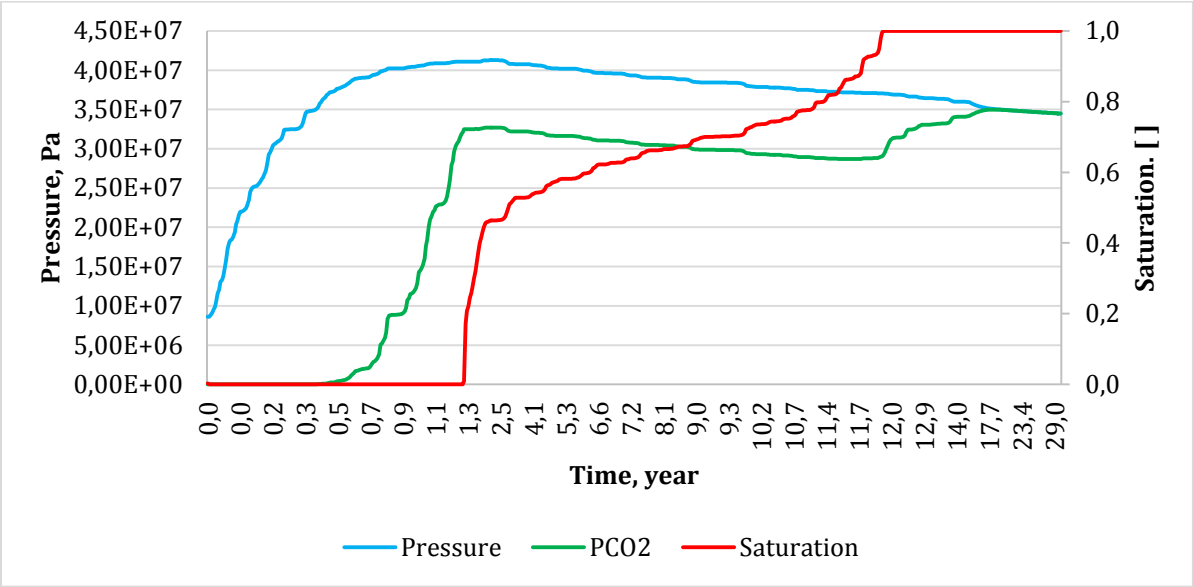

Figure 3.2.2: Base case pressure, partial pressure and saturation profiles at production.

The temperature profile within the reservoir correlates with the partial pressure, and reservoir pressure. Figure 3.2.3 show the temperature profile at production, the temperature decreased with time, for which it dropped drastically as the gas saturation switched to one. At this point the temperature of the fluid decreased, owing to the fact that water vapor which had being boiled by CO_2, had higher enthalpy than CO_2. Therefore transition to one phase and one component should cause temperature drop as shown in figure 3.2.3.

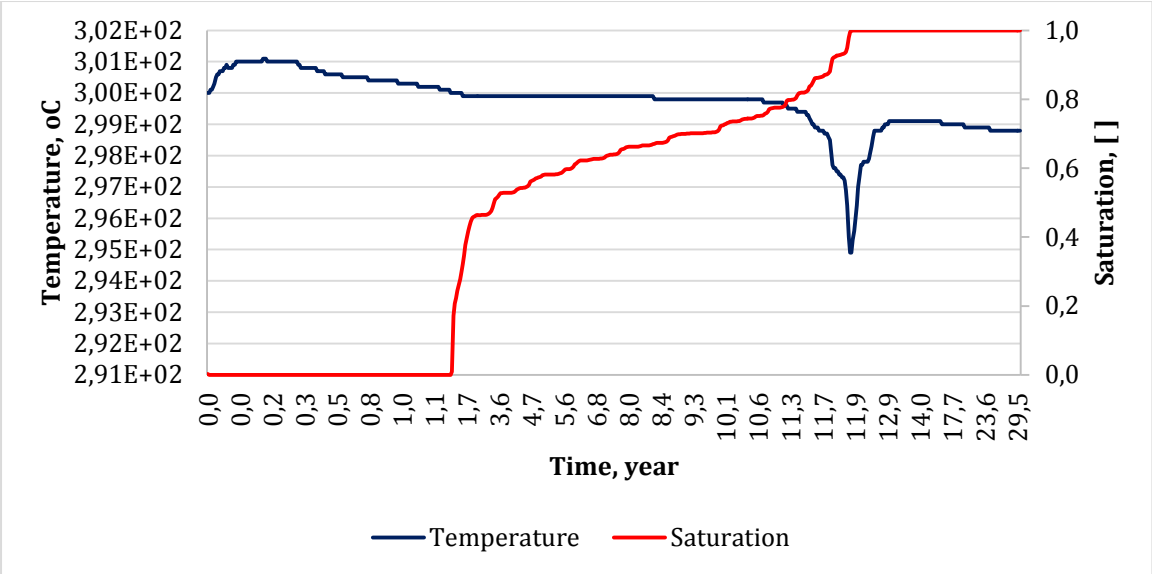

Figure 3.2.3 Base case temperature & saturation profile at production

The diagram 3.2.4 shows the direct correlation between the energy extracted and CO_2 mole faction at production block. When the CO_2 mole fraction increased, the enthalpy decreased too, this reflects lower energy carried by CO_2 compared to water vapor. The initial higher energy flowing, reflect the boiling activities causes by CO_2. When CO_2 was injected, it boiled the water in the reservoir, generating more water vapor, which in turn initially gives high flow of energy at production. The higher energy remained constant until when CO_2 reached the production at one year after injection, then it started to drop as CO_2 amount started to increase at production. The energy remained constant when CO_2 mole fraction remained also constant. It dropped again when CO_2 mole fraction increased at twelve years of production. At this stage, CO_2 mole fraction increased to one, which indicates zero water vapor in the gas phase. As result we got a drastic reduction of energy flow owing to CO_2 lower energy carrying capacity, than water vapor. This trend was also observed in all simulation cases when we varied parameters and the plots are enclosed in appendix B.

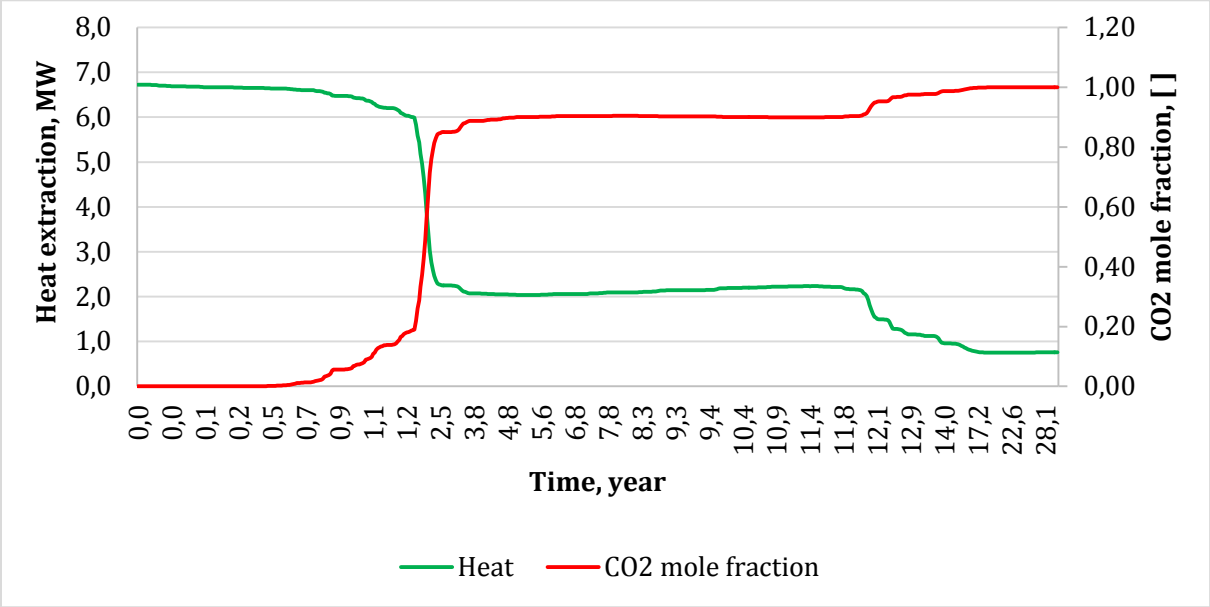

Figure 3.2.4: Base case heat extraction & CO_2 mole fraction flow profile at production

3.2.2.1 Effect of fracture porosity

Fracture porosity is another parameter, which in particular need to be assessed. The base case had fracture porosity of about 60%. We decided to decrease the fracture porosity to 30 % that simply means fractures occupied 30 % of total porosity of the reservoir. The

result for pressure, partial pressure and gas saturation was plotted in figure 3.2.5. Equivalently, for temperature and gas saturation in figure 3.2.6

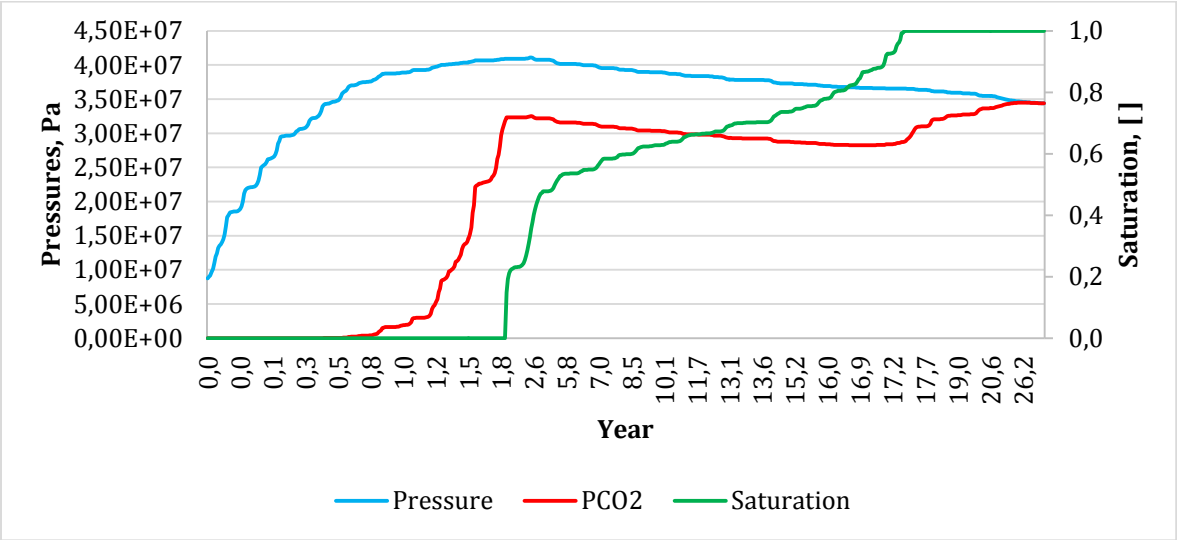

Figure 3.2.5: Pressure, partial pressure and saturation profiles at production [Ø= 30 %].

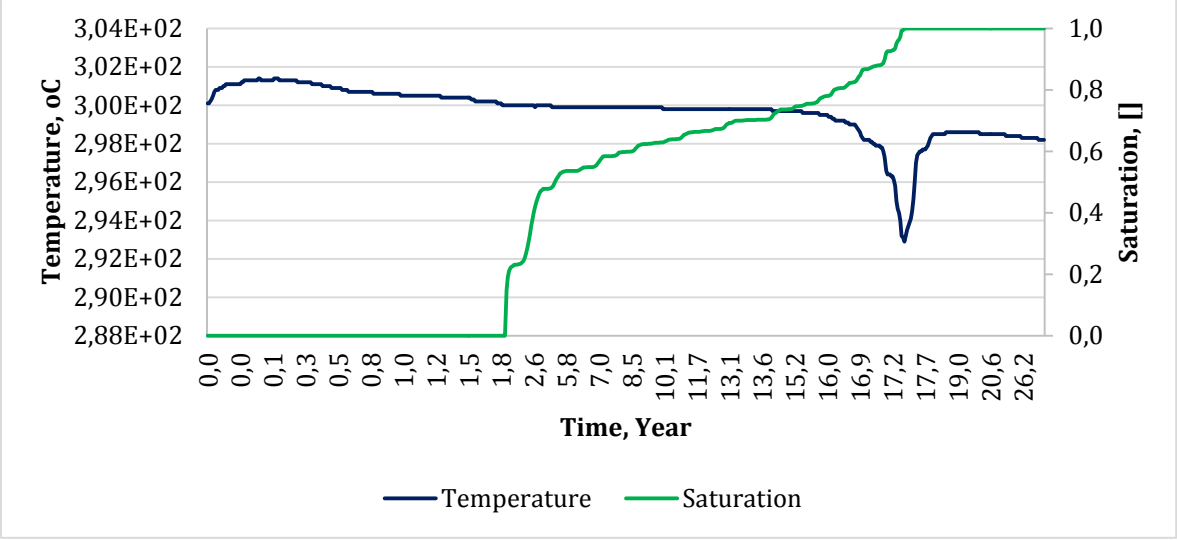

Figure 3.2.6 Temperature & saturation profile at production [Ø = 30 %].

The result showed longer time it took for the system to attain the steady state than the base case, with the quasi- steady state achieved at seventeen years. It also took almost the same period for the reservoir to be fully gas saturated. Same trend was also observed for the time taken for CO_2 to reach the production block, for which it took one and two years for 60 % and 30% fracture porosity respectively. In order to have a clear view of the fracture the impact on energy production, we had to increase the porosity above the base

case. Figure 3.2.7 and 3.2.8 shows the results obtained from the increasing of porosity to 70 %.

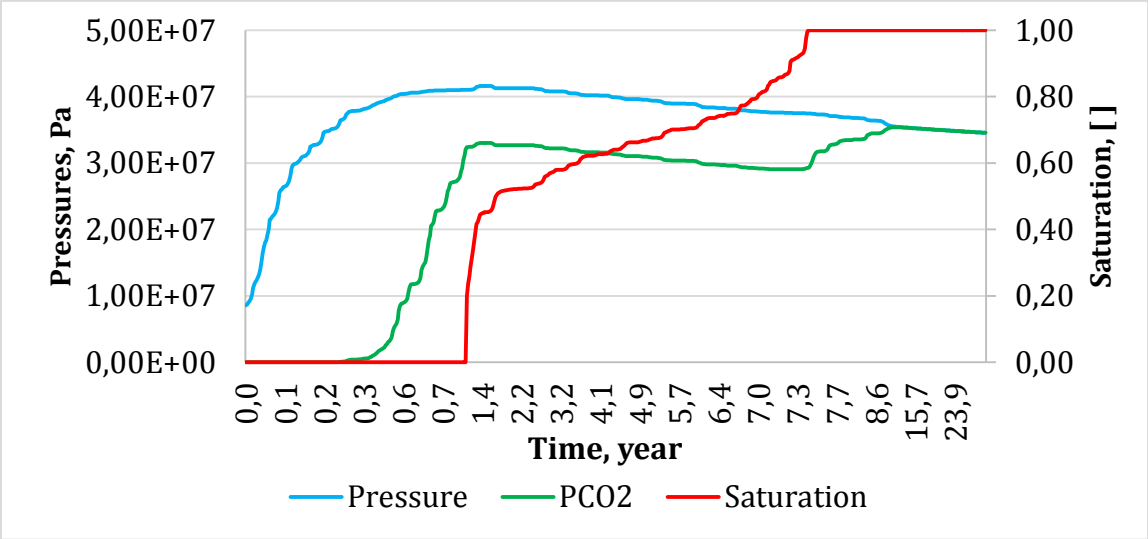

Figure 3.2.7: Pressure, partial pressure and saturation profiles at production [Ø= 70 %].

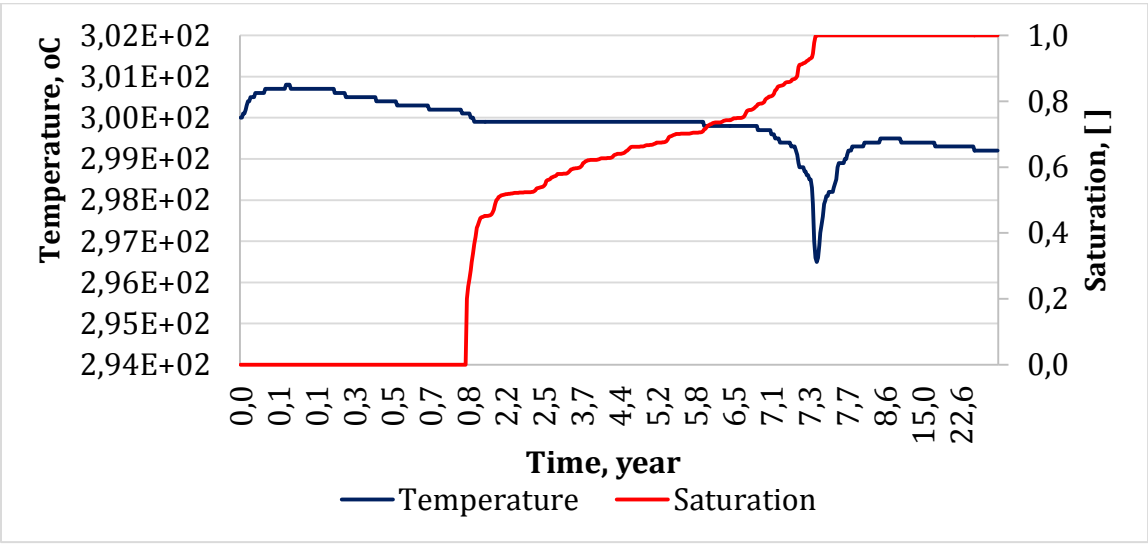

Figure 3.2.8: Temperature & saturation profile at production [Ø = 70 %].

The result shows lowest time for acquiring the quasi-steady state compare to the base case and 30%. The 30 % porosity showed the best trend, favorable for longer production of high enthalpy. The result also for 70% showed, the earliest time it took for CO_2 to reach the production block for the all three cases. The overall result of all the three cases is presented in diagram 3.2.9 showing the enthalpy flow at production. 30 % had longest time with high enthalpy production, while 70% possessed the least value. The time for

which the enthalpy start dropping to the least value for all three case, is equivalent to the time for which the gas saturation becomes one, thus the reservoir becomes fully gas saturated. In this case also, 30 % possessed the longest time, followed by 50 % (base case) and finally 70% fracture porosity.

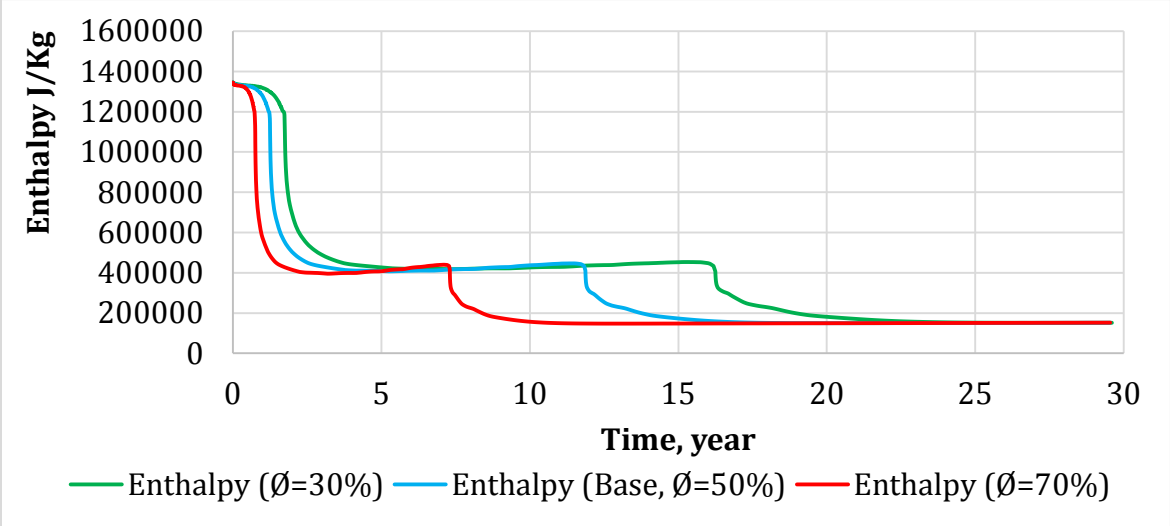

Figure 3.2.9: Flow enthalpy at production block for porosity.

3.2.2.2 Effect of flow rate

We increased the fluid flow rate from 5 kg/s to 7 kg/s. We observed that, the time for which the system reach the steady state decreased from almost fourteen years to nine years. The phenomena could be also observed with CO_2 saturation at production. The time it took for production point to be fully saturated with CO_2 was also shortened, from twelve years to almost eight years.

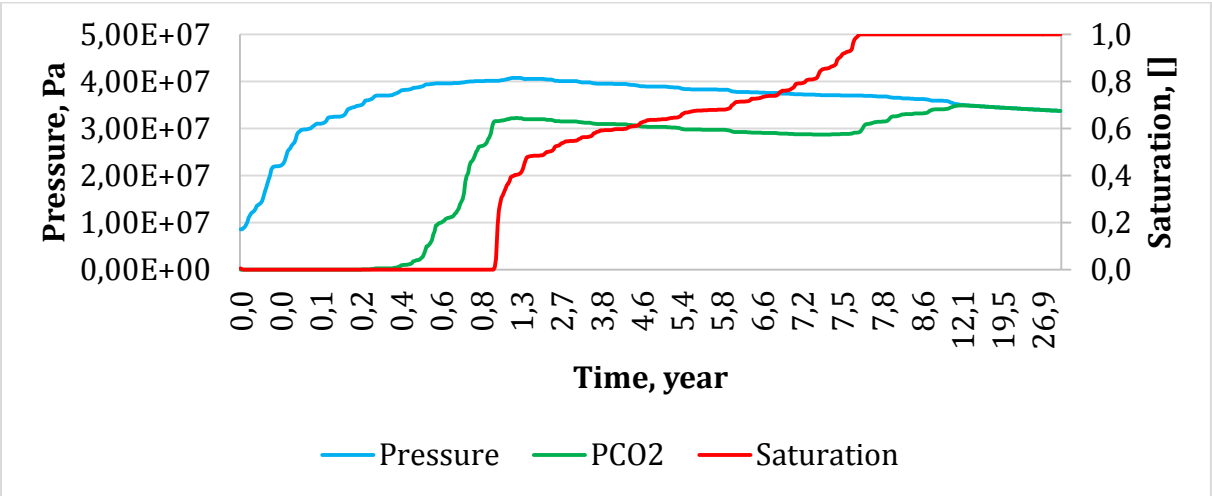

Figure 3.3.0: Effect of 7.0 kg/s flow rate on pressure, partial pressure and saturation profiles at production for.

The same trend was also observed for temperature and saturation profile as shown in figure 3.3.1. The drop in temperature was also achieved at eight years, when the gas saturation switched to one, then it becomes lower after that time.

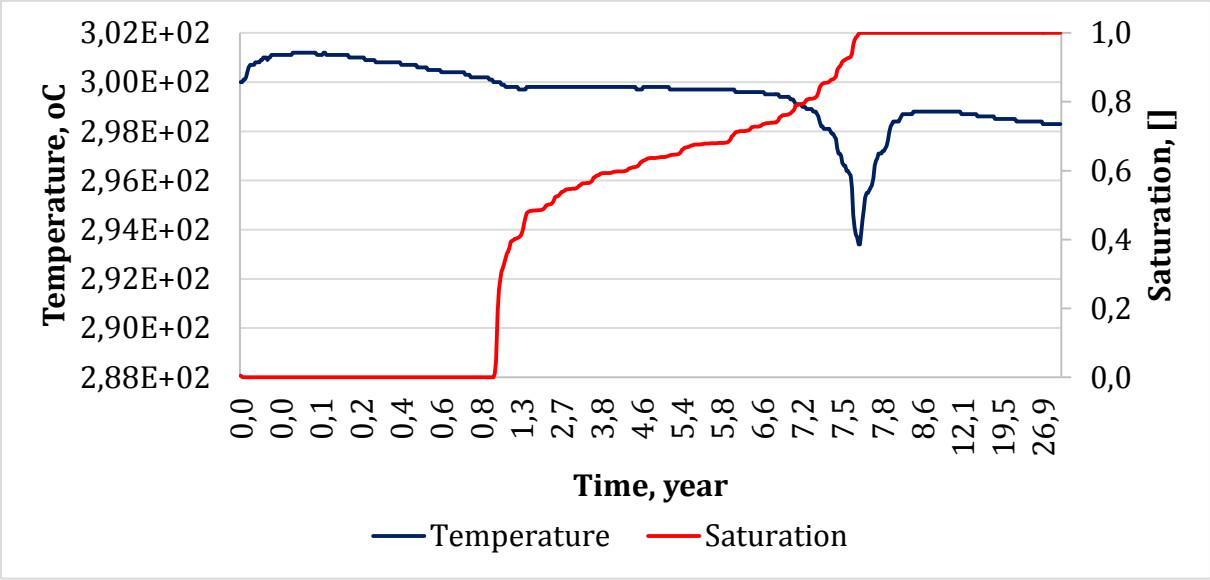

Figure 3.3.1: Effect of 7.0 kg/s injection mass rate on temperature & saturation profile at production.

The flow was then decreased to 2.5 Kg/s. We observed that the system took longest time compared to the base case and when flow rates was 7 kg/s to reach the quasi-steady state, with the quasi-steady state achieved at almost twenty- eight years. At the same time CO_2 took more than two years to reach the production block. The CO_2 saturation also follows the same trend, reaching the maximum value of one after twenty-six years. The three flow rate cases were summarized in figure 3.3.3, which again represent enthalpy produced at production. Enthalpy production was direct proportional to time it took for the system to be fully saturated with CO_2. The longer it took the system to be fully gas saturated, the longer it also took for the fluid with higher enthalpy value to be produced. Figure 3.3.3 shows fluid flow rate of 2.5 Kg/s had longest time to reach gas saturation of one, therefore, longer time for higher enthalpy production. Followed by the flow rate of the base case 5 Kg/s and finally, 7 Kg/s. But the highest cumulative energy produced showed opposite tendencies, with the highest energy produced recorded from the highest flow rate (7 kg/s), then followed by the base case (5 kg/s) and the least value with (2.5 kg/s). These tendencies are further discussed in section 5.2

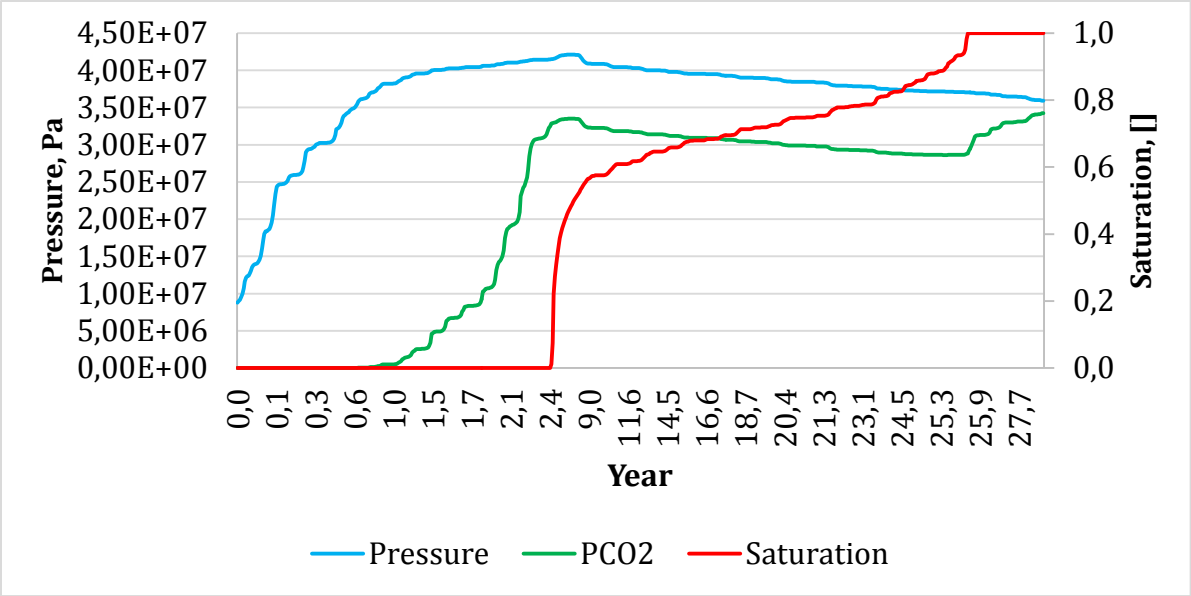

Figure 3.3.2: Effect of 2.5 kg/s injection mass rate on pressure, partial pressure and saturation profiles at production.

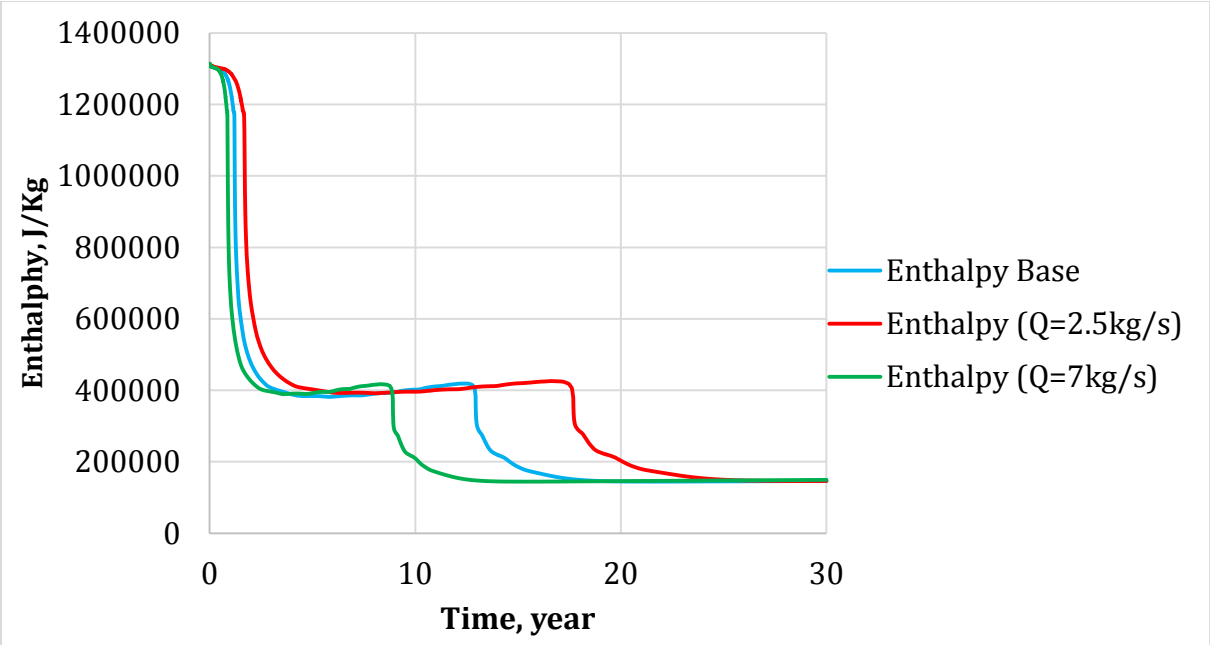

Figure 3.3.3 Flow enthalpy at production block for flow rates.

3.2.2.3 Effect of fracture spacing and permeability

Fracture spacing and permeability were also other parameters to be assessed. The pressure, temperature and saturation profile observed were of the same trends for almost all rest parameters as shown in figure 3.3.4 and 3.3.5 below:

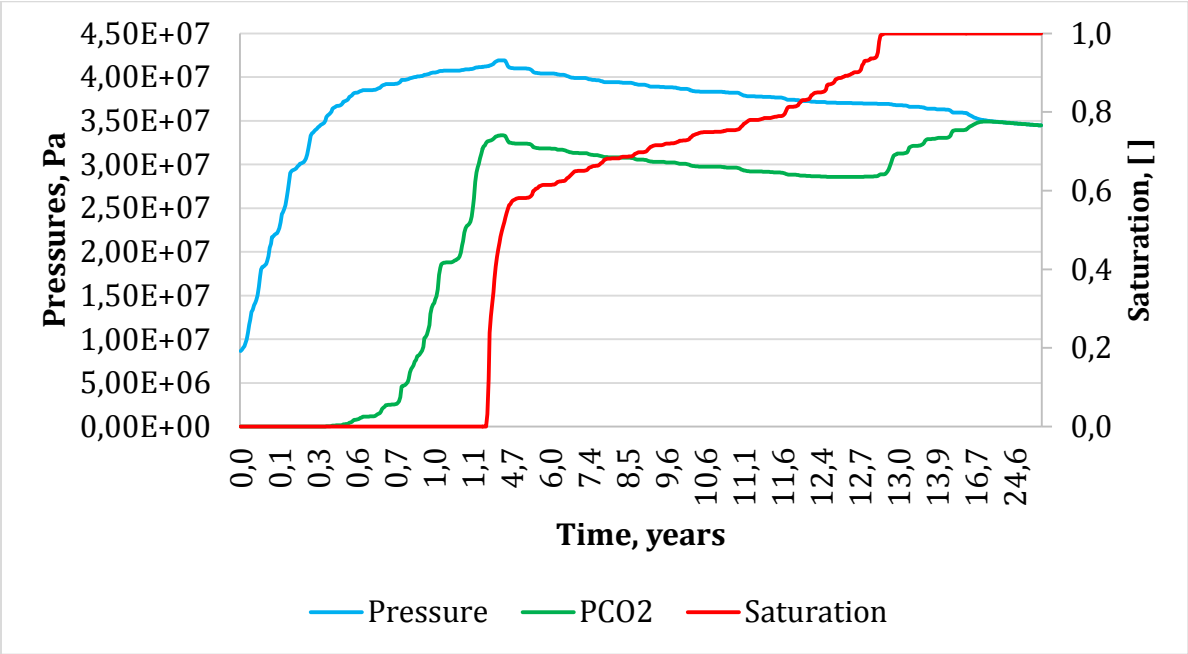

Figure 3.3.4: Effect of permeability on pressure, partial pressure and saturation profiles at production.

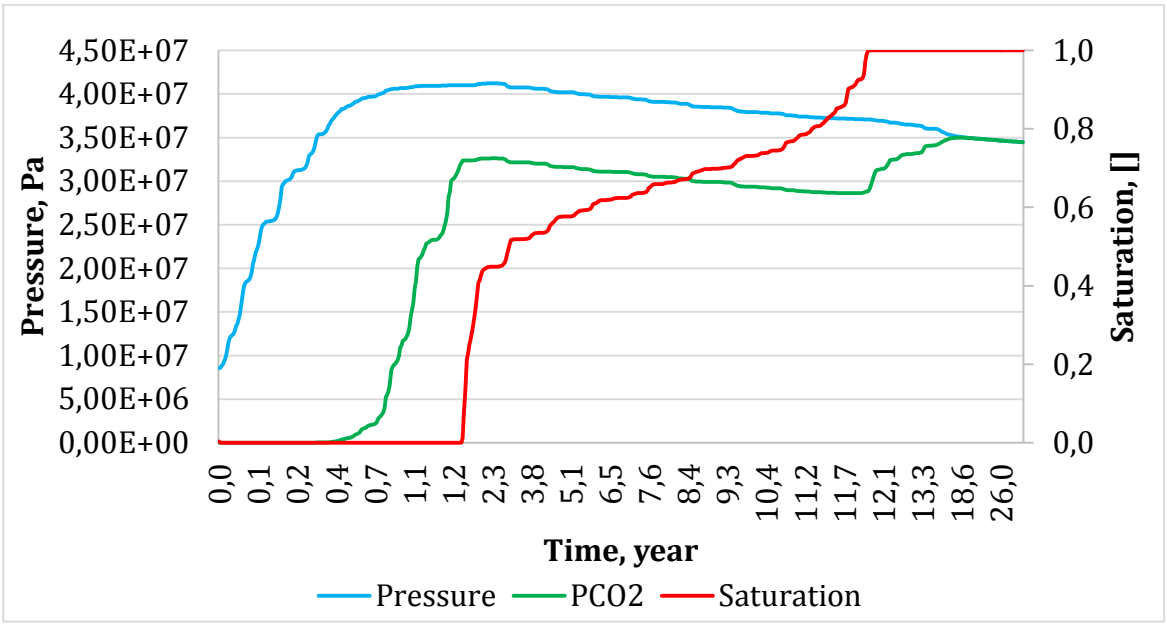

Figure 3.3.5: Effect of fracture spacing (D=30m) on pressure, partial pressure and saturation profiles at production.

Both permeability and fracture spacing showed minor impact or almost no change for the time it took for the reservoir to be fully saturated with gas. Same result was also observed with time for steady state attainting. Showing little or no difference when the values were dropped or increased from the base case. The variation of these parameters did not affect

the time it took CO_2 to reach the production block; the time was almost constant compared to the base value. For better overview, the flow enthalpies for both parameters are presented in figure 3.3.6 and 3.3.7, with all cases showing the same profile as the base case. Figure 3.3.6 shows the flow enthalpy obtained by varying the fracture spacing, with almost the same values for all the three cases, but the difference could be seen on the cumulative energy produced presented in section 5.3, while fracture permeability, the value was also dropped to 0.075 D and increased to 0.15 D from the base case, they also showed almost the same tendency as shown in figure 3.3.7, the little difference could be observed on the cumulative energy presented in section 5.3 too.

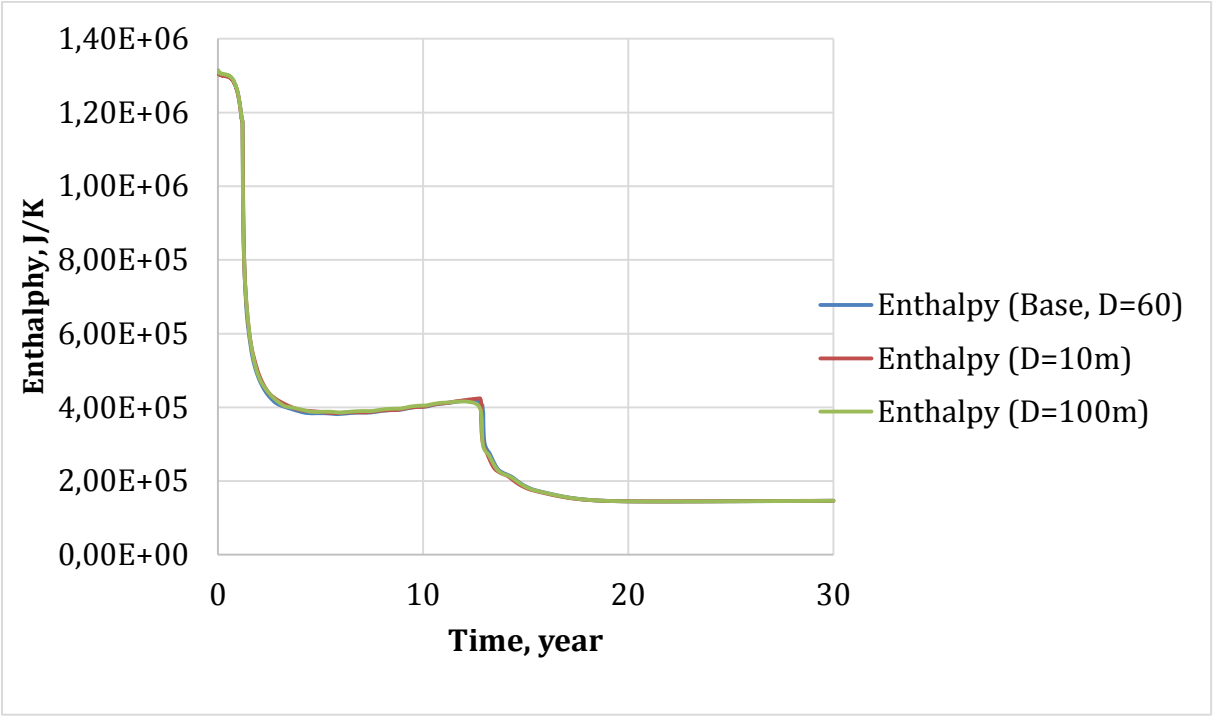

Figure 3.3.6 Flow enthalpy at production block for fracture spacing.

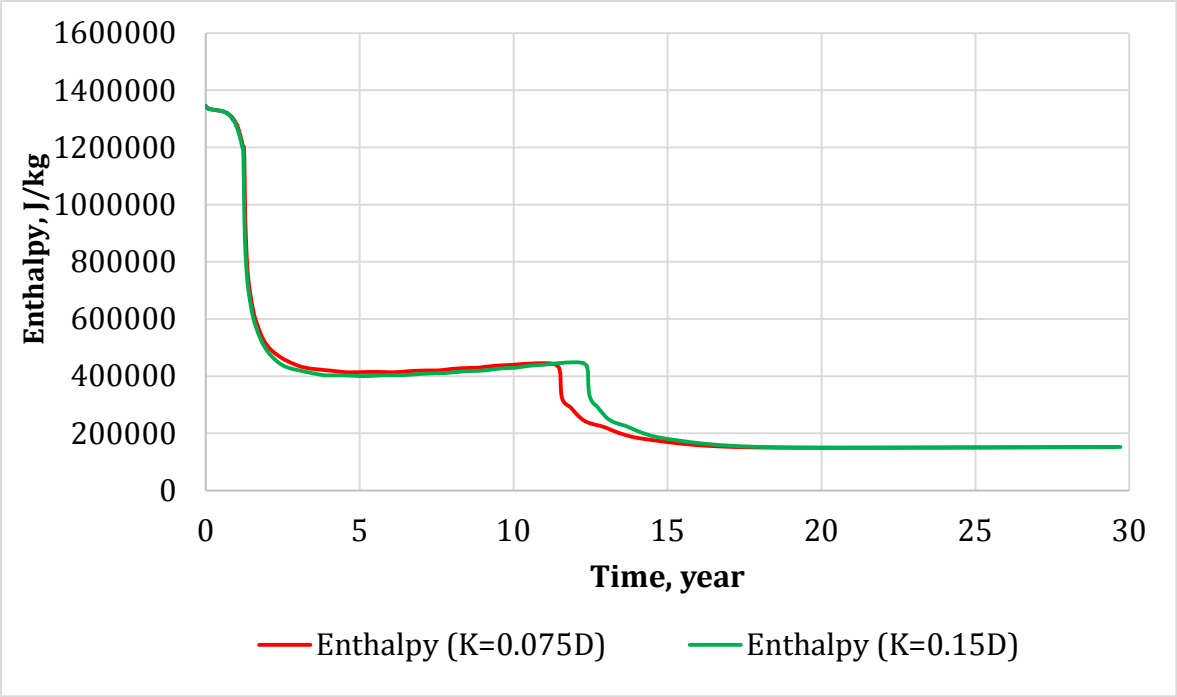

Figure 3.3.7 Flow enthalpy at production block for fracture permeability.

4 Radial heat transfer mechanisms in the wellbore simulation

This chapter presents the modeling for overall heat transfer coefficient and heat-loss calculations across the production tubing to well formation. The analysis is based on the classical paper published by (Willhite, 1967). The idea of this analysis is as the fluid well flowing to surface, we will try to analyze the heat loss in the presence of insulator and in the absence of insulator for various cement heat conductivity.

As shown in figure 4.1.1, steam (water/CO_2) flows from reservoir to surface or injected downward to the reservoir, there exist heat transfer mechanisms, which were described in section 2.5, and hence the fluid flow losses heat energy to the surrounding formation. This heat loss may result in the change of thermodynamic states and hence phase change with subsequent reduction in steam quality and enthalpy may occur.

4.1 Assumption

As indicated by (Willhite, 1967), heat loss attains a quasi-steady state at which the rate of heat loss is a monotonically decrease with as time increases. However, for simplicity, in this thesis the assumptions for the modeling are:

1. Steady state heat transfer takes place in and around the wellbore, which assumes that time independent constant heat rate.
2. The heat diffusivity and the conductivity of the well components are constant.
3. Production fluid is flowing from the hydrothermal fluid obtained at the production well from TOUGH2 simulator section 3.1
4. Forced convection inside tubing is neglected, gives the temperature of the fluid is equal to the temperature of the tubing.
5. Pressure and phase behavior of annulus fluid is excluded.

Packer fluid is seawater and will not be connected with the fluid temperature at tailpipe due to the production packer seals completely.

Consider a typical well construction, which contains tubing, annular completion fluid, casing, cement and formation. Figure 4.1.2a and 4.1.2b illustrate the horizontal and the vertical cross-sections of the overburden part of production well. As fluid flows along the

tubing, as mentioned earlier, the heat transfer occurs through the three mechanisms from well to the undisturbed formation temperature.

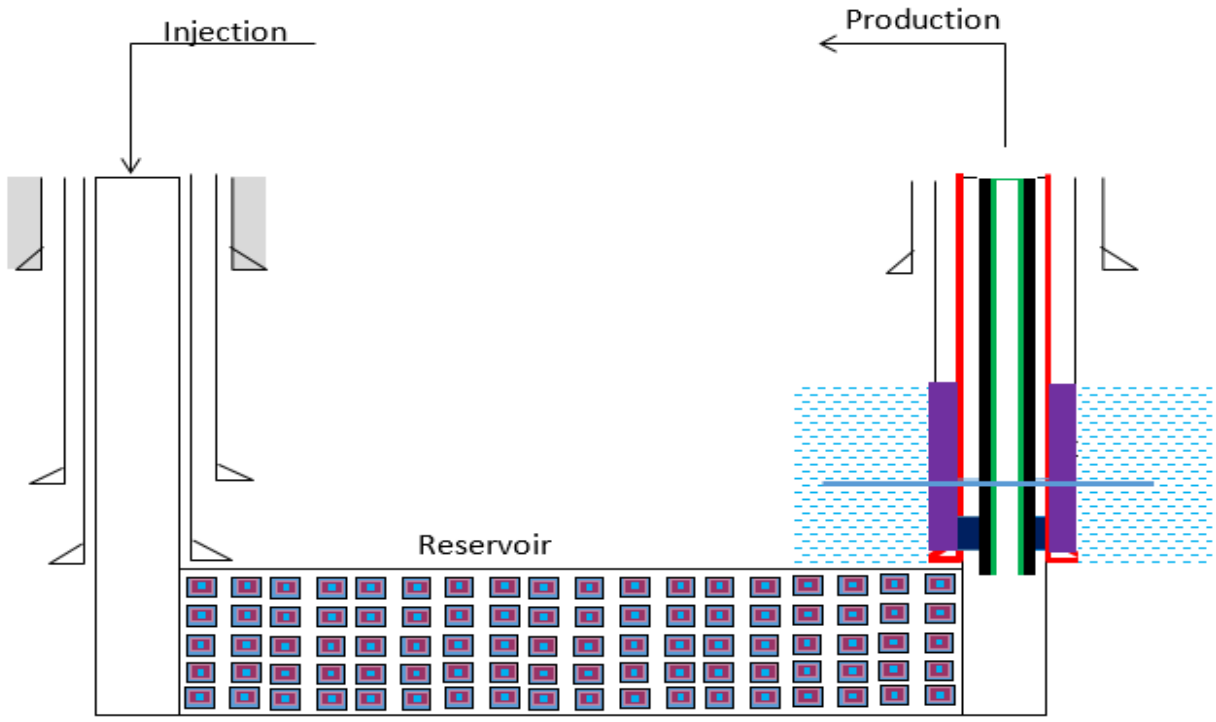

Figure 4.1.1: Illustration of injection well, reservoir and production well

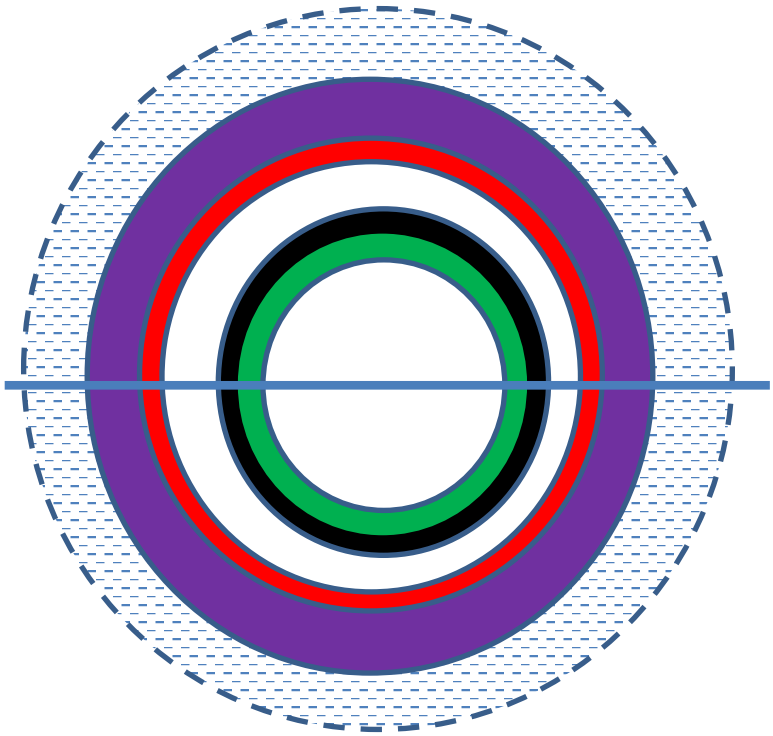

Figure 4.1.2a: Illustration of the horizontal cross-section of the well

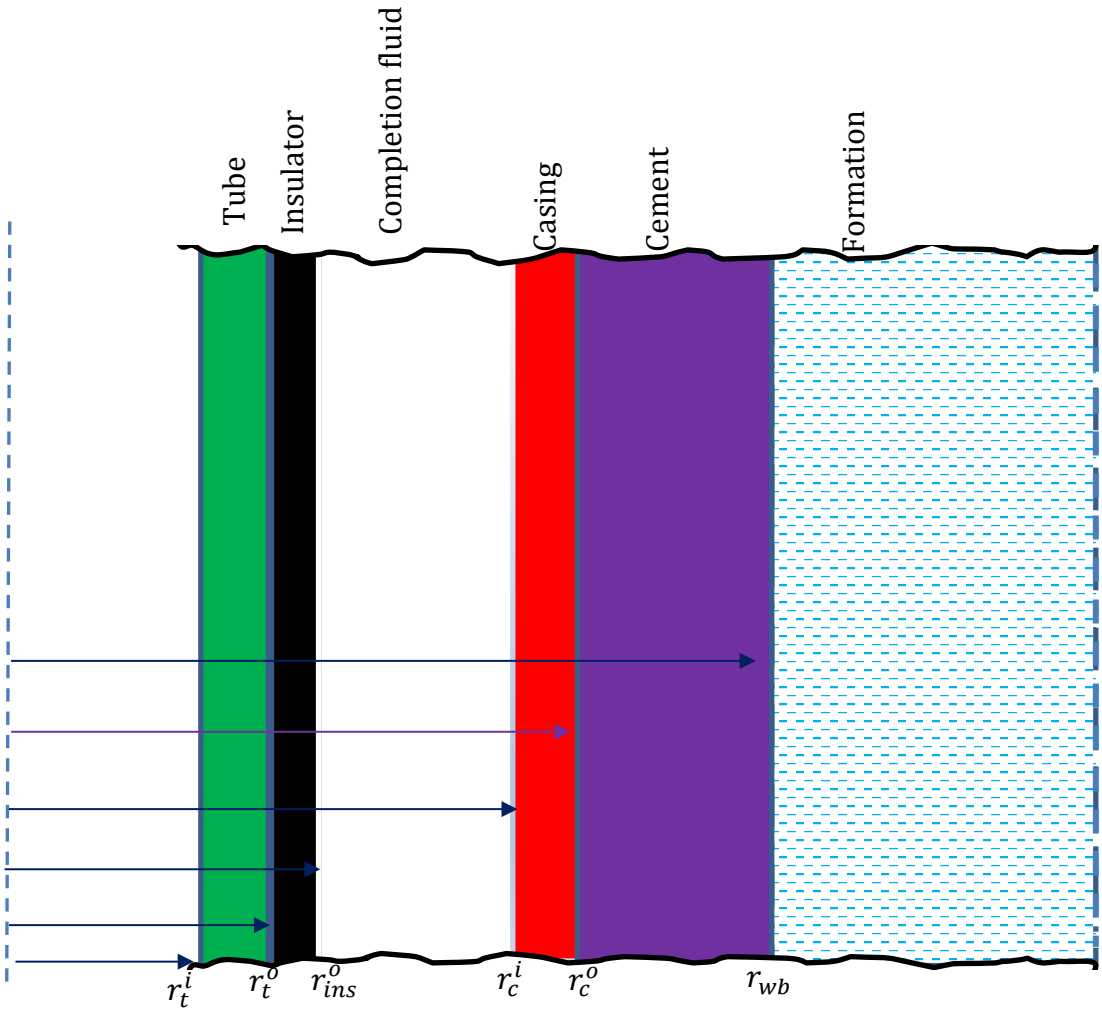

Figure 4.1.2b: Illustration of the vertical cross-section of the well

4.2 Heat transfer modeling

The rate of heat flow through a wellbore is proportional to the temperature difference between the fluid and formation, and the cross-sectional area perpendicular to the direction of heat flow. The proportionality factor, called the over-all heat transfer coefficient, represents the net resistance of the flowing fluid, tubing, insulating material, casing annulus completion fluid, casing wall and cement sheath to the flow of heat.

The three-heat transfer mechanisms presented in equation 2.9 – 3.0 are independent. The effective heat flow in the completion fluid (Annulus fluid) is the resulting sum of these. According to (Willhite, 1967), the heat transfer rate in the annulus is described in terms

of heat transfer coefficient, h_c, (which is the combined effect of natural convection and conduction) and radiation, hr. Since the insulator outer radius is in contact with the completion fluid, using the surface area and the temperature difference between the inner casing and the insulator, Q can be given as (Willhite, 1967):

$$Q = 2\pi r_{ins}^{o}(h_c + h_r)(T_{ins}^{o} - T_c^{i})\Delta L \qquad 4.1$$

The heat transfer rate between the flowing fluid in the tube and the inside wall the tubing is given as:

$$Q = 2\pi r_t^{i} h_f (T_f - T_t^{i})\Delta L \qquad 4.2$$

Where, h_f is the film heat transfer coefficient on the inside surface of the tube. The temperature difference $(T_f - T_t^{i})$ is the temperature between fluid flowing and the temperature at the inner wall.

Heat transfer through conduction in each components is given as (Willhite, 1967):

Tubing

$$Q = \frac{2\pi k_t (T_t^{i} - T_t^{o})\Delta L}{\ln(\frac{r_t^{o}}{r_t^{i}})} \qquad 4.3$$

Insulator

$$Q = \frac{2\pi k_{ins} (T_t^{o} - T_{ins}^{o})\Delta L}{\ln(\frac{r_{ins}^{o}}{r_t^{o}})} \qquad 4.4$$

Casing

$$Q = \frac{2\pi k_{csg} (T_c^{i} - T_c^{o})\Delta L}{\ln(\frac{r_c^{o}}{r_c^{i}})} \qquad 4.5$$

Cément

$$Q = \frac{2\pi k_{cem} (T_c^{o} - T_{wb})\Delta L}{\ln(\frac{r_{wb}}{r_c^{o}})} \qquad 4.6$$

The temperature difference between the well and the formation can be written as the sum of the temperature difference across each components of figure 4.1.2 given as Equation 4.7:

$$T_f - T_{wb} = (T_f - T_t^i) + (T_t^i - T_t^o) + (T_t^o - T_{ins}^o) + (T_{ins}^o - T_c^i) + (T_c^i - T_c^o) + (T_c^o - T_{wb}) \quad 4.7$$

Inserting the temperature differences obtained from Eq. 4.1- 4.6 into Eq. 4.7, we get:

$$T_f - T_{wb} = \frac{Q}{2\pi\Delta L}\left[\frac{r_t^o}{r_t^i h_f} + \frac{r_t^o \ln(\frac{r_t^o}{r_t^i})}{k_t} + \frac{r_t^o \ln(\frac{r_{ins}^o}{r_t^o})}{k_{ins}} + \frac{r_t^o}{r_{ins}^o(h_c + h_r)} + \frac{r_t^o \ln(\frac{r_c^o}{r_c^i})}{k_{csg}} + \frac{r_t^o \ln(\frac{r_{wb}}{r_c^o})}{k_{cem}}\right] \quad 4.8$$

Assuming that a hot reservoir fluid, which is obtained from Tough2, is flowing through the production tube. Using the temperature difference between the flowing fluid (T_f) and the formation, (T_{wb}) at the formation/cement interface and the outer surface area of the tubing, the steady state heat transfer rate can be given by equation 4.7 as (Willhite, 1967):

$$Q = 2\pi r_t^o U(T_f - T_{wb})\Delta L \quad 4.9$$

Using 4.8 and Eq. 4.9, the overall heat transfer coefficient, which accounts for the net-resistance to the heat flow through the components of the well structure shown on Figure 5.1.2 is given as:

$$\frac{1}{U} = \frac{r_t^o}{r_t^i h_f} + \frac{r_t^o \ln(\frac{r_t^o}{r_t^i})}{k_t} + \frac{r_t^o \ln(\frac{r_{ins}^o}{r_t^o})}{k_{ins}} + \frac{r_t^o}{r_{ins}^o(h_c+h_r)} + \frac{r_t^o \ln(\frac{r_c^o}{r_c^i})}{k_{csg}} + \frac{r_t^o \ln(\frac{r_{wb}}{r_c^o})}{k_{cem}} \quad 5.0$$

4.3 Simulation setup

Table 7 shows the well, fluid and properties used for the simulation. Equations 4.8, 4.9 and 5.0 were used to model heat loss along the horizontal components of the well. As we

mentioned earlier, for the first case, as the object is to assess the impact insulation thickness on heat loss, then we kept the heat conductivity constant at 0.025 W/ht and we varied the insulation thickness from 0.005 to 0.15in. In the same manner, for the second, we also assessed the impact of insulation thermal conductivity on horizontal heat loss. We varied the thermal conductivity and kept all other parameters constant.

Table 7: Pipe simulation input parameters

Parameters	Value
r_{to} – tubing outside radius	0,2291658
r_{ci} – casing inside radius	0,3593736
r_{ti} – tubing inside radius	0,2038325
r_{co} – casing outside radius	0,4010401
r_{ins} – insulation radius	0,3791658
r_{wb} - wellbore radius	0,5208313
h_f – liquid convective heat transfer coefficient,	500
k_t – conductivity of tubing material	25
h_c – convective heat transfer coefficient	100
k_c – conductivity of casing material	25
h_r – radiative heat transfer coefficient	2
k_{cem} – conductivity of settled cement	
k_{ins}- thermal conductivity of insulation	0,025
t-Insulation thickness	0,15

4.4 Simulation results

4.4.1 Effect of insulator's thickness

Figure 4.1.3 shows heat loss of the well system without insulating material plotted as function cement 's thermal conductivity. We can observe that the amount of heat loss increases with increasing cement's thermal conductivity. In figure 4.1.4 we varied the thickness of insulating materials, the result shows that cement's thermal conductivity plays no role on heat insulating, with the insulator's thickness taking over.

The thickest insulator preserves most heat, and the thinner insulating materials losing more heat. However the loss is insignificant. As illustrated in Figure 4.1.4, as the insulation thickness increase from 0.015ft to 0.15ft, the heat loss reduced by an average of 300 BTU/hr-ft for any thermal conductivity of cement.

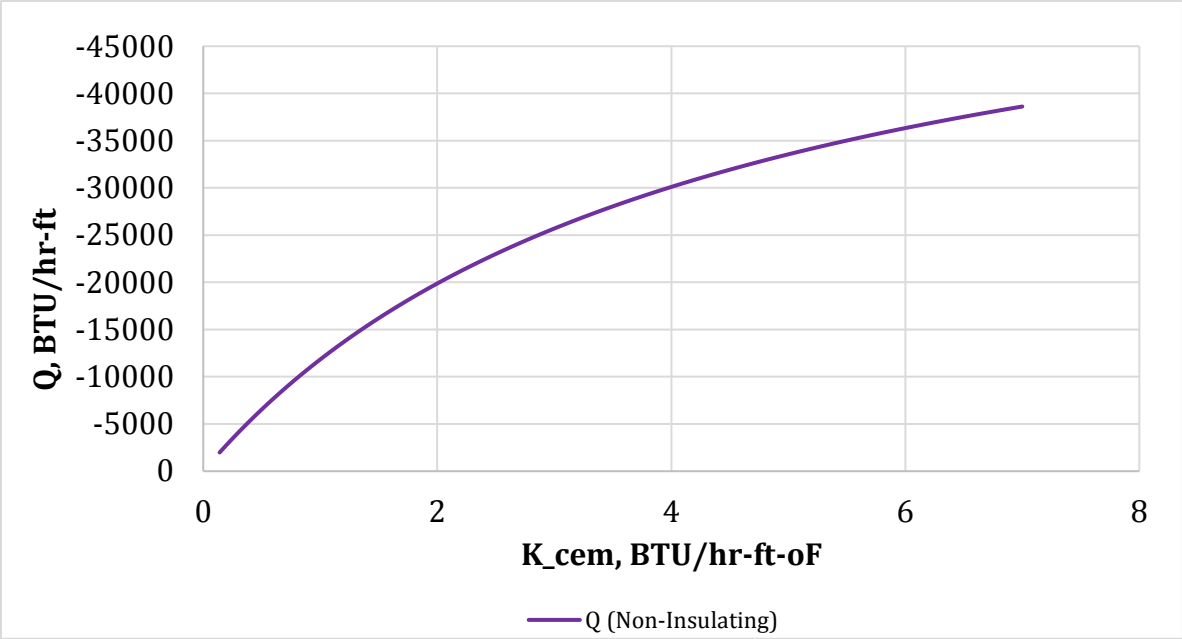

Figure 4.1.3: Heat loss for a non-insulating well

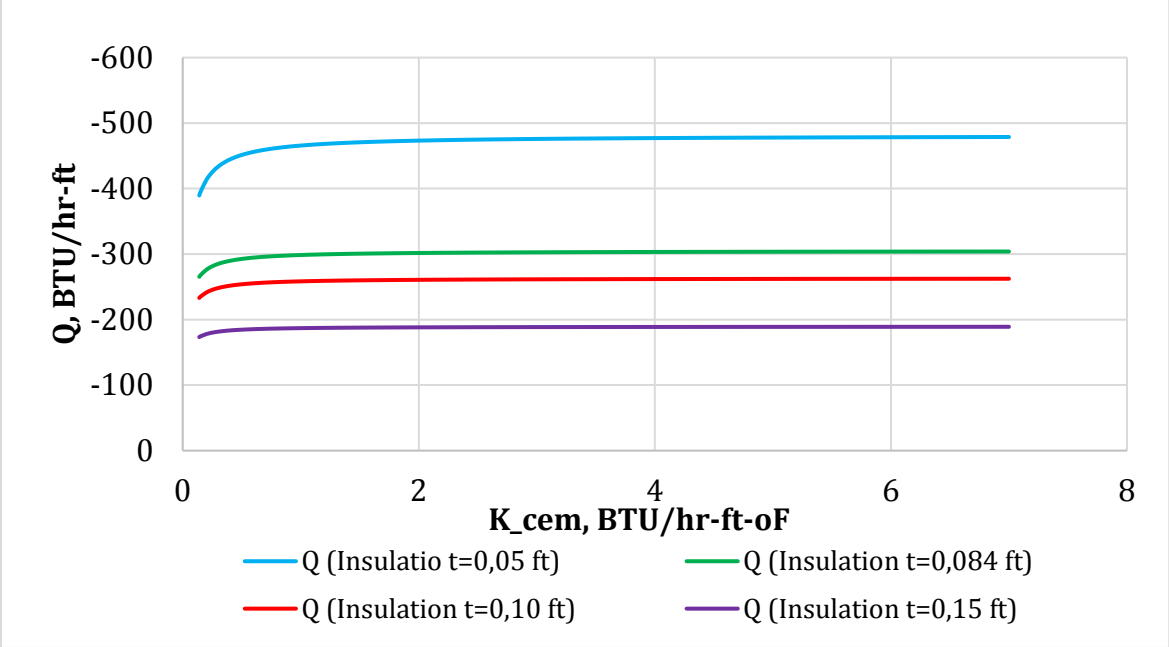

Figure 4.1.4: Effect of insulation thickness on well heat loss.

4.4.1 Effect of insulator's thermal conductivity

We extended our research as mentioned, by varying different insulating materials in order to assess the impact of material's thermal conductivity. The result shows that materials with lower thermal conductivity preserve more heat than those with higher conductivity as shown in figure 4.1.5

We mentioned earlier that, the heat transfer or loss through all layers along the horizontal line of the well, could be represented by the over – all heat coefficient factor. We plotted the heat coefficient factor as function of insulator's thickness and thermal conductivity. The result showed the same results we obtained for the heat loss simulation cases. Therefore, without the insulator the coefficient increased significantly as cement thermal conductivity increased as well. When we implemented the insulator's thickness and thermal conductivity, the cement thermal conductivity had no influence on the variation of the heat coefficient values. The result results are enclosed in appendix D.

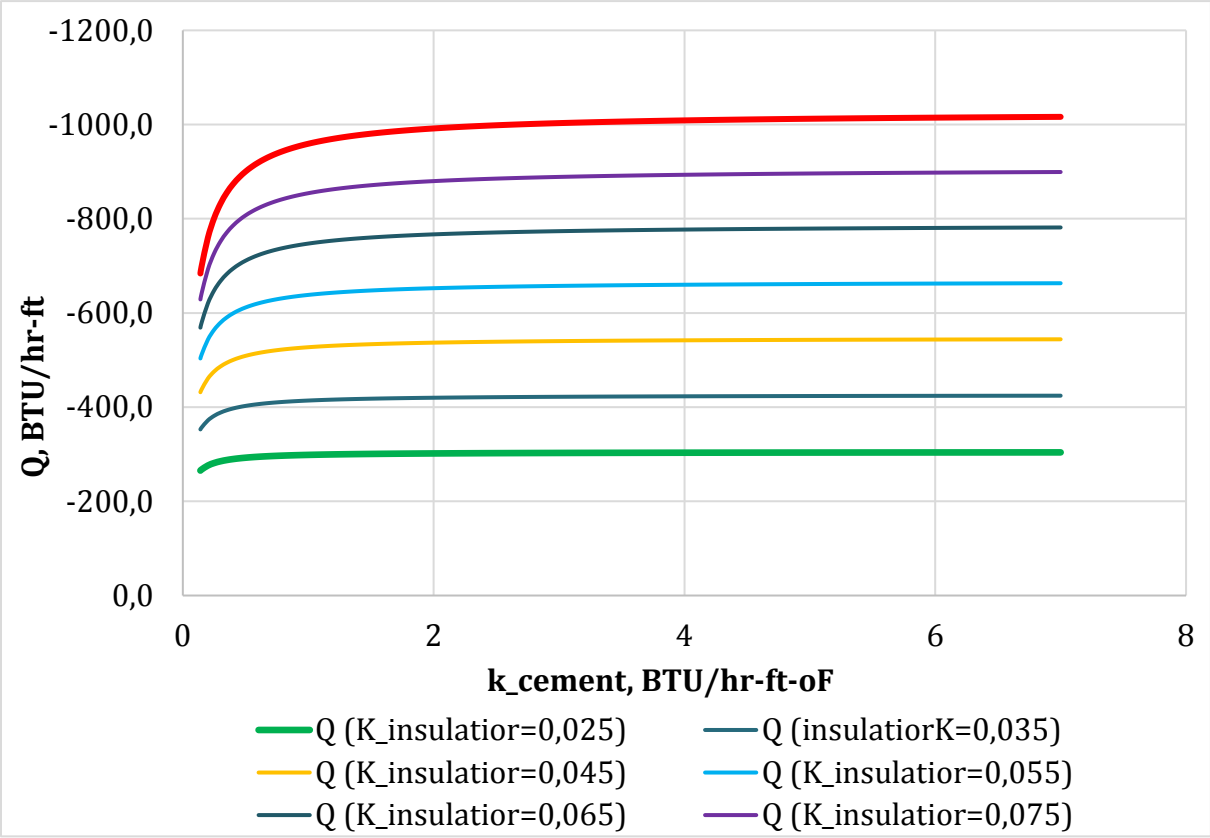

Figure 4.1.5: Effect of thermal insulator 's thermal conductivity

5 Summary and discussion

5.1 Geothermal reservoir simulations

The engineering designed processes are found everywhere and touch every aspect of our lives, with main objective to create functional products and processes. These processes are applied in almost all sub-disciplines of engineering, from materials, process, thermal and energy engineering. In this thesis we assessed different variable fractured reservoir properties, which could play a key role for designing of an optimal fractured non-condensable gas geothermal reservoir. These properties include fluid injection rate, fracture permeability, spacing, and porosity. The sensitivity studies of these reservoir parameters were conducted for both traditional geothermal reservoir using a reservoir simulator TOUGH2 module EOS1, and for non-condensable reservoir by using module EOS2. CO_2 and water were chosen as working fluid for both non-condensable and traditional reservoir respectively.

The results showed that, all these parameters could affect reservoir temperature and pressure distribution during production, which in turn affected the heat mined at early stage of production for a traditional reservoir. For the case of a traditional reservoir, as the heat productions continued, parameters impacts on heat production became minor, with almost no difference in the amount of heat produced after some time. While for a non-condensable reservoir, fluid injection rate and fracture porosity showed positive impacts on heat mined, for which the amount of heat produced increased with increasing injection rate and decreasing fracture porosity. All other varied parameters had no impacts on pressure and temperature distribution in a non-condensable reservoir for the chosen time of simulation. This is so because, when CO_2 was injected into the reservoir it reduced the flash point pressure of the water-CO_2 mixture and improved boiling. In turn the boiling induced the formation of gas, which could be observed by the increment of gas saturation. Since CO_2 was the most part of the gas saturation, and owing to the fact that it had larger compressibility and expansivity than water, it helped maintaining higher total reservoir pressure. On the other hand, all parameter variations had impact on the time the system took to attain the quasi-steady state and to be fully gas saturated, which in turn affected amount of the amount of energy which was being mined with the exception of flow rate and fracture permeability. For which the amount of heat mined was totally

dependent of speed at which the fluid traveled, than the time it took for the system to achieve the steady-state. Below are the amounts of cumulative energy produced for each case.

5.1.1 Fracture porosity

As mentioned before that, fracture porosity values represent a fraction of total porosity of the system. The base case value was at 50% for both traditional and non-condensable geothermal reservoir. Lowest fracture porosity showed the most positive for energy production for both reservoir types, with the results for non-condensable reservoir presented below. Fracture porosity determines how much contact the injected fluid can have with the hot rock or formation. For which a given fluid volume in lower fracture porosity will have more contact and energy access than the same fluid volume in higher fracture porosity. This is the background behind having higher cumulative energy when the fracture porosity is small as shown in 5.1.1a & 5.1.1b. We also observed that, fracture porosity was also affecting the time for which the system attained the quasi-steady state, which in turn was correlated to the amount of energy produced. For which, the lowest fracture porosity had the longest time to the achievement of the steady –state.

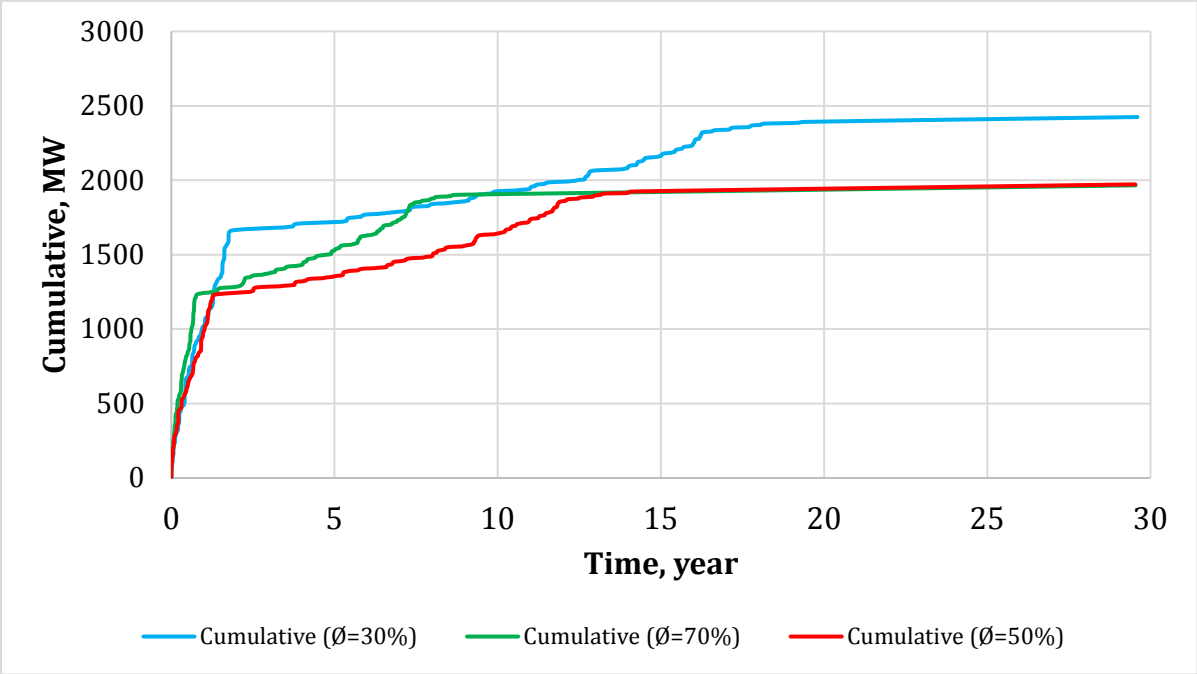

Figure 5.1.1a: Cumulative energy produced for different fracture porosity.

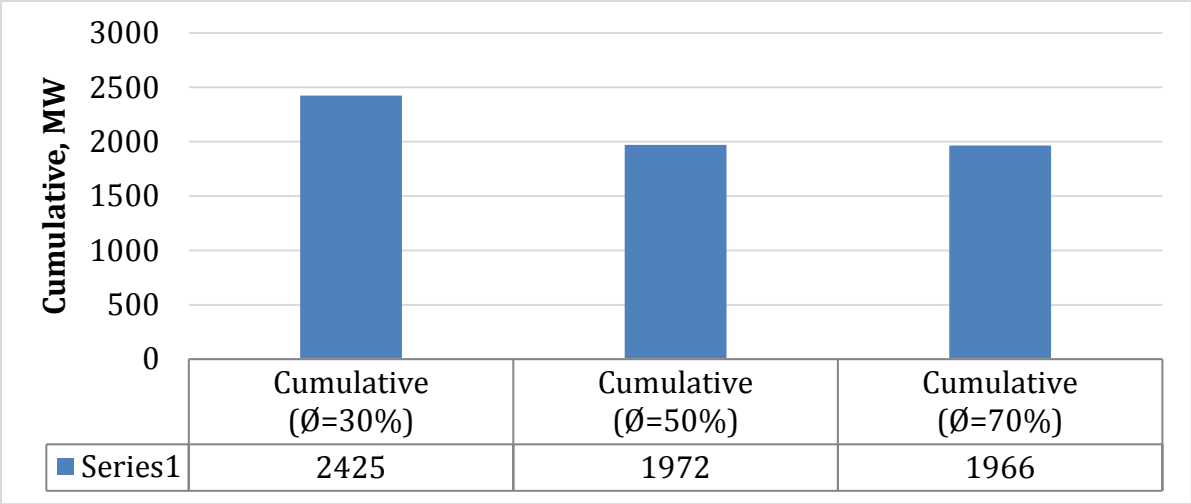

Figure 5.1.1b: Cumulative energy produced for different fracture porosity.

5.1.2 Fluid flow rate

Flow rate is a parameter, which showed a different energy production tendency. This is because it energy production was inversely proportional to the time it took for the system to reach the steady state. In contrast to all other parameters, the energy produced from the flow rate variation showed that the fluid rate had played the main part, for which the highest cumulative was produced with the highest flow rate as shown in figure 5.1.2a & 5.1.3b. At the same time the highest flow rate achieved earliest the steady state. This shows how important is the flow rate for energy production in a geothermal system. In other word, fast production of energy increased the heat sweep efficiency from reservoir.

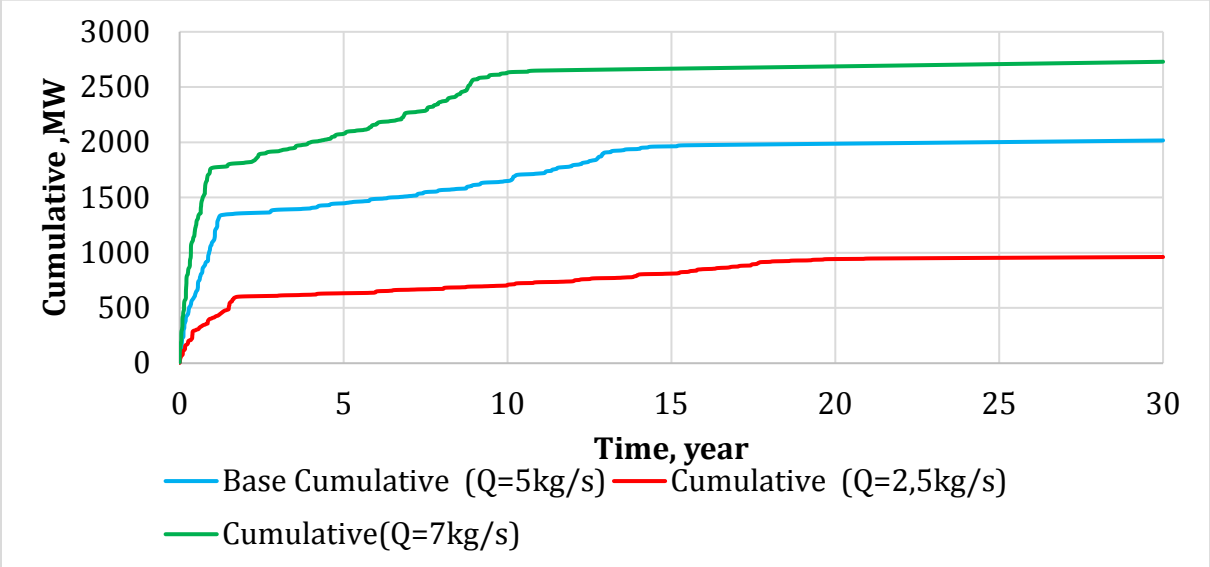

Figure 5.1.2a: Cumulative energy produced for different flow rate.

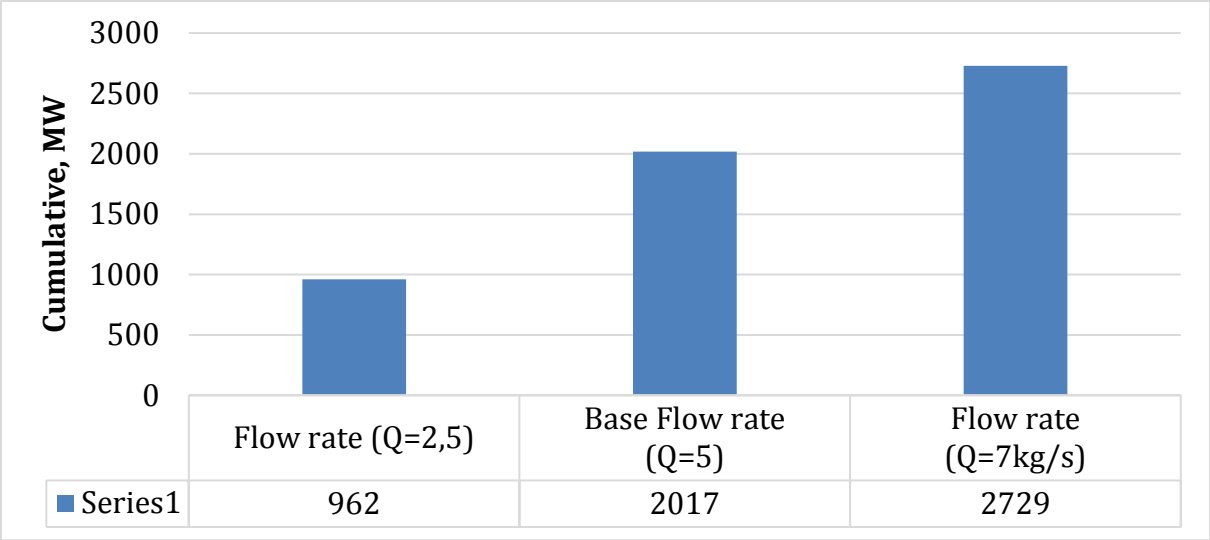

Figure 5.1.2b: Cumulative energy produced for different flow rate.

5.1.3 Fracture spacing

Fracture spacing determines the number of fractures for a reservoir system. In such way that lower number of fractures spacing, have more fracture than higher number of fracture spacing. Fracture spacing showed the same tendency of producing more energy when spacing was low, and lower energy when the spacing was higher. In overall the impact was not as big as in the case of flow rate and fracture porosity. This showed meaningless of having many fracture when other parameters such as flow rate and fracture porosity are not at their optimal values. Figure 5.1.3a & 5.1.3b represent the fracture spacing impacts on cumulative energy produced.

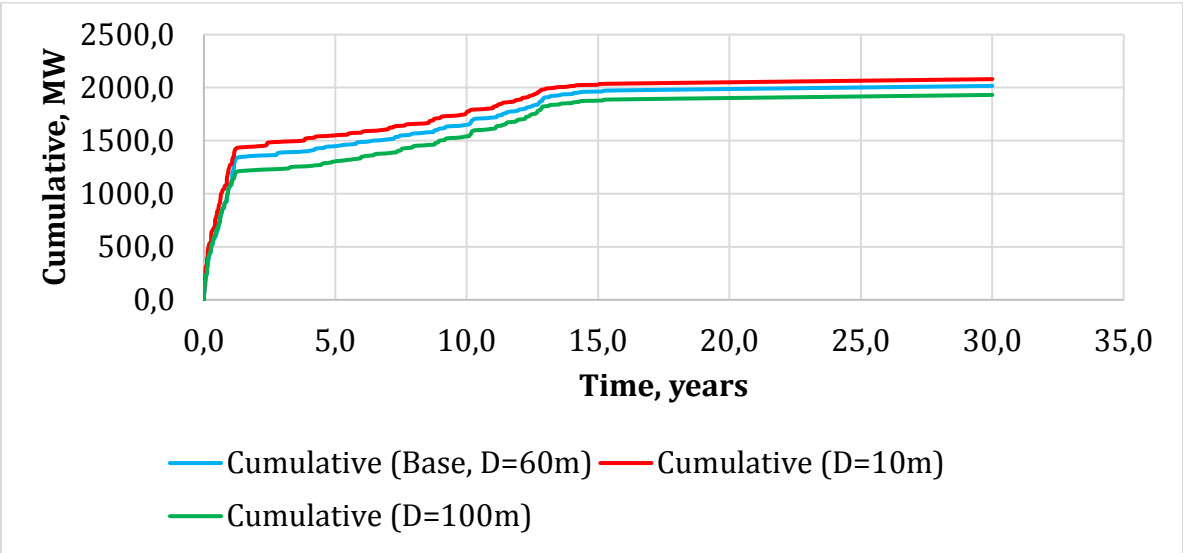

Figure 5.1.3a: Cumulative energy produced for different fracture spacing.

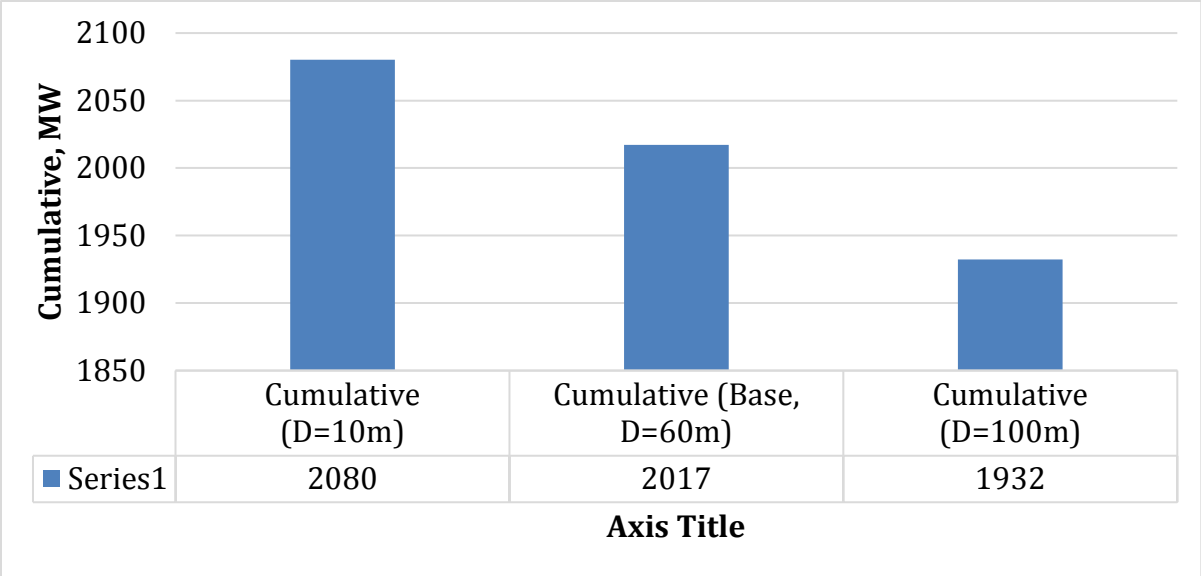

Figure 5.1.3b: Cumulative energy produced for different fracture spacing.

5.1.4 Fracture permeability

Fracture permeability showed also little impacts as fracture spacing. Basically, fracture permeability should have shown the same impact as the flow rate, since both parameters represents how fast the injected fluid move through the porous medium. Owing to the fact that the variation represents a very small difference in terms of flow, then the impact on the energy produced was of little value. Note that, the fracture permeability was correlating with the time the system took to achieve the steady –state just as for flow rate, with longer time for achieving steady state observed with lower permeability.

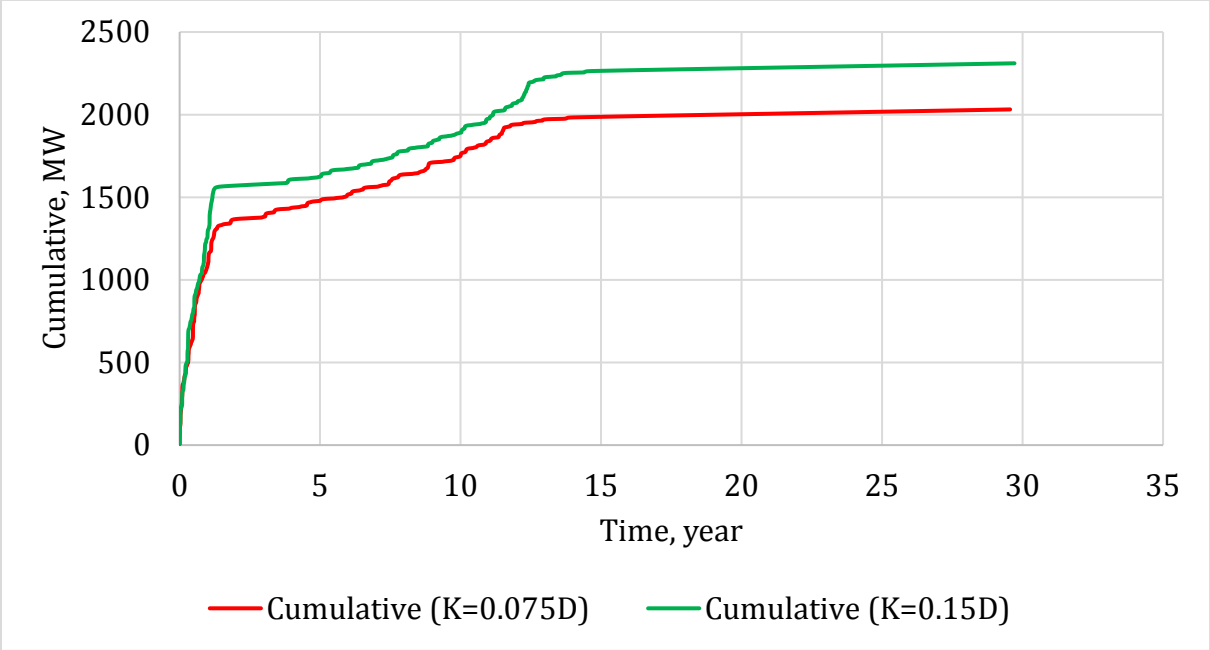

Figure 5.1.4a: Cumulative energy produced for different permeability.

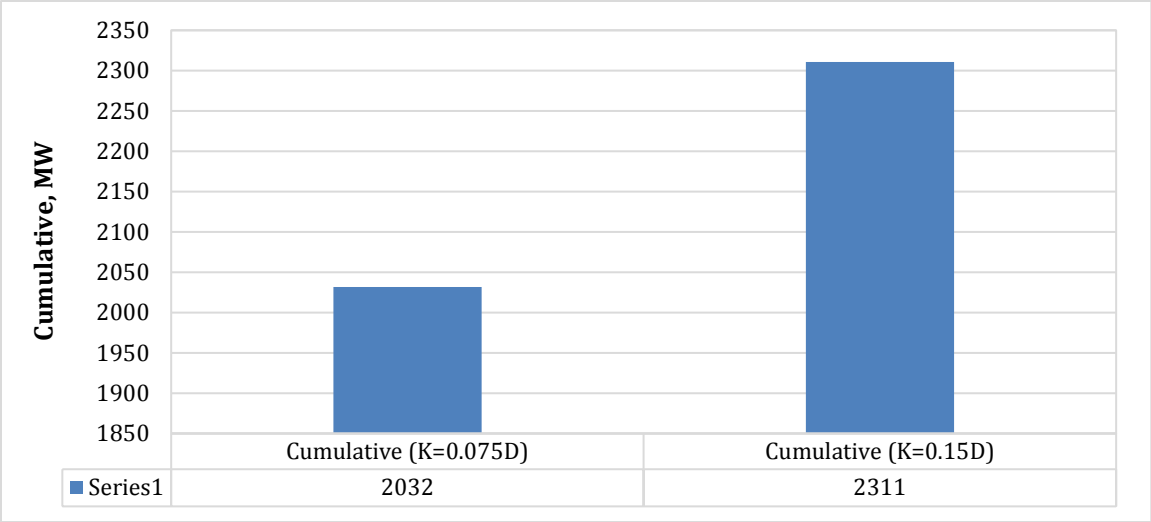

Figure 5.1.4b: Cumulative energy produced for different permeability.

5.2 Heat flow across wellbore

On this part we considered how we could preserve the heat mined during the designing of well, which could be of particular interest for the full system design, with the consideration of optimal heat productivity. The well structure was designed, with Calcium silicate as insulating material for the tubing for the first case and assessed the impact of thickness insulating materials on heat preservation. For the second case, we varied the heat conductivity by choosing different insulating materials and assessed the impact of material heat conductivity on heat preservation. Other heat conductive materials around the wellbore were casing, cement and finally the formation. The models were tested for the well with and without the insulating materials. For the first case, the result showed very high heat loss without insulating material, but choosing the cement with very low heat conductivity could solve this problem. When the thickness of insulating material was varied, the cement heat conductivity seemed to play a minor role on heat preservation, for which thicker insulating material was better in preserving heat. For the second case, lower heat conductivity preserves more heat, and the cement play minor role on preserving heat when low conductive insulating materials were again chosen.

6 Conclusion

From the two simulations we can claim that CO_2 is an enhanced geothermal working fluid. From water simulations, we observed that, even though the parameters were varied to assess their effects on heat recovery, the effect was very little; it did not take that long time before the energy from these varied parameters matched. Therefore, with water as a working, optimizing parameters in order to obtain most energy from a geothermal system functioned only for early stages of production and for a short period of time. On the other, this approach seemed to work very well for CO_2 and the main reason behind this is CO2 higher mobility compared to water. CO_2 has low viscosity which result to larger flow velocities for a given pressure drop (Karsten Pruess, 2006) .

We also observed the importance of high fluid flow rate on the case flow rate and permeability. Therefore, when the fluid flow was considered as a working parameter, then phenomenon of reaching steady state at a longer time in order to extract more became an inversely proportioned to the fluid flow rate. After all these studies we can concludes with the following points:

- Water is a poor geothermal working fluids, even when different parameters are stimulated in order to extract more energy, the impact is very little and not durable.
- CO_2 can be used as an enhanced working fluid in non – condensable reservoirs, owing the fact that it promote liquid mixture boiling and induces the formation of gas, which helps maintain the reservoir pressure.
- Fracture spacing and porosity optimization can enhance the energy extraction from a geothermal system, these two parameter also help prolong the time at which the system attain steady-state, which in turn gives higher energy extraction
- After all these sensitivity parameter studies, we can conclude by claiming that the most important parameters to control in non- condensable reservoir was the fracture porosity and fluid flow rate. This because they had most impacts on heat extracted.
- The heat produced from controlling the flow rate and fracture permeability was inversely proportional to the time at which the system will achieve the steady state.

When considering extracting most energy from a non- condensable reservoir, both water and CO_2 should be used as working fluid, this because CO_2 is used as a boiling fluid and water as energy carrying fluid. But more research on proportional amount should be done, to avoid over flooding the reservoir with more water which can reduce CO_2 enhanced recovery abilities ability, and assessed the optimal proportional. We have also seen that the heat production with flow rate as working parameter was inversely proportional to the system steady state achievement, therefore more research on the reducing the fluid flow rate after a given flow rate has achieved the steady state. This can enhance the heat extraction.

Concerning the heat insulating in the well, we observed that a non- insulating well looses more heat to the formation, cement with low thermal conductivity should be implemented, as a compensation of a non-insulating well. Secondly, we assessed the impact of insulator's thickness, for which thicker insulator preserved more heat than less thick insulators. We finalized our research by also assessing the impact of insulator's thermal conductivity, for which those with lower thermal conductivity preserved more heat than the ones with higher thermal conductivity. For both insulator's thickness and thermal conductivity, the cement played little or no of insulating when these two were implemented. The advices for insulating design are:

- When considering designing a well without an insulator, make sure the cement with low thermal conductivity is implemented.
- When considering using the insulator with either higher thickness or law thermal conductivity, never take the cement conductivity into consideration, because the cement has little role to play in this regard.

References

Bertani, R., & Thain, I. (2002). Geothermal power genrating plant CO2 emission survey. IGA News 49. 1-3.

Biagi, J., Agarwal, R., & Zhang, Z. (2015). Simulation and optimization of enhanced geothermal systems using CO2 as a working fluid. *Energy, 86*, 627-637. doi:10.1016/j.energy.2015.04.020

Botros, F. E., Hassan, A. E., Reeves, D. M., & Pohll, G. (2008). On mapping fracture networks onto continuum. *Water Resources Research, 44*(8), n/a-n/a. doi:10.1029/2007wr006092

Brown, D. (2000). A Hot Dry Rock geothermal energy concept utilizing supercritical carbon dioxide instead of water . In: Proceedings of the Twenty -Fifth Workshop on Geothermal Reservoir Engineering, Stanford University,. 233-238.

Buscheck T, C. M., Sun Y, Hao Y Elliot T. (2012). Two Stage, Intergrated geothermal CO2 storage reservoirs: An approach for suitable energy production, CO2 sequestration security, and reduced environment risk. Livermore, CA: Lawrence Livermore National Laboratory. .

Dickson, M. a. F., M., . (2004). What is geothermal energy . Instituto di Geoscienze Georisorse; CNR, Pisa, Italy.

ESMAP. (2006). Greenhouse gases from geothermal power production Energy Sector Management Assistance Program-The World Bank Technical Report 009/16.

Fidan, S. (2011). Wellbore Heat Loss Calculation During Steam Injection in Onshore & Offshore Environments.

G.E.A. (2016). 2016 Annula U.S & Global Geothermal Power Production Report. . 3-33.

Geraud, F. S. a. Y. (2003). Porosity and Thermal Conductivity of the Soultz Sous-Foret Granite. Pure Appl. Geophys. 160. 1125-1136. 1122.1121.1121.

Grant, M. A. (1977). Broadlands- A gas- dominated geothermal field. Geothermics, 6(1). 9-29.

IEA. (2015). Special Report on Energy and Climate Change., 1-196.

IPCC. (2012). Special Report on Renewable Energy Sources and Climate Change Mitigation. Cambridge University Press, Cambridge, United Kingdom and New York, NY.USA.

John, H. L. I. (2008). A Heat Transfer Text Book

Karsten Pruess, C. O., George Moridis. (2012). Tough2 user's guide, version 2.0 LBNL-43134., 1-197.

Karsten Pruess, T. N. N. (1985). A Practical Method for Modelling Fluid and Heat Flow in Fractured Porous Media. 1-13.

Lehua Pan, B. F., Christine Doughty Steven Zakem. (2015). Fully Coupled wellbore - reservoir modelling of geothermal heat extraction using CO2 as the working fluid. 100-113. doi:0.1016/j.geothermics.2014.05.005

Luo, F., Xu, R.-N., & Jiang, P.-X. (2014). Numerical investigation of fluid flow and heat transfer in a doublet enhanced geothermal system with CO2 as the working fluid (CO2–EGS). *Energy, 64*, 307-322. doi:10.1016/j.energy.2013.10.048

O'Sullivan, M. J., Bodvarsson; G.S., Pruess, K., and Blakeley, M.R. . (1985). Fluid and heat flow in gas-rich geothermal reservoirs, Society of Petroleum Engineers Journal. *25*, 215-226.

Ozcan, N. Y., & Gokcen, G. . (April 2010). Performance Analysis of Single - Flash Geothermal Power Plants: Gas Removal Stystem Points of View. Proceeding World Geothermal Congress. 25-29.

Pruess, K. (1983). GMINC- A Mesh Generator for Flow Simulation in Fractured Reservoirs. 1-64.

Pruess, K. (2006). Enhanced geothermal systems (EGS) using CO2 as working fluid—A novel approach for generating renewable energy with simultaneous sequestration of carbon. *Geothermics, 35*(4), 351-367. doi:10.1016/j.geothermics.2006.08.002

Randolph, J. B., & Saar, M. O. (2011a). Combining geothermal energy capture with geologic carbon dioxide sequestration. *Geophysical Research Letters, 38*(10), n/a-n/a. doi:10.1029/2011gl047265

Randolph, J. B., & Saar, M. O. (2011b). Coupling carbon dioxide sequestration with geothermal energy capture in naturally permeable, porous geologic formations: Implications for CO2 sequestration. *Energy Procedia, 4*, 2206-2213. doi:10.1016/j.egypro.2011.02.108

Salimi, H., & Wolf, K.-H. (2012). Integration of heat-energy recovery and carbon sequestration. *International Journal of Greenhouse Gas Control, 6*, 56-68. doi:10.1016/j.ijggc.2011.11.010

Sciencedirect. http://msduncanchem.com/Unit_11/phase_diagrams_ws.htm.

Singh., P. (2015). Techological Review of the Geothermal Energy System from Indian Perspective// International Journal of Mechanics and Thermodynamics. . *6*, 23-32.

Van Genuten, M. T. (1980). A closed -form equation for predicting the conductivity of unsaturated soils. Soil Sci.Soc,44,. 892-898.

Willhite, G. P. (1967). Over - all Heat Transfer Coefficients in Steam and Hot Water Injection Wells. 607-615.

Wu, Y. S. (1999). «On the effective continuum method for modelling multiphase flow, multicomponents transport and heat transfer in fracture rock» Lawrence Berkley Laboratory Report LBL-42720, Berkley, California.

Yue Hao, P. F., Scott M.Johnson and Charles R. Carrigan. (2012). Numerical Studies of Couple Flow and Heat Processes in Hydraulically Fractured Geothermal Reservoirs. *36*, 453-458.

Zhang, L., Ezekiel, J., Li, D., Pei, J., & Ren, S. (2014). Potential assessment of CO2 injection for heat mining and geological storage in geothermal reservoirs of China. *Applied Energy, 122*, 237-246. doi:10.1016/j.apenergy.2014.02.027

Appendix

Appendix A

TOUGH2 input and output data

CO2 simulation input file

```
ROCKS----1----*----2----*----3----*----4----*----5----*----6----*----7-
---*----8
SAND1    1     2650.      .025    1.E-13    1.E-13    1.E-13      2.51
1000.
   1.0E-10       0.0       0.0       0.0       0.0       0.0
FRACT    1     2650.       .50   1.0E-13   1.0E-13   1.0E-13      2.51
1000.
                 0.0       0.0       0.0       0.0       0.0
MATRX    1     2650.     0.254    1.E-20    1.E-20    1.E-20      2.51
1000.
   1.0E-10       0.0       0.0       0.0       0.0       0.0

START----1----*----2----*----3----*----4----*----5----*----6----*----7-
---*----8
----*----1 MOP: 123456789*123456789*1234 ---*----5----*----6----*----7-
---*----8
PARAM----1----*----2----*----3----*----4----*----5----*----6----*----7-
---*----8
   2  99       31000200000000014    3
           9.460800E8       -1.   7.776E6 KA 1
  2.592E6
    1.E-5      1.E00                                  1.E-8
                 300            0.00000           0.0000E0
RPCAP----1----*----2----*----3----*----4----*----5----*----6----*----7-
---*----8
    7           0.65      0.05        1.      0.05
    7          0.412      0.03   6.08E-5     6.4E7        1.

GOFT ----1----*----2----*----3----*----4----*----5----*----6----*----7-
---*----8

 KA 1

FOFT ----1----*----2----*----3----*----4----*----5----*----6----*----7-
---*----8
 KA 1

ELEME----1----*----2----*----3----*----4----*----5----*----6----*----7-
---*----8
 AA 1          SAND10.1906E+060.1250E+04          0.        0.
0.1525E+03
 BA 1          SAND10.7625E+060.5000E+04          0.7071E+020.
0.1525E+03
 CA 1          SAND10.7625E+060.5000E+04          0.1414E+030.
0.1525E+03
 DA 1          SAND10.7625E+060.5000E+04          0.2121E+030.
0.1525E+03
```

```
 EA 1          SAND10.7625E+060.5000E+04          0.2828E+030.
0.1525E+03
 FA 1          SAND10.7625E+060.5000E+04          0.3536E+030.
0.1525E+03
 GA 1          SAND10.7625E+060.5000E+04          0.4243E+030.
0.1525E+03
 HA 1          POMED0.7625E+060.5000E+04          0.4950E+030.
0.1525E+03
 IA 1          SAND10.7625E+060.5000E+04          0.5657E+030.
0.1525E+03
 JA 1          SAND10.7625E+060.5000E+04          0.6364E+030.
0.1525E+03
 KA 1          SAND10.1906E+060.1250E+04          0.7071E+030.
0.1525E+03
 BB 1          SAND10.7625E+060.5000E+04
0.7071E+020.7071E+020.1525E+03
 CB 1          SAND10.1525E+070.1000E+05
0.1414E+030.7071E+020.1525E+03
 DB 1          SAND10.1525E+070.1000E+05
0.2121E+030.7071E+020.1525E+03
 EB 1          SAND10.1525E+070.1000E+05
0.2828E+030.7071E+020.1525E+03
 FB 1          SAND10.1525E+070.1000E+05
0.3536E+030.7071E+020.1525E+03
 GB 1          SAND10.1525E+070.1000E+05
0.4243E+030.7071E+020.1525E+03
 HB 1          SAND10.1525E+070.1000E+05
0.4950E+030.7071E+020.1525E+03
 IB 1          SAND10.1525E+070.1000E+05
0.5657E+030.7071E+020.1525E+03
 JB 1          SAND10.7625E+060.5000E+04
0.6364E+030.7071E+020.1525E+03
 CC 1          SAND10.7625E+060.5000E+04
0.1414E+030.1414E+030.1525E+03
 DC 1          SAND10.1525E+070.1000E+05
0.2121E+030.1414E+030.1525E+03
 EC 1          SAND10.1525E+070.1000E+05
0.2828E+030.1414E+030.1525E+03
 FC 1          SAND10.1525E+070.1000E+05
0.3536E+030.1414E+030.1525E+03
 GC 1          SAND10.1525E+070.1000E+05
0.4243E+030.1414E+030.1525E+03
 HC 1          SAND10.1525E+070.1000E+05
0.4950E+030.1414E+030.1525E+03
 IC 1          SAND10.7625E+060.5000E+04
0.5657E+030.1414E+030.1525E+03
 DD 1          SAND10.7625E+060.5000E+04
0.2121E+030.2121E+030.1525E+03
 ED 1          SAND10.1525E+070.1000E+05
0.2828E+030.2121E+030.1525E+03
 FD 1          SAND10.1525E+070.1000E+05
0.3536E+030.2121E+030.1525E+03
 GD 1          SAND10.1525E+070.1000E+05
0.4243E+030.2121E+030.1525E+03
 HD 1          SAND10.7625E+060.5000E+04
0.4950E+030.2121E+030.1525E+03
 EE 1          SAND10.7625E+060.5000E+04
0.2828E+030.2828E+030.1525E+03
```

```
 FE 1          SAND10.1525E+070.1000E+05
0.3536E+030.2828E+030.1525E+03
 GE 1          SAND10.7625E+060.5000E+04
0.4243E+030.2828E+030.1525E+03
 FF 1          SAND10.3812E+060.2500E+04
0.3536E+030.3536E+030.1525E+03
HTX00          SAND1        0.

CONNE----1----*----2----*----3----*----4----*----5----*----6----*----7-
---*----8
 AA 1 BA 1                    10.3536E+020.3536E+020.1078E+05
 BA 1 CA 1                    10.3536E+020.3536E+020.1078E+05
 BA 1 BB 1                    20.3536E+020.3536E+020.2157E+05
 CA 1 DA 1                    10.3536E+020.3536E+020.1078E+05
 CA 1 CB 1                    20.3536E+020.3536E+020.2157E+05
 DA 1 EA 1                    10.3536E+020.3536E+020.1078E+05
 DA 1 DB 1                    20.3536E+020.3536E+020.2157E+05
 EA 1 FA 1                    10.3536E+020.3536E+020.1078E+05
 EA 1 EB 1                    20.3536E+020.3536E+020.2157E+05
 FA 1 GA 1                    10.3536E+020.3536E+020.1078E+05
 FA 1 FB 1                    20.3536E+020.3536E+020.2157E+05
 GA 1 HA 1                    10.3536E+020.3536E+020.1078E+05
 GA 1 GB 1                    20.3536E+020.3536E+020.2157E+05
 HA 1 IA 1                    10.3536E+020.3536E+020.1078E+05
 HA 1 HB 1                    20.3536E+020.3536E+020.2157E+05
 IA 1 JA 1                    10.3536E+020.3536E+020.1078E+05
 IA 1 IB 1                    20.3536E+020.3536E+020.2157E+05
 JA 1 KA 1                    10.3536E+020.3536E+020.1078E+05
 JA 1 JB 1                    20.3536E+020.3536E+020.2157E+05
 BB 1 CB 1                    10.3536E+020.3536E+020.2157E+05
 CB 1 DB 1                    10.3536E+020.3536E+020.2157E+05
 CB 1 CC 1                    20.3536E+020.3536E+020.2157E+05
 DB 1 EB 1                    10.3536E+020.3536E+020.2157E+05
 DB 1 DC 1                    20.3536E+020.3536E+020.2157E+05
 EB 1 FB 1                    10.3536E+020.3536E+020.2157E+05
 EB 1 EC 1                    20.3536E+020.3536E+020.2157E+05
 FB 1 GB 1                    10.3536E+020.3536E+020.2157E+05
 FB 1 FC 1                    20.3536E+020.3536E+020.2157E+05
 GB 1 HB 1                    10.3536E+020.3536E+020.2157E+05
 GB 1 GC 1                    20.3536E+020.3536E+020.2157E+05
 HB 1 IB 1                    10.3536E+020.3536E+020.2157E+05
 HB 1 HC 1                    20.3536E+020.3536E+020.2157E+05
 IB 1 JB 1                    10.3536E+020.3536E+020.2157E+05
 IB 1 IC 1                    20.3536E+020.3536E+020.2157E+05
 CC 1 DC 1                    10.3536E+020.3536E+020.2157E+05
 DC 1 EC 1                    10.3536E+020.3536E+020.2157E+05
 DC 1 DD 1                    20.3536E+020.3536E+020.2157E+05
 EC 1 FC 1                    10.3536E+020.3536E+020.2157E+05
 EC 1 ED 1                    20.3536E+020.3536E+020.2157E+05
 FC 1 GC 1                    10.3536E+020.3536E+020.2157E+05
 FC 1 FD 1                    20.3536E+020.3536E+020.2157E+05
 GC 1 HC 1                    10.3536E+020.3536E+020.2157E+05
 GC 1 GD 1                    20.3536E+020.3536E+020.2157E+05
 HC 1 IC 1                    10.3536E+020.3536E+020.2157E+05
 HC 1 HD 1                    20.3536E+020.3536E+020.2157E+05
 DD 1 ED 1                    10.3536E+020.3536E+020.2157E+05
 ED 1 FD 1                    10.3536E+020.3536E+020.2157E+05
 ED 1 EE 1                    20.3536E+020.3536E+020.2157E+05
```

```
 FD 1 GD 1                    10.3536E+020.3536E+020.2157E+05
 FD 1 FE 1                    20.3536E+020.3536E+020.2157E+05
 GD 1 HD 1                    10.3536E+020.3536E+020.2157E+05
 GD 1 GE 1                    20.3536E+020.3536E+020.2157E+05
 EE 1 FE 1                    10.3536E+020.3536E+020.2157E+05
 FE 1 GE 1                    10.3536E+020.3536E+020.2157E+05
 FE 1 FF 1                    20.3536E+020.3536E+020.2157E+05

GENER----1----*----2----*----3----*----4----*----5----*----6----*----7-
---*----8
 AA 1INJ 1                          COM2          5
 KA 1PRO 1                          MASS         -5

MESHMAKER1----*----2----*----3----*----4----*----5----*----6----*----7-
---*----8
MINC
PART THRED     DFLT
  3  2OUT         60
       .03       .09

ENDCY----1----*----2----*----3----*----4----*----5----*----6----*----7-
---*----8
```

Water Simulations input file

```
ROCKS----1----*----2----*----3----*----4----*----5----*----6----*----7-
---*----8
SANDS    1     2650.      .025    1.E-13    1.E-13    1.E-13      2.51
1000.
   1.0E-10       0.0       0.0       0.0       0.0       0.0
FRACT    1     2650.       .50    1.E-13    1.E-13    1.E-13      2.51
1000.
                 0.0       0.0       0.0       0.0       0.0
MATRX    1     2650.     0.254    0.E-13    0.E-13    0.E-13      2.51
1000.
   1.0E-10       0.0       0.0       0.0       0.0       0.0

START----1----*----2----*----3----*----4----*----5----*----6----*----7-
---*----8
----*----1 MOP: 123456789*123456789*1234 ---*----5----*----6----*----7-
---*----8
PARAM----1----*----2----*----3----*----4----*----5----*----6----*----7-
---*----8
   29999       31000101000000014    3
          9.460800E8       -1. 3.15360E7 KA 1
   1.58E7
    1.E-5      1.E00                                  1.E-8
               3.0E6                    1             2.5E5

RPCAP----1----*----2----*----3----*----4----*----5----*----6----*----7-
---*----8
    7           0.65     0.025        1.      0.05
    7          0.412      0.03   6.08E-5     6.4E7        1.

TIMES----1----*----2----*----3----*----4----*----5----*----6----*----7-
---*----8
```

```
    5    5
 6.30720E7 9.46080E7 1.26144E8 1.57680E8 1.89216E8

GOFT ----1----*----2----*----3----*----4----*----5----*----6----*----7-
---*----8

 KA 1

FOFT ----1----*----2----*----3----*----4----*----5----*----6----*----7-
---*----8
 KA 1

ELEME----1----*----2----*----3----*----4----*----5----*----6----*----7-
---*----8
 AA 1          SANDS0.1906E+060.1250E+04          0.        0.
0.1525E+03
 BA 1          SANDS0.7625E+060.5000E+04          0.7071E+020.
0.1525E+03
 CA 1          SANDS0.7625E+060.5000E+04          0.1414E+030.
0.1525E+03
 DA 1          SANDS0.7625E+060.5000E+04          0.2121E+030.
0.1525E+03
 EA 1          SANDS0.7625E+060.5000E+04          0.2828E+030.
0.1525E+03
 FA 1          SANDS0.7625E+060.5000E+04          0.3536E+030.
0.1525E+03
 GA 1          SANDS0.7625E+060.5000E+04          0.4243E+030.
0.1525E+03
 HA 1          SANDS0.7625E+060.5000E+04          0.4950E+030.
0.1525E+03
 IA 1          SANDS0.7625E+060.5000E+04          0.5657E+030.
0.1525E+03
 JA 1          SANDS0.7625E+060.5000E+04          0.6364E+030.
0.1525E+03
 KA 1          SANDS0.1906E+060.1250E+04          0.7071E+030.
0.1525E+03
 BB 1          SANDS0.7625E+060.5000E+04
0.7071E+020.7071E+020.1525E+03
 CB 1          SANDS0.1525E+070.1000E+05
0.1414E+030.7071E+020.1525E+03
 DB 1          SANDS0.1525E+070.1000E+05
0.2121E+030.7071E+020.1525E+03
 EB 1          SANDS0.1525E+070.1000E+05
0.2828E+030.7071E+020.1525E+03
 FB 1          SANDS0.1525E+070.1000E+05
0.3536E+030.7071E+020.1525E+03
 GB 1          SANDS0.1525E+070.1000E+05
0.4243E+030.7071E+020.1525E+03
 HB 1          SANDS0.1525E+070.1000E+05
0.4950E+030.7071E+020.1525E+03
 IB 1          SANDS0.1525E+070.1000E+05
0.5657E+030.7071E+020.1525E+03
 JB 1          SANDS0.7625E+060.5000E+04
0.6364E+030.7071E+020.1525E+03
 CC 1          SANDS0.7625E+060.5000E+04
0.1414E+030.1414E+030.1525E+03
 DC 1          SANDS0.1525E+070.1000E+05
0.2121E+030.1414E+030.1525E+03
```

```
 EC 1          SANDS0.1525E+070.1000E+05
0.2828E+030.1414E+030.1525E+03
 FC 1          SANDS0.1525E+070.1000E+05
0.3536E+030.1414E+030.1525E+03
 GC 1          SANDS0.1525E+070.1000E+05
0.4243E+030.1414E+030.1525E+03
 HC 1          SANDS0.1525E+070.1000E+05
0.4950E+030.1414E+030.1525E+03
 IC 1          SANDS0.7625E+060.5000E+04
0.5657E+030.1414E+030.1525E+03
 DD 1          SANDS0.7625E+060.5000E+04
0.2121E+030.2121E+030.1525E+03
 ED 1          SANDS0.1525E+070.1000E+05
0.2828E+030.2121E+030.1525E+03
 FD 1          SANDS0.1525E+070.1000E+05
0.3536E+030.2121E+030.1525E+03
 GD 1          SANDS0.1525E+070.1000E+05
0.4243E+030.2121E+030.1525E+03
 HD 1          SANDS0.7625E+060.5000E+04
0.4950E+030.2121E+030.1525E+03
 EE 1          SANDS0.7625E+060.5000E+04
0.2828E+030.2828E+030.1525E+03
 FE 1          SANDS0.1525E+070.1000E+05
0.3536E+030.2828E+030.1525E+03
 GE 1          SANDS0.7625E+060.5000E+04
0.4243E+030.2828E+030.1525E+03
 FF 1          SANDS0.3812E+060.2500E+04
0.3536E+030.3536E+030.1525E+03
HTX00          SANDS        0.

CONNE----1----*----2----*----3----*----4----*----5----*----6----*----7-
---*----8
 AA 1 BA 1                   10.3536E+020.3536E+020.1078E+05
 BA 1 CA 1                   10.3536E+020.3536E+020.1078E+05
 BA 1 BB 1                   20.3536E+020.3536E+020.2157E+05
 CA 1 DA 1                   10.3536E+020.3536E+020.1078E+05
 CA 1 CB 1                   20.3536E+020.3536E+020.2157E+05
 DA 1 EA 1                   10.3536E+020.3536E+020.1078E+05
 DA 1 DB 1                   20.3536E+020.3536E+020.2157E+05
 EA 1 FA 1                   10.3536E+020.3536E+020.1078E+05
 EA 1 EB 1                   20.3536E+020.3536E+020.2157E+05
 FA 1 GA 1                   10.3536E+020.3536E+020.1078E+05
 FA 1 FB 1                   20.3536E+020.3536E+020.2157E+05
 GA 1 HA 1                   10.3536E+020.3536E+020.1078E+05
 GA 1 GB 1                   20.3536E+020.3536E+020.2157E+05
 HA 1 IA 1                   10.3536E+020.3536E+020.1078E+05
 HA 1 HB 1                   20.3536E+020.3536E+020.2157E+05
 IA 1 JA 1                   10.3536E+020.3536E+020.1078E+05
 IA 1 IB 1                   20.3536E+020.3536E+020.2157E+05
 JA 1 KA 1                   10.3536E+020.3536E+020.1078E+05
 JA 1 JB 1                   20.3536E+020.3536E+020.2157E+05
 BB 1 CB 1                   10.3536E+020.3536E+020.2157E+05
 CB 1 DB 1                   10.3536E+020.3536E+020.2157E+05
 CB 1 CC 1                   20.3536E+020.3536E+020.2157E+05
 DB 1 EB 1                   10.3536E+020.3536E+020.2157E+05
 DB 1 DC 1                   20.3536E+020.3536E+020.2157E+05
 EB 1 FB 1                   10.3536E+020.3536E+020.2157E+05
 EB 1 EC 1                   20.3536E+020.3536E+020.2157E+05
```

```
 FB 1 GB 1                    10.3536E+020.3536E+020.2157E+05
 FB 1 FC 1                    20.3536E+020.3536E+020.2157E+05
 GB 1 HB 1                    10.3536E+020.3536E+020.2157E+05
 GB 1 GC 1                    20.3536E+020.3536E+020.2157E+05
 HB 1 IB 1                    10.3536E+020.3536E+020.2157E+05
 HB 1 HC 1                    20.3536E+020.3536E+020.2157E+05
 IB 1 JB 1                    10.3536E+020.3536E+020.2157E+05
 IB 1 IC 1                    20.3536E+020.3536E+020.2157E+05
 CC 1 DC 1                    10.3536E+020.3536E+020.2157E+05
 DC 1 EC 1                    10.3536E+020.3536E+020.2157E+05
 DC 1 DD 1                    20.3536E+020.3536E+020.2157E+05
 EC 1 FC 1                    10.3536E+020.3536E+020.2157E+05
 EC 1 ED 1                    20.3536E+020.3536E+020.2157E+05
 FC 1 GC 1                    10.3536E+020.3536E+020.2157E+05
 FC 1 FD 1                    20.3536E+020.3536E+020.2157E+05
 GC 1 HC 1                    10.3536E+020.3536E+020.2157E+05
 GC 1 GD 1                    20.3536E+020.3536E+020.2157E+05
 HC 1 IC 1                    10.3536E+020.3536E+020.2157E+05
 HC 1 HD 1                    20.3536E+020.3536E+020.2157E+05
 DD 1 ED 1                    10.3536E+020.3536E+020.2157E+05
 ED 1 FD 1                    10.3536E+020.3536E+020.2157E+05
 ED 1 EE 1                    20.3536E+020.3536E+020.2157E+05
 FD 1 GD 1                    10.3536E+020.3536E+020.2157E+05
 FD 1 FE 1                    20.3536E+020.3536E+020.2157E+05
 GD 1 HD 1                    10.3536E+020.3536E+020.2157E+05
 GD 1 GE 1                    20.3536E+020.3536E+020.2157E+05
 EE 1 FE 1                    10.3536E+020.3536E+020.2157E+05
 FE 1 GE 1                    10.3536E+020.3536E+020.2157E+05
 FE 1 FF 1                    20.3536E+020.3536E+020.2157E+05

GENER----1----*----2----*----3----*----4----*----5----*----6----*----7-
---*----8
 AA 1INJ 1                        MASS          8     1.0E5
 KA 1PRO 1                        MASS         -8

MESHMAKER1----*----2----*----3----*----4----*----5----*----6----*----7-
---*----8
MINC
PART THRED     DFLT
  4  3OUT        60.
       .03       .06       .40

ENDCY----1----*----2----*----3----*----4----*----5----*----6----*----7-
---*----8
```

The Secondary mesh process by the MINC

```
ELEME
 AA 1               20.5718E+040.1250E+04
0.0000E+000.0000E+000.1525E+03
2AA 1               30.1144E+050.0000E+00
0.0000E+000.0000E+000.1525E+03
3AA 1               30.7624E+050.0000E+00
0.0000E+000.0000E+000.1525E+03
4AA 1               30.9721E+050.0000E+00
0.0000E+000.0000E+000.1525E+03
 BA 1               20.2288E+050.5000E+04
0.7071E+020.0000E+000.1525E+03
2BA 1               30.4575E+050.0000E+00
0.7071E+020.0000E+000.1525E+03
3BA 1               30.3050E+060.0000E+00
0.7071E+020.0000E+000.1525E+03
4BA 1               30.3889E+060.0000E+00
0.7071E+020.0000E+000.1525E+03
 CA 1               20.2288E+050.5000E+04
0.1414E+030.0000E+000.1525E+03
2CA 1               30.4575E+050.0000E+00
0.1414E+030.0000E+000.1525E+03
3CA 1               30.3050E+060.0000E+00
0.1414E+030.0000E+000.1525E+03
4CA 1               30.3889E+060.0000E+00
0.1414E+030.0000E+000.1525E+03
 DA 1               20.2288E+050.5000E+04
0.2121E+030.0000E+000.1525E+03
2DA 1               30.4575E+050.0000E+00
0.2121E+030.0000E+000.1525E+03
3DA 1               30.3050E+060.0000E+00
0.2121E+030.0000E+000.1525E+03
4DA 1               30.3889E+060.0000E+00
0.2121E+030.0000E+000.1525E+03
 EA 1               20.2288E+050.5000E+04
0.2828E+030.0000E+000.1525E+03
2EA 1               30.4575E+050.0000E+00
0.2828E+030.0000E+000.1525E+03
3EA 1               30.3050E+060.0000E+00
0.2828E+030.0000E+000.1525E+03
4EA 1               30.3889E+060.0000E+00
0.2828E+030.0000E+000.1525E+03
 FA 1               20.2288E+050.5000E+04
0.3536E+030.0000E+000.1525E+03
2FA 1               30.4575E+050.0000E+00
0.3536E+030.0000E+000.1525E+03
3FA 1               30.3050E+060.0000E+00
0.3536E+030.0000E+000.1525E+03
4FA 1               30.3889E+060.0000E+00
0.3536E+030.0000E+000.1525E+03
 GA 1               20.2288E+050.5000E+04
0.4243E+030.0000E+000.1525E+03
2GA 1               30.4575E+050.0000E+00
0.4243E+030.0000E+000.1525E+03
3GA 1               30.3050E+060.0000E+00
0.4243E+030.0000E+000.1525E+03
4GA 1               30.3889E+060.0000E+00
0.4243E+030.0000E+000.1525E+03
```

```
 HA 1              20.2288E+050.5000E+04
0.4950E+030.0000E+000.1525E+03
2HA 1              30.4575E+050.0000E+00
0.4950E+030.0000E+000.1525E+03
3HA 1              30.3050E+060.0000E+00
0.4950E+030.0000E+000.1525E+03
4HA 1              30.3889E+060.0000E+00
0.4950E+030.0000E+000.1525E+03
 IA 1              20.2288E+050.5000E+04
0.5657E+030.0000E+000.1525E+03
2IA 1              30.4575E+050.0000E+00
0.5657E+030.0000E+000.1525E+03
3IA 1              30.3050E+060.0000E+00
0.5657E+030.0000E+000.1525E+03
4IA 1              30.3889E+060.0000E+00
0.5657E+030.0000E+000.1525E+03
 JA 1              20.2288E+050.5000E+04
0.6364E+030.0000E+000.1525E+03
2JA 1              30.4575E+050.0000E+00
0.6364E+030.0000E+000.1525E+03
3JA 1              30.3050E+060.0000E+00
0.6364E+030.0000E+000.1525E+03
4JA 1              30.3889E+060.0000E+00
0.6364E+030.0000E+000.1525E+03
 KA 1              20.5718E+040.1250E+04
0.7071E+030.0000E+000.1525E+03
2KA 1              30.1144E+050.0000E+00
0.7071E+030.0000E+000.1525E+03
3KA 1              30.7624E+050.0000E+00
0.7071E+030.0000E+000.1525E+03
4KA 1              30.9721E+050.0000E+00
0.7071E+030.0000E+000.1525E+03
 BB 1              20.2288E+050.5000E+04
0.7071E+020.7071E+020.1525E+03
2BB 1              30.4575E+050.0000E+00
0.7071E+020.7071E+020.1525E+03
3BB 1              30.3050E+060.0000E+00
0.7071E+020.7071E+020.1525E+03
4BB 1              30.3889E+060.0000E+00
0.7071E+020.7071E+020.1525E+03
 CB 1              20.4575E+050.1000E+05
0.1414E+030.7071E+020.1525E+03
2CB 1              30.9150E+050.0000E+00
0.1414E+030.7071E+020.1525E+03
3CB 1              30.6100E+060.0000E+00
0.1414E+030.7071E+020.1525E+03
4CB 1              30.7778E+060.0000E+00
0.1414E+030.7071E+020.1525E+03
 DB 1              20.4575E+050.1000E+05
0.2121E+030.7071E+020.1525E+03
2DB 1              30.9150E+050.0000E+00
0.2121E+030.7071E+020.1525E+03
3DB 1              30.6100E+060.0000E+00
0.2121E+030.7071E+020.1525E+03
4DB 1              30.7778E+060.0000E+00
0.2121E+030.7071E+020.1525E+03
 EB 1              20.4575E+050.1000E+05
0.2828E+030.7071E+020.1525E+03
```

```
2EB 1              30.9150E+050.0000E+00
0.2828E+030.7071E+020.1525E+03
3EB 1              30.6100E+060.0000E+00
0.2828E+030.7071E+020.1525E+03
4EB 1              30.7778E+060.0000E+00
0.2828E+030.7071E+020.1525E+03
 FB 1              20.4575E+050.1000E+05
0.3536E+030.7071E+020.1525E+03
2FB 1              30.9150E+050.0000E+00
0.3536E+030.7071E+020.1525E+03
3FB 1              30.6100E+060.0000E+00
0.3536E+030.7071E+020.1525E+03
4FB 1              30.7778E+060.0000E+00
0.3536E+030.7071E+020.1525E+03
 GB 1              20.4575E+050.1000E+05
0.4243E+030.7071E+020.1525E+03
2GB 1              30.9150E+050.0000E+00
0.4243E+030.7071E+020.1525E+03
3GB 1              30.6100E+060.0000E+00
0.4243E+030.7071E+020.1525E+03
4GB 1              30.7778E+060.0000E+00
0.4243E+030.7071E+020.1525E+03
 HB 1              20.4575E+050.1000E+05
0.4950E+030.7071E+020.1525E+03
2HB 1              30.9150E+050.0000E+00
0.4950E+030.7071E+020.1525E+03
3HB 1              30.6100E+060.0000E+00
0.4950E+030.7071E+020.1525E+03
4HB 1              30.7778E+060.0000E+00
0.4950E+030.7071E+020.1525E+03
 IB 1              20.4575E+050.1000E+05
0.5657E+030.7071E+020.1525E+03
2IB 1              30.9150E+050.0000E+00
0.5657E+030.7071E+020.1525E+03
3IB 1              30.6100E+060.0000E+00
0.5657E+030.7071E+020.1525E+03
4IB 1              30.7778E+060.0000E+00
0.5657E+030.7071E+020.1525E+03
 JB 1              20.2288E+050.5000E+04
0.6364E+030.7071E+020.1525E+03
2JB 1              30.4575E+050.0000E+00
0.6364E+030.7071E+020.1525E+03
3JB 1              30.3050E+060.0000E+00
0.6364E+030.7071E+020.1525E+03
4JB 1              30.3889E+060.0000E+00
0.6364E+030.7071E+020.1525E+03
 CC 1              20.2288E+050.5000E+04
0.1414E+030.1414E+030.1525E+03
2CC 1              30.4575E+050.0000E+00
0.1414E+030.1414E+030.1525E+03
3CC 1              30.3050E+060.0000E+00
0.1414E+030.1414E+030.1525E+03
4CC 1              30.3889E+060.0000E+00
0.1414E+030.1414E+030.1525E+03
 DC 1              20.4575E+050.1000E+05
0.2121E+030.1414E+030.1525E+03
2DC 1              30.9150E+050.0000E+00
0.2121E+030.1414E+030.1525E+03
```

```
3DC 1              30.6100E+060.0000E+00
0.2121E+030.1414E+030.1525E+03
4DC 1              30.7778E+060.0000E+00
0.2121E+030.1414E+030.1525E+03
 EC 1              20.4575E+050.1000E+05
0.2828E+030.1414E+030.1525E+03
2EC 1              30.9150E+050.0000E+00
0.2828E+030.1414E+030.1525E+03
3EC 1              30.6100E+060.0000E+00
0.2828E+030.1414E+030.1525E+03
4EC 1              30.7778E+060.0000E+00
0.2828E+030.1414E+030.1525E+03
 FC 1              20.4575E+050.1000E+05
0.3536E+030.1414E+030.1525E+03
2FC 1              30.9150E+050.0000E+00
0.3536E+030.1414E+030.1525E+03
3FC 1              30.6100E+060.0000E+00
0.3536E+030.1414E+030.1525E+03
4FC 1              30.7778E+060.0000E+00
0.3536E+030.1414E+030.1525E+03
 GC 1              20.4575E+050.1000E+05
0.4243E+030.1414E+030.1525E+03
2GC 1              30.9150E+050.0000E+00
0.4243E+030.1414E+030.1525E+03
3GC 1              30.6100E+060.0000E+00
0.4243E+030.1414E+030.1525E+03
4GC 1              30.7778E+060.0000E+00
0.4243E+030.1414E+030.1525E+03
 HC 1              20.4575E+050.1000E+05
0.4950E+030.1414E+030.1525E+03
2HC 1              30.9150E+050.0000E+00
0.4950E+030.1414E+030.1525E+03
3HC 1              30.6100E+060.0000E+00
0.4950E+030.1414E+030.1525E+03
4HC 1              30.7778E+060.0000E+00
0.4950E+030.1414E+030.1525E+03
 IC 1              20.2288E+050.5000E+04
0.5657E+030.1414E+030.1525E+03
2IC 1              30.4575E+050.0000E+00
0.5657E+030.1414E+030.1525E+03
3IC 1              30.3050E+060.0000E+00
0.5657E+030.1414E+030.1525E+03
4IC 1              30.3889E+060.0000E+00
0.5657E+030.1414E+030.1525E+03
 DD 1              20.2288E+050.5000E+04
0.2121E+030.2121E+030.1525E+03
2DD 1              30.4575E+050.0000E+00
0.2121E+030.2121E+030.1525E+03
3DD 1              30.3050E+060.0000E+00
0.2121E+030.2121E+030.1525E+03
4DD 1              30.3889E+060.0000E+00
0.2121E+030.2121E+030.1525E+03
 ED 1              20.4575E+050.1000E+05
0.2828E+030.2121E+030.1525E+03
2ED 1              30.9150E+050.0000E+00
0.2828E+030.2121E+030.1525E+03
3ED 1              30.6100E+060.0000E+00
0.2828E+030.2121E+030.1525E+03
```

```
4ED 1              30.7778E+060.0000E+00
0.2828E+030.2121E+030.1525E+03
 FD 1              20.4575E+050.1000E+05
0.3536E+030.2121E+030.1525E+03
2FD 1              30.9150E+050.0000E+00
0.3536E+030.2121E+030.1525E+03
3FD 1              30.6100E+060.0000E+00
0.3536E+030.2121E+030.1525E+03
4FD 1              30.7778E+060.0000E+00
0.3536E+030.2121E+030.1525E+03
 GD 1              20.4575E+050.1000E+05
0.4243E+030.2121E+030.1525E+03
2GD 1              30.9150E+050.0000E+00
0.4243E+030.2121E+030.1525E+03
3GD 1              30.6100E+060.0000E+00
0.4243E+030.2121E+030.1525E+03
4GD 1              30.7778E+060.0000E+00
0.4243E+030.2121E+030.1525E+03
 HD 1              20.2288E+050.5000E+04
0.4950E+030.2121E+030.1525E+03
2HD 1              30.4575E+050.0000E+00
0.4950E+030.2121E+030.1525E+03
3HD 1              30.3050E+060.0000E+00
0.4950E+030.2121E+030.1525E+03
4HD 1              30.3889E+060.0000E+00
0.4950E+030.2121E+030.1525E+03
 EE 1              20.2288E+050.5000E+04
0.2828E+030.2828E+030.1525E+03
2EE 1              30.4575E+050.0000E+00
0.2828E+030.2828E+030.1525E+03
3EE 1              30.3050E+060.0000E+00
0.2828E+030.2828E+030.1525E+03
4EE 1              30.3889E+060.0000E+00
0.2828E+030.2828E+030.1525E+03
 FE 1              20.4575E+050.1000E+05
0.3536E+030.2828E+030.1525E+03
2FE 1              30.9150E+050.0000E+00
0.3536E+030.2828E+030.1525E+03
3FE 1              30.6100E+060.0000E+00
0.3536E+030.2828E+030.1525E+03
4FE 1              30.7778E+060.0000E+00
0.3536E+030.2828E+030.1525E+03
 GE 1              20.2288E+050.5000E+04
0.4243E+030.2828E+030.1525E+03
2GE 1              30.4575E+050.0000E+00
0.4243E+030.2828E+030.1525E+03
3GE 1              30.3050E+060.0000E+00
0.4243E+030.2828E+030.1525E+03
4GE 1              30.3889E+060.0000E+00
0.4243E+030.2828E+030.1525E+03
 FF 1              20.1144E+050.2500E+04
0.3536E+030.3536E+030.1525E+03
2FF 1              30.2287E+050.0000E+00
0.3536E+030.3536E+030.1525E+03
3FF 1              30.1525E+060.0000E+00
0.3536E+030.3536E+030.1525E+03
4FF 1              30.1944E+060.0000E+00
0.3536E+030.3536E+030.1525E+03
```

```
HTX 0               10.0000E+000.0000E+00
0.0000E+000.0000E+000.0000E+00

CONNE
 AA 1 BA 1                    10.3536E+020.3536E+020.1078E+050.0000E+00
 BA 1 CA 1                    10.3536E+020.3536E+020.1078E+050.0000E+00
 BA 1 BB 1                    20.3536E+020.3536E+020.2157E+050.0000E+00
 CA 1 DA 1                    10.3536E+020.3536E+020.1078E+050.0000E+00
 CA 1 CB 1                    20.3536E+020.3536E+020.2157E+050.0000E+00
 DA 1 EA 1                    10.3536E+020.3536E+020.1078E+050.0000E+00
 DA 1 DB 1                    20.3536E+020.3536E+020.2157E+050.0000E+00
 EA 1 FA 1                    10.3536E+020.3536E+020.1078E+050.0000E+00
 EA 1 EB 1                    20.3536E+020.3536E+020.2157E+050.0000E+00
 FA 1 GA 1                    10.3536E+020.3536E+020.1078E+050.0000E+00
 FA 1 FB 1                    20.3536E+020.3536E+020.2157E+050.0000E+00
 GA 1 HA 1                    10.3536E+020.3536E+020.1078E+050.0000E+00
 GA 1 GB 1                    20.3536E+020.3536E+020.2157E+050.0000E+00
 HA 1 IA 1                    10.3536E+020.3536E+020.1078E+050.0000E+00
 HA 1 HB 1                    20.3536E+020.3536E+020.2157E+050.0000E+00
 IA 1 JA 1                    10.3536E+020.3536E+020.1078E+050.0000E+00
 IA 1 IB 1                    20.3536E+020.3536E+020.2157E+050.0000E+00
 JA 1 KA 1                    10.3536E+020.3536E+020.1078E+050.0000E+00
 JA 1 JB 1                    20.3536E+020.3536E+020.2157E+050.0000E+00
 BB 1 CB 1                    10.3536E+020.3536E+020.2157E+050.0000E+00
 CB 1 DB 1                    10.3536E+020.3536E+020.2157E+050.0000E+00
 CB 1 CC 1                    20.3536E+020.3536E+020.2157E+050.0000E+00
 DB 1 EB 1                    10.3536E+020.3536E+020.2157E+050.0000E+00
 DB 1 DC 1                    20.3536E+020.3536E+020.2157E+050.0000E+00
 EB 1 FB 1                    10.3536E+020.3536E+020.2157E+050.0000E+00
 EB 1 EC 1                    20.3536E+020.3536E+020.2157E+050.0000E+00
 FB 1 GB 1                    10.3536E+020.3536E+020.2157E+050.0000E+00
 FB 1 FC 1                    20.3536E+020.3536E+020.2157E+050.0000E+00
 GB 1 HB 1                    10.3536E+020.3536E+020.2157E+050.0000E+00
 GB 1 GC 1                    20.3536E+020.3536E+020.2157E+050.0000E+00
 HB 1 IB 1                    10.3536E+020.3536E+020.2157E+050.0000E+00
 HB 1 HC 1                    20.3536E+020.3536E+020.2157E+050.0000E+00
 IB 1 JB 1                    10.3536E+020.3536E+020.2157E+050.0000E+00
 IB 1 IC 1                    20.3536E+020.3536E+020.2157E+050.0000E+00
 CC 1 DC 1                    10.3536E+020.3536E+020.2157E+050.0000E+00
 DC 1 EC 1                    10.3536E+020.3536E+020.2157E+050.0000E+00
 DC 1 DD 1                    20.3536E+020.3536E+020.2157E+050.0000E+00
 EC 1 FC 1                    10.3536E+020.3536E+020.2157E+050.0000E+00
 EC 1 ED 1                    20.3536E+020.3536E+020.2157E+050.0000E+00
 FC 1 GC 1                    10.3536E+020.3536E+020.2157E+050.0000E+00
 FC 1 FD 1                    20.3536E+020.3536E+020.2157E+050.0000E+00
 GC 1 HC 1                    10.3536E+020.3536E+020.2157E+050.0000E+00
 GC 1 GD 1                    20.3536E+020.3536E+020.2157E+050.0000E+00
 HC 1 IC 1                    10.3536E+020.3536E+020.2157E+050.0000E+00
 HC 1 HD 1                    20.3536E+020.3536E+020.2157E+050.0000E+00
 DD 1 ED 1                    10.3536E+020.3536E+020.2157E+050.0000E+00
 ED 1 FD 1                    10.3536E+020.3536E+020.2157E+050.0000E+00
 ED 1 EE 1                    20.3536E+020.3536E+020.2157E+050.0000E+00
 FD 1 GD 1                    10.3536E+020.3536E+020.2157E+050.0000E+00
 FD 1 FE 1                    20.3536E+020.3536E+020.2157E+050.0000E+00
 GD 1 HD 1                    10.3536E+020.3536E+020.2157E+050.0000E+00
 GD 1 GE 1                    20.3536E+020.3536E+020.2157E+050.0000E+00
 EE 1 FE 1                    10.3536E+020.3536E+020.2157E+050.0000E+00
 FE 1 GE 1                    10.3536E+020.3536E+020.2157E+050.0000E+00
```

```
 FE 1 FF 1                    20.3536E+020.3536E+020.2157E+050.0000E+00
 AA 12AA 1                    10.0000E+000.3159E+000.1849E+05
2AA 13AA 1                    10.3159E+000.2577E+010.1772E+05
3AA 14AA 1                    10.2577E+010.4843E+010.1204E+05
 BA 12BA 1                    10.0000E+000.3159E+000.7396E+05
2BA 13BA 1                    10.3159E+000.2577E+010.7088E+05
3BA 14BA 1                    10.2577E+010.4843E+010.4818E+05
 CA 12CA 1                    10.0000E+000.3159E+000.7396E+05
2CA 13CA 1                    10.3159E+000.2577E+010.7088E+05
3CA 14CA 1                    10.2577E+010.4843E+010.4818E+05
 DA 12DA 1                    10.0000E+000.3159E+000.7396E+05
2DA 13DA 1                    10.3159E+000.2577E+010.7088E+05
3DA 14DA 1                    10.2577E+010.4843E+010.4818E+05
 EA 12EA 1                    10.0000E+000.3159E+000.7396E+05
2EA 13EA 1                    10.3159E+000.2577E+010.7088E+05
3EA 14EA 1                    10.2577E+010.4843E+010.4818E+05
 FA 12FA 1                    10.0000E+000.3159E+000.7396E+05
2FA 13FA 1                    10.3159E+000.2577E+010.7088E+05
3FA 14FA 1                    10.2577E+010.4843E+010.4818E+05
 GA 12GA 1                    10.0000E+000.3159E+000.7396E+05
2GA 13GA 1                    10.3159E+000.2577E+010.7088E+05
3GA 14GA 1                    10.2577E+010.4843E+010.4818E+05
 HA 12HA 1                    10.0000E+000.3159E+000.7396E+05
2HA 13HA 1                    10.3159E+000.2577E+010.7088E+05
3HA 14HA 1                    10.2577E+010.4843E+010.4818E+05
 IA 12IA 1                    10.0000E+000.3159E+000.7396E+05
2IA 13IA 1                    10.3159E+000.2577E+010.7088E+05
3IA 14IA 1                    10.2577E+010.4843E+010.4818E+05
 JA 12JA 1                    10.0000E+000.3159E+000.7396E+05
2JA 13JA 1                    10.3159E+000.2577E+010.7088E+05
3JA 14JA 1                    10.2577E+010.4843E+010.4818E+05
 KA 12KA 1                    10.0000E+000.3159E+000.1849E+05
2KA 13KA 1                    10.3159E+000.2577E+010.1772E+05
3KA 14KA 1                    10.2577E+010.4843E+010.1204E+05
 BB 12BB 1                    10.0000E+000.3159E+000.7396E+05
2BB 13BB 1                    10.3159E+000.2577E+010.7088E+05
3BB 14BB 1                    10.2577E+010.4843E+010.4818E+05
 CB 12CB 1                    10.0000E+000.3159E+000.1479E+06
2CB 13CB 1                    10.3159E+000.2577E+010.1418E+06
3CB 14CB 1                    10.2577E+010.4843E+010.9636E+05
 DB 12DB 1                    10.0000E+000.3159E+000.1479E+06
2DB 13DB 1                    10.3159E+000.2577E+010.1418E+06
3DB 14DB 1                    10.2577E+010.4843E+010.9636E+05
 EB 12EB 1                    10.0000E+000.3159E+000.1479E+06
2EB 13EB 1                    10.3159E+000.2577E+010.1418E+06
3EB 14EB 1                    10.2577E+010.4843E+010.9636E+05
 FB 12FB 1                    10.0000E+000.3159E+000.1479E+06
2FB 13FB 1                    10.3159E+000.2577E+010.1418E+06
3FB 14FB 1                    10.2577E+010.4843E+010.9636E+05
 GB 12GB 1                    10.0000E+000.3159E+000.1479E+06
2GB 13GB 1                    10.3159E+000.2577E+010.1418E+06
3GB 14GB 1                    10.2577E+010.4843E+010.9636E+05
 HB 12HB 1                    10.0000E+000.3159E+000.1479E+06
2HB 13HB 1                    10.3159E+000.2577E+010.1418E+06
3HB 14HB 1                    10.2577E+010.4843E+010.9636E+05
 IB 12IB 1                    10.0000E+000.3159E+000.1479E+06
2IB 13IB 1                    10.3159E+000.2577E+010.1418E+06
3IB 14IB 1                    10.2577E+010.4843E+010.9636E+05
```

```
 JB 12JB 1                    10.0000E+000.3159E+000.7396E+05
2JB 13JB 1                    10.3159E+000.2577E+010.7088E+05
3JB 14JB 1                    10.2577E+010.4843E+010.4818E+05
 CC 12CC 1                    10.0000E+000.3159E+000.7396E+05
2CC 13CC 1                    10.3159E+000.2577E+010.7088E+05
3CC 14CC 1                    10.2577E+010.4843E+010.4818E+05
 DC 12DC 1                    10.0000E+000.3159E+000.1479E+06
2DC 13DC 1                    10.3159E+000.2577E+010.1418E+06
3DC 14DC 1                    10.2577E+010.4843E+010.9636E+05
 EC 12EC 1                    10.0000E+000.3159E+000.1479E+06
2EC 13EC 1                    10.3159E+000.2577E+010.1418E+06
3EC 14EC 1                    10.2577E+010.4843E+010.9636E+05
 FC 12FC 1                    10.0000E+000.3159E+000.1479E+06
2FC 13FC 1                    10.3159E+000.2577E+010.1418E+06
3FC 14FC 1                    10.2577E+010.4843E+010.9636E+05
 GC 12GC 1                    10.0000E+000.3159E+000.1479E+06
2GC 13GC 1                    10.3159E+000.2577E+010.1418E+06
3GC 14GC 1                    10.2577E+010.4843E+010.9636E+05
 HC 12HC 1                    10.0000E+000.3159E+000.1479E+06
2HC 13HC 1                    10.3159E+000.2577E+010.1418E+06
3HC 14HC 1                    10.2577E+010.4843E+010.9636E+05
 IC 12IC 1                    10.0000E+000.3159E+000.7396E+05
2IC 13IC 1                    10.3159E+000.2577E+010.7088E+05
3IC 14IC 1                    10.2577E+010.4843E+010.4818E+05
 DD 12DD 1                    10.0000E+000.3159E+000.7396E+05
2DD 13DD 1                    10.3159E+000.2577E+010.7088E+05
3DD 14DD 1                    10.2577E+010.4843E+010.4818E+05
 ED 12ED 1                    10.0000E+000.3159E+000.1479E+06
2ED 13ED 1                    10.3159E+000.2577E+010.1418E+06
3ED 14ED 1                    10.2577E+010.4843E+010.9636E+05
 FD 12FD 1                    10.0000E+000.3159E+000.1479E+06
2FD 13FD 1                    10.3159E+000.2577E+010.1418E+06
3FD 14FD 1                    10.2577E+010.4843E+010.9636E+05
 GD 12GD 1                    10.0000E+000.3159E+000.1479E+06
2GD 13GD 1                    10.3159E+000.2577E+010.1418E+06
3GD 14GD 1                    10.2577E+010.4843E+010.9636E+05
 HD 12HD 1                    10.0000E+000.3159E+000.7396E+05
2HD 13HD 1                    10.3159E+000.2577E+010.7088E+05
3HD 14HD 1                    10.2577E+010.4843E+010.4818E+05
 EE 12EE 1                    10.0000E+000.3159E+000.7396E+05
2EE 13EE 1                    10.3159E+000.2577E+010.7088E+05
3EE 14EE 1                    10.2577E+010.4843E+010.4818E+05
 FE 12FE 1                    10.0000E+000.3159E+000.1479E+06
2FE 13FE 1                    10.3159E+000.2577E+010.1418E+06
3FE 14FE 1                    10.2577E+010.4843E+010.9636E+05
 GE 12GE 1                    10.0000E+000.3159E+000.7396E+05
2GE 13GE 1                    10.3159E+000.2577E+010.7088E+05
3GE 14GE 1                    10.2577E+010.4843E+010.4818E+05
 FF 12FF 1                    10.0000E+000.3159E+000.3698E+05
2FF 13FF 1                    10.3159E+000.2577E+010.3544E+05
3FF 14FF 1                    10.2577E+010.4843E+010.2409E+05
```

Appendix B

CO2 mole fraction and energy at production for different parameters

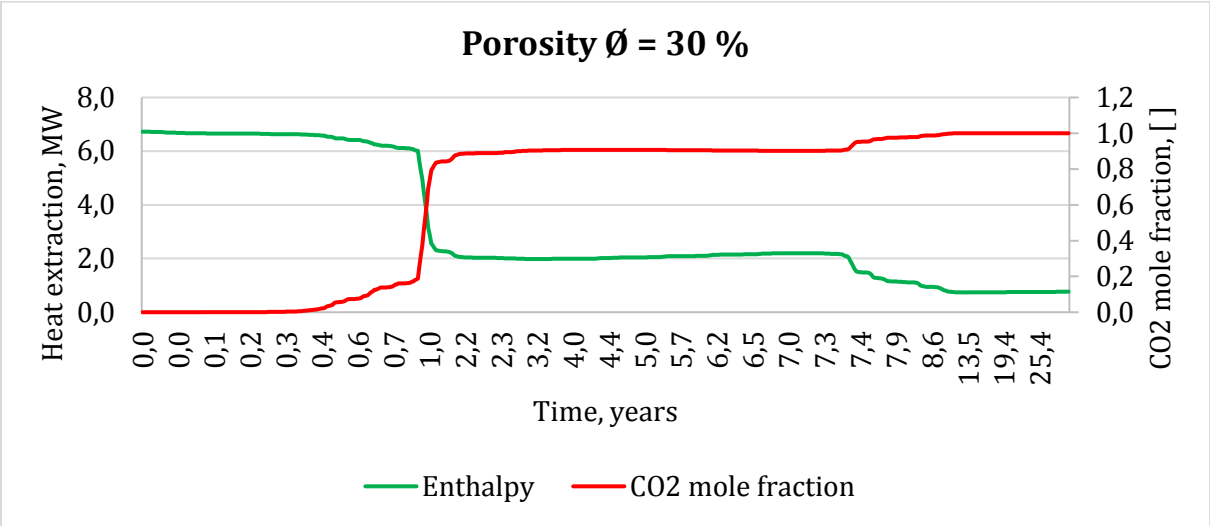

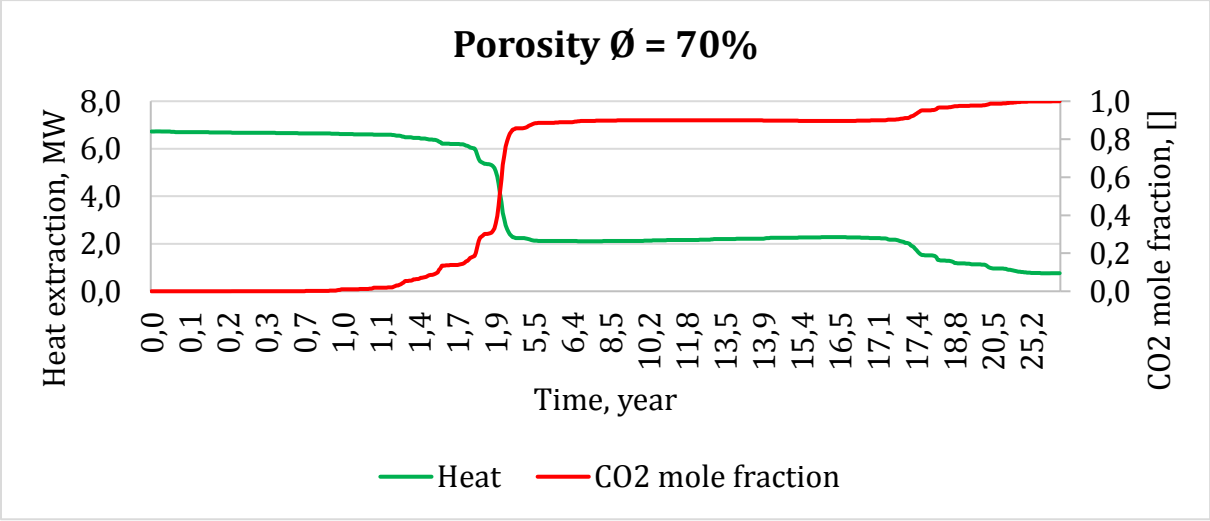

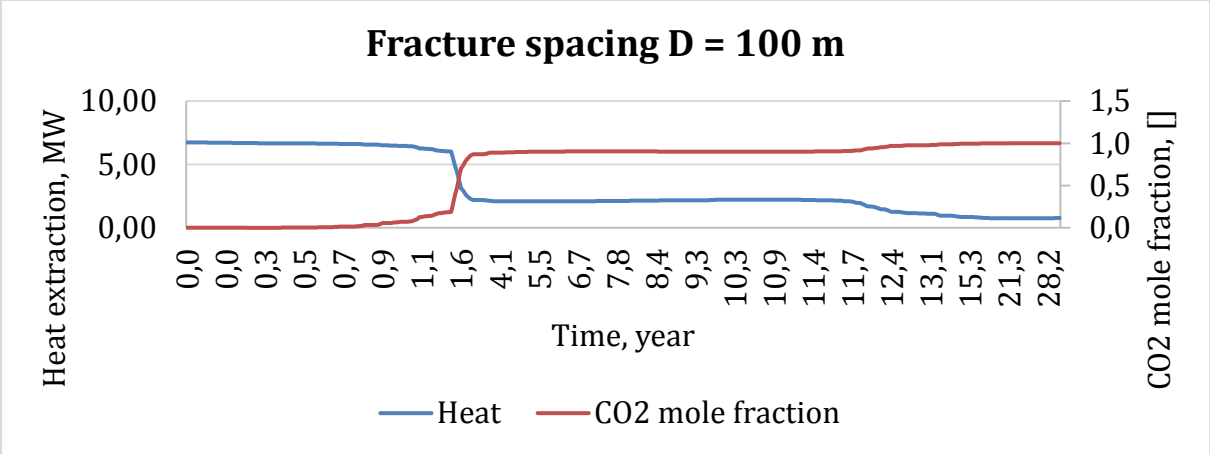

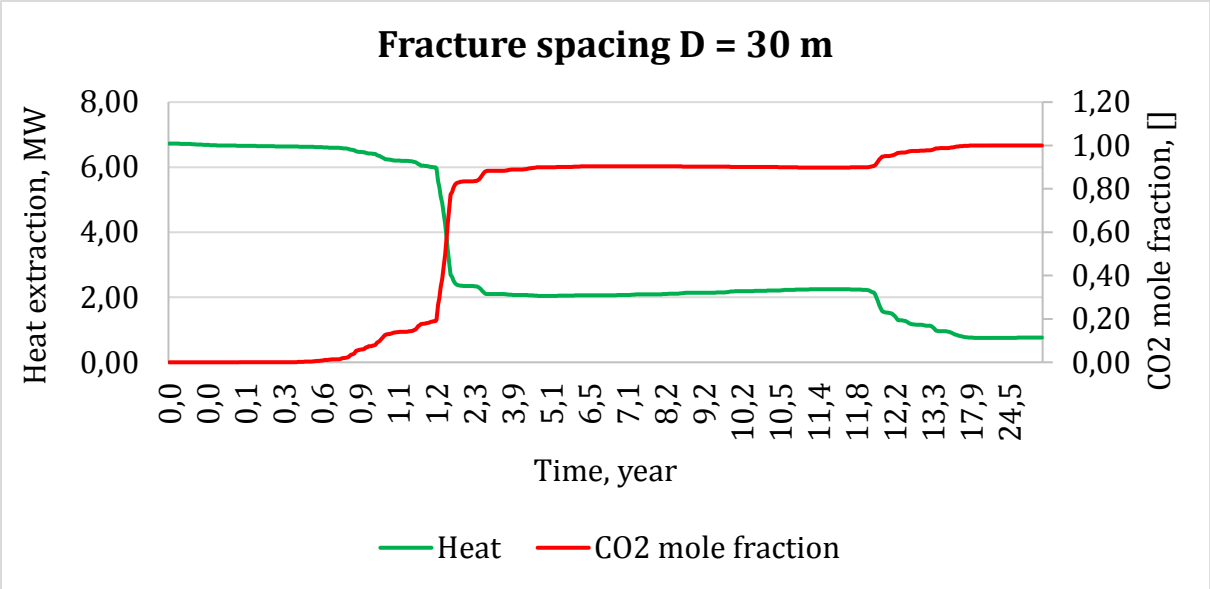
Fracture spacing D = 30 m
Heat extraction, MW
8,00
6,00
4,00
2,00
0,00
1,20
1,00
0,80
0,60
0,40
0,20
0,00
CO2 mole fraction, []
0,0 0,0 0,1 0,3 0,6 0,9 1,1 1,2 2,3 3,9 5,1 6,5 7,1 8,2 9,2 10,2 10,5 11,4 11,8 12,2 13,3 17,9 24,5
Time, year
Heat
CO2 mole fraction

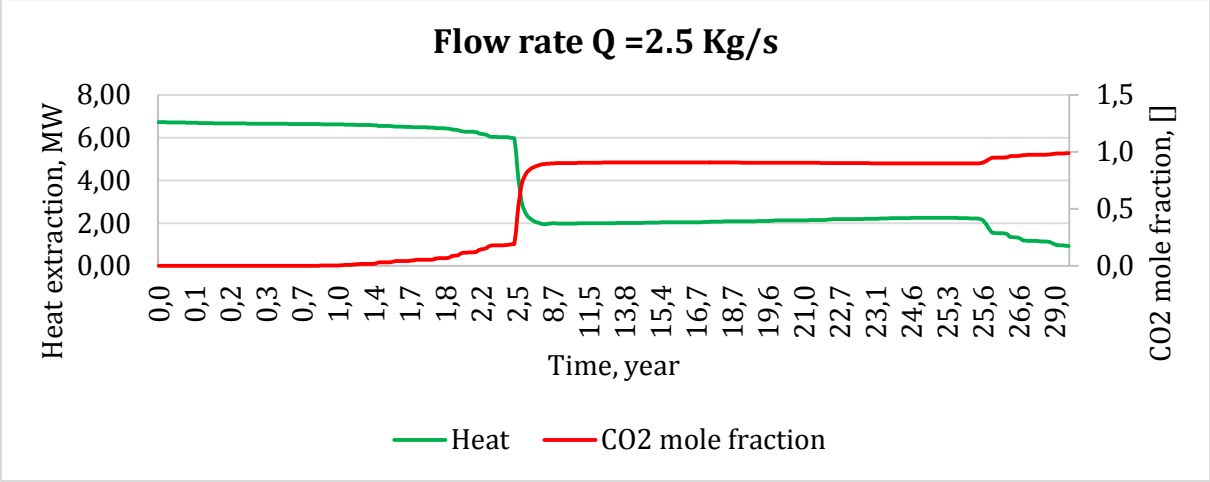
Flow rate Q =2.5 Kg/s
Heat extraction, MW
8,00
6,00
4,00
2,00
0,00
1,5
1,0
0,5
0,0
CO2 mole fraction, []
0,0 0,1 0,2 0,3 0,7 1,0 1,4 1,7 1,8 2,2 2,5 8,7 11,5 13,8 15,4 16,7 18,7 19,6 21,0 22,7 23,1 24,6 25,3 25,6 26,6 29,0
Time, year
Heat
CO2 mole fraction

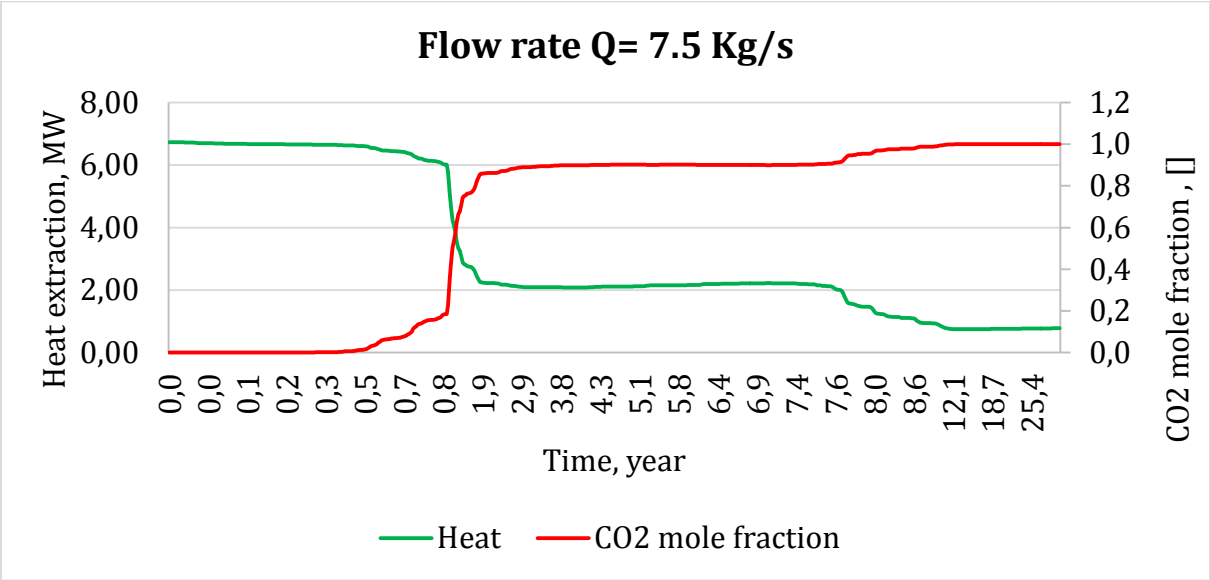
Flow rate Q= 7.5 Kg/s
Heat extraction, MW
8,00
6,00
4,00
2,00
0,00
1,2
1,0
0,8
0,6
0,4
0,2
0,0
CO2 mole fraction , []
0,0 0,0 0,1 0,2 0,3 0,5 0,7 0,8 1,9 2,9 3,8 4,3 5,1 5,8 6,4 6,9 7,4 7,6 8,0 8,6 12,1 18,7 25,4
Time, year
Heat
CO2 mole fraction

Appendix C

Heat extraction for CO2 injection

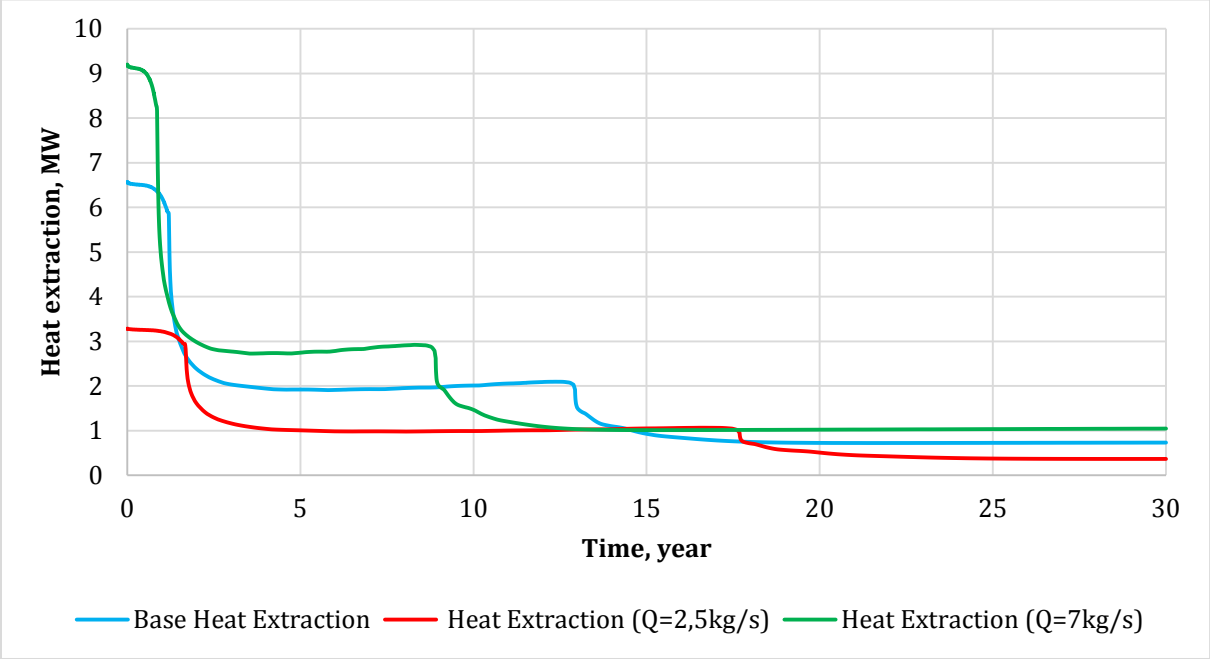

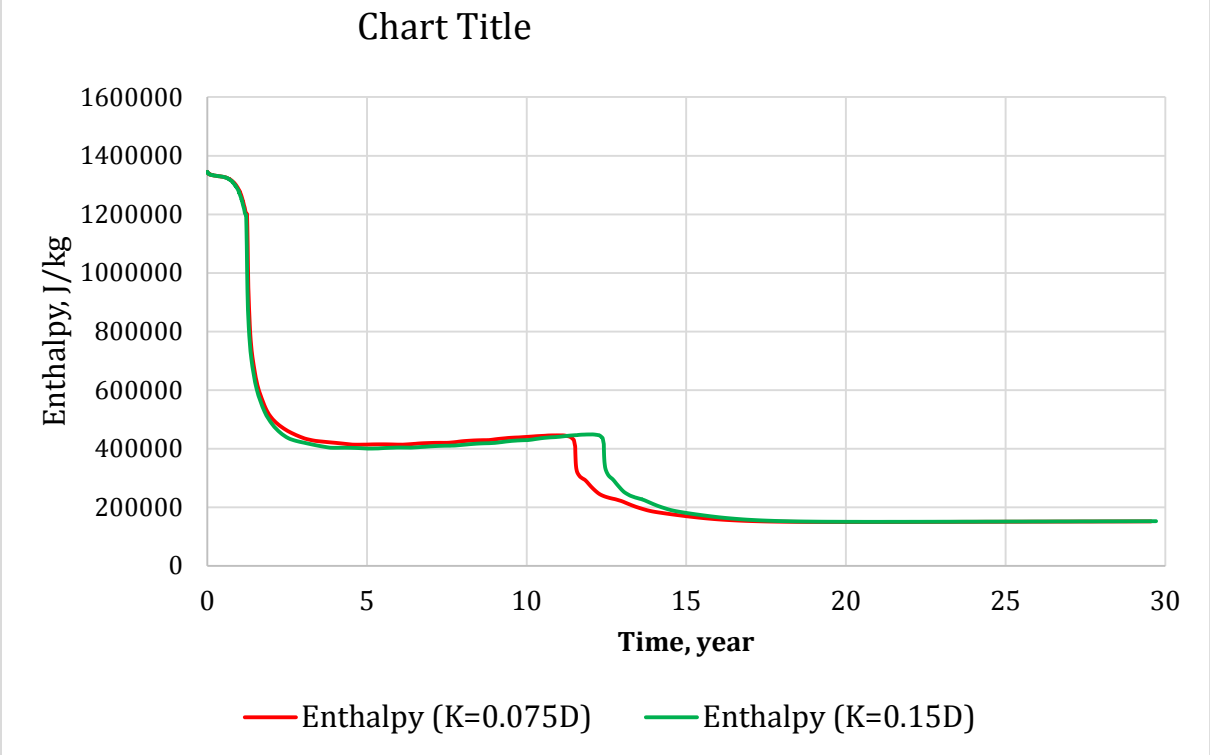

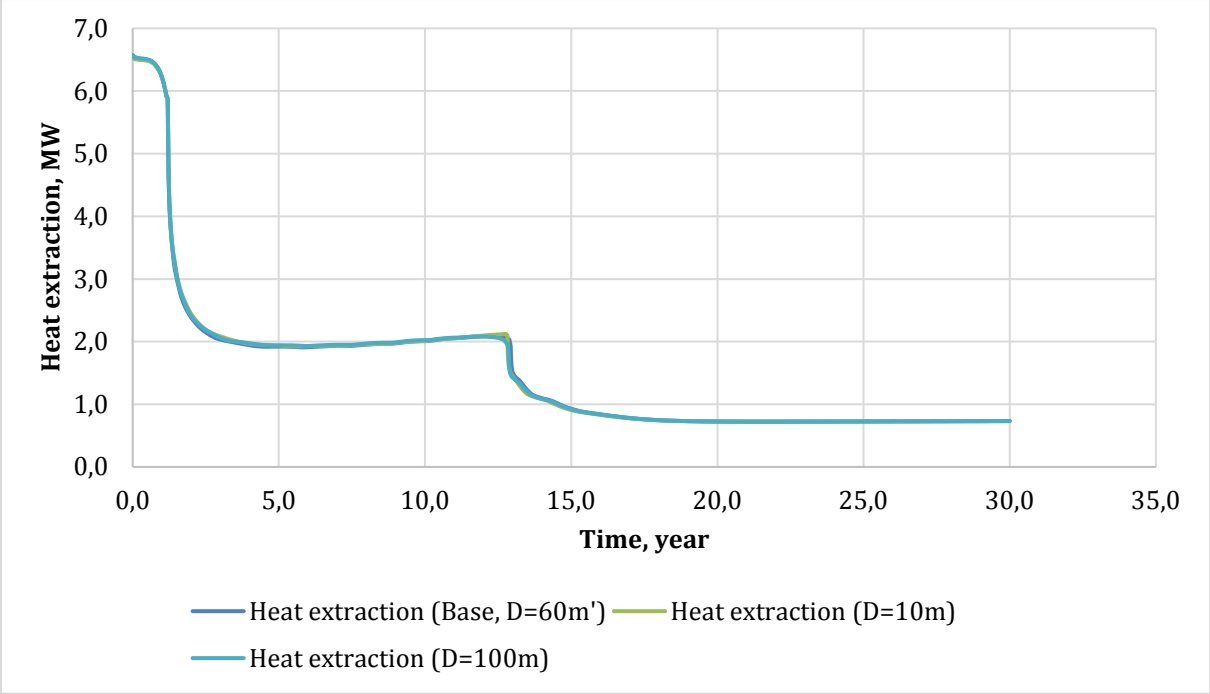
7,0
6,0
5,0
4,0
3,0
2,0
1,0
0,0
Heat extraction, MW
0,0
5,0
10,0
15,0
20,0
25,0
30,0
35,0
Time, year
Heat extraction (Base, D=60m')
Heat extraction (D=10m)
Heat extraction (D=100m)

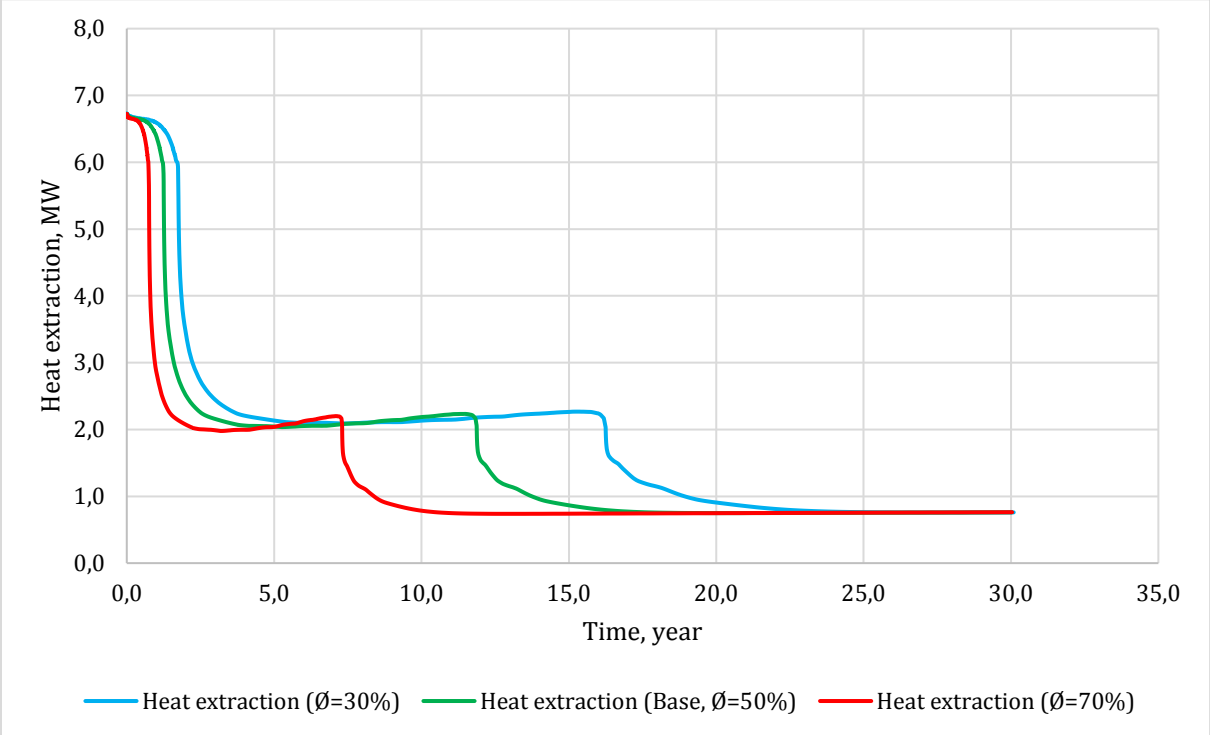
8,0
7,0
6,0
5,0
4,0
3,0
2,0
1,0
0,0
Heat extraction, MW
0,0
5,0
10,0
15,0
20,0
25,0
30,0
35,0
Time, year
Heat extraction (Ø=30%)
Heat extraction (Base, Ø=50%)
Heat extraction (Ø=70%)

Appendix D

Overall – heat coefficient

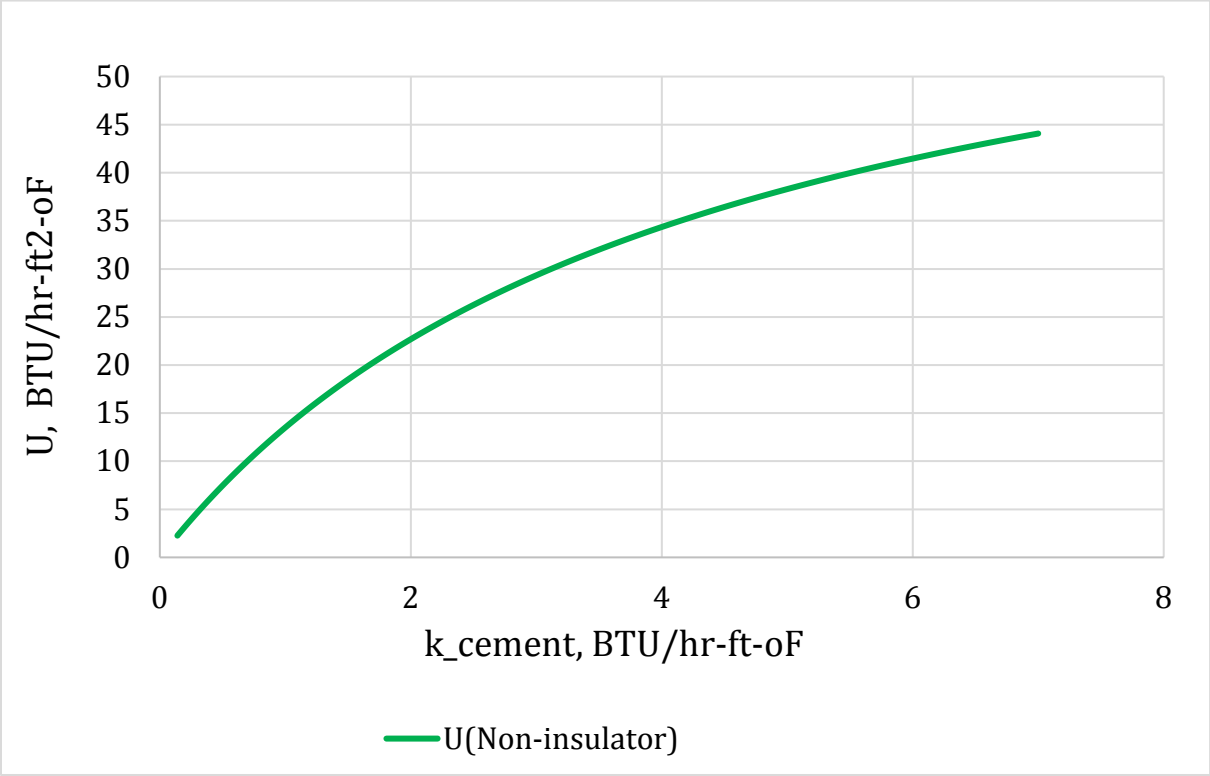

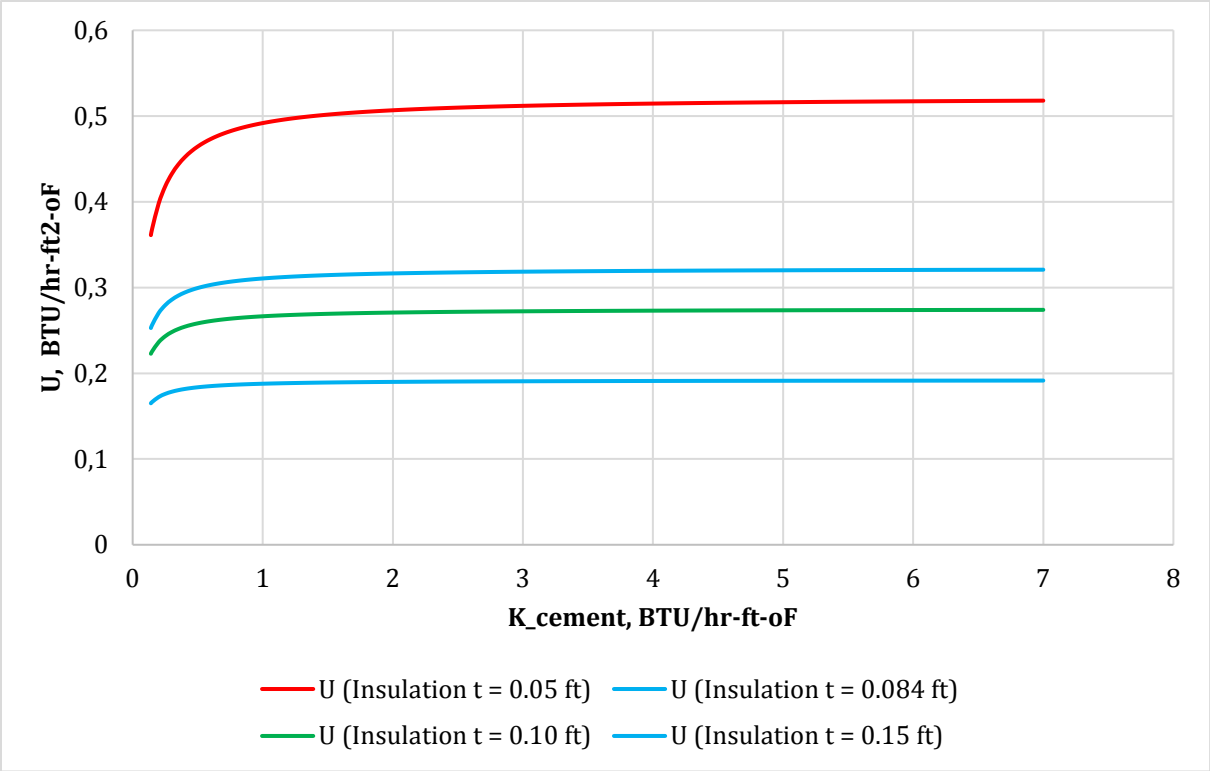
0,6
0,5
0,4
0,3
0,2
0,1
0
U, BTU/hr-ft2-oF
0
1
2
3
4
5
6
7
8
K_cement, BTU/hr-ft-oF
U (Insulation t = 0.05 ft)
U (Insulation t = 0.084 ft)
U (Insulation t = 0.10 ft)
U (Insulation t = 0.15 ft)

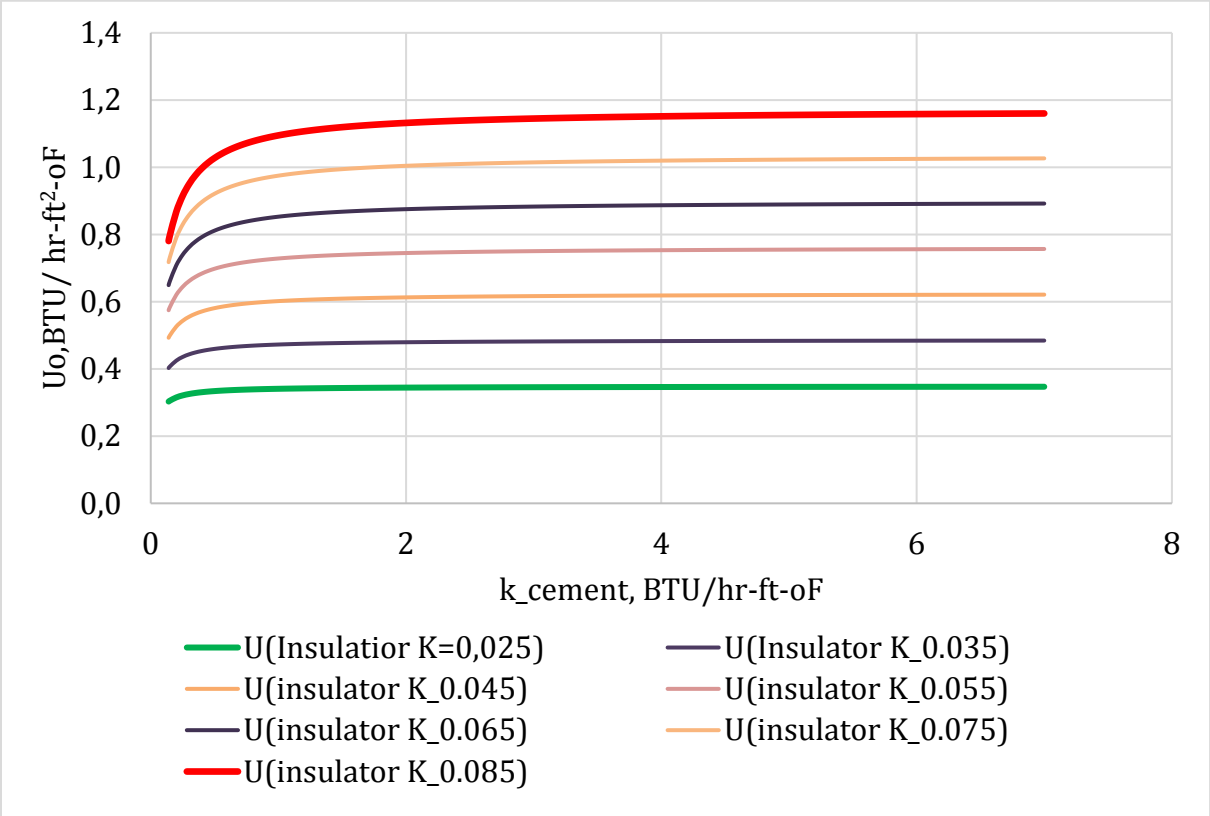
1,4
1,2
1,0
0,8
0,6
0,4
0,2
0,0
Uo,BTU/ hr-ft2-oF
0
2
4
6
8
k_cement, BTU/hr-ft-oF
U(Insulatior K=0,025)
U(Insulator K_0.035)
U(insulator K_0.045)
U(insulator K_0.055)
U(insulator K_0.065)
U(insulator K_0.075)
U(insulator K_0.085)

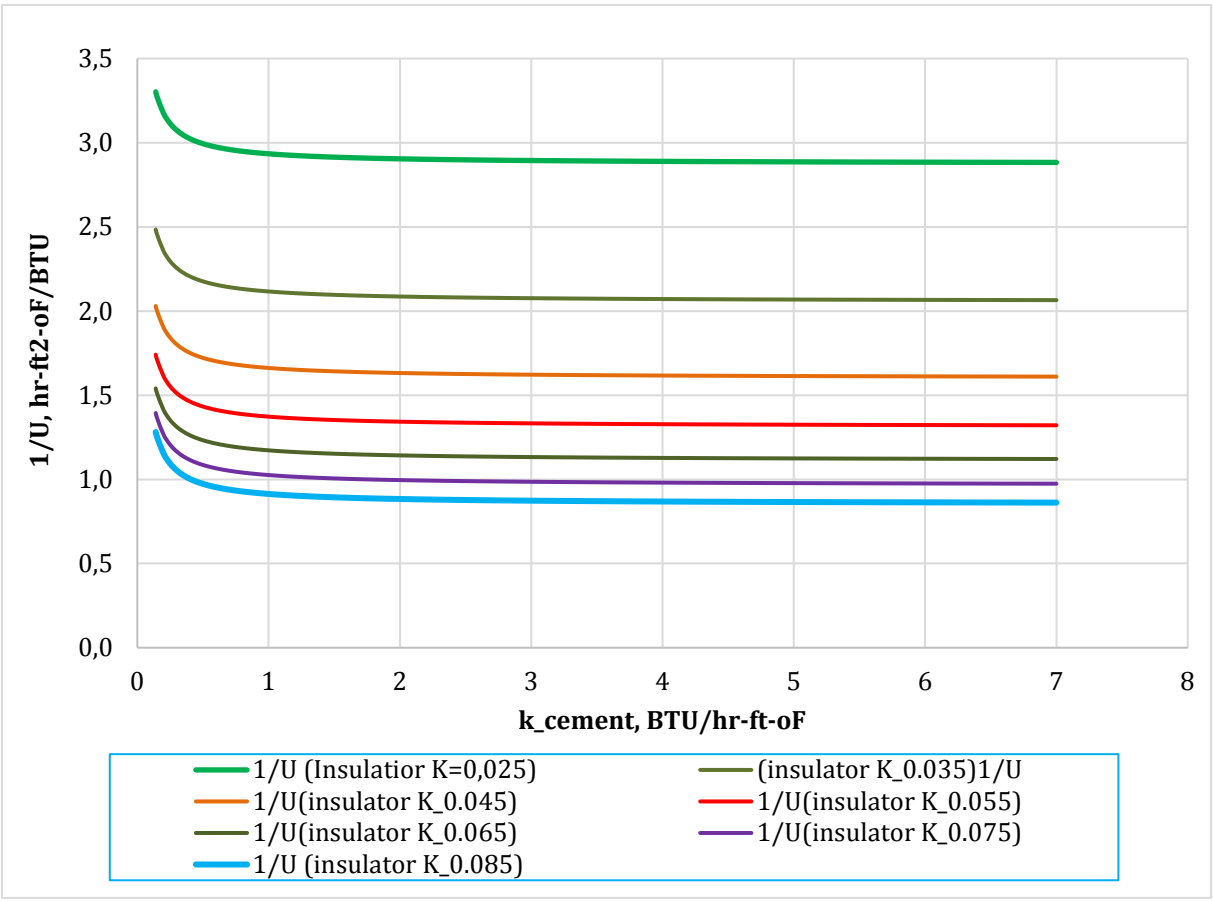
3,5
3,0
2,5
2,0
1,5
1,0
0,5
0,0
1/U, hr-ft2-oF/BTU
0
1
2
3
4
5
6
7
8
k_cement, BTU/hr-ft-oF
1/U (Insulatior K=0,025)
(insulator K_0.035)1/U
1/U(insulator K_0.045)
1/U(insulator K_0.055)
1/U(insulator K_0.065)
1/U(insulator K_0.075)
1/U (insulator K_0.085)

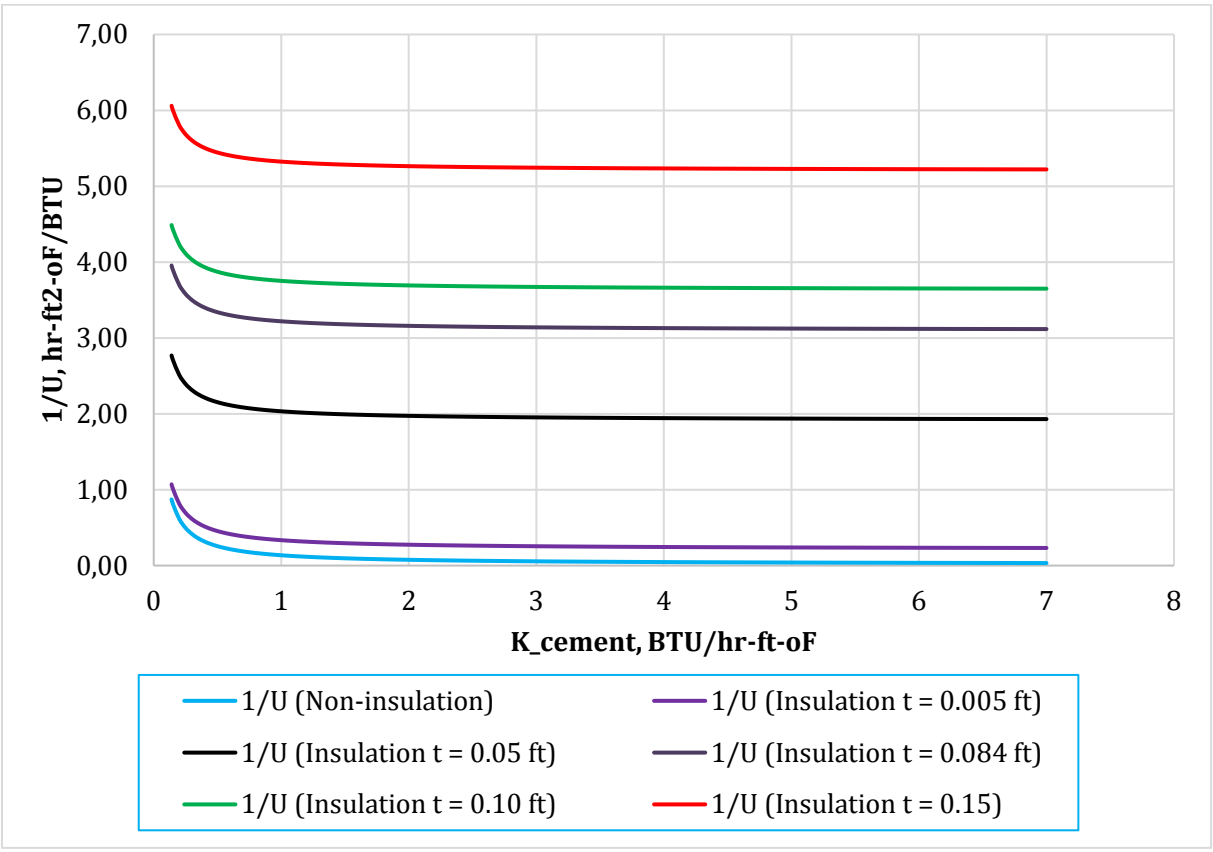
7,00
6,00
5,00
4,00
3,00
2,00
1,00
0,00
1/U, hr-ft2-oF/BTU
0
1
2
3
4
5
6
7
8
K_cement, BTU/hr-ft-oF
1/U (Non-insulation)
1/U (Insulation t = 0.005 ft)
1/U (Insulation t = 0.05 ft)
1/U (Insulation t = 0.084 ft)
1/U (Insulation t = 0.10 ft)
1/U (Insulation t = 0.15)

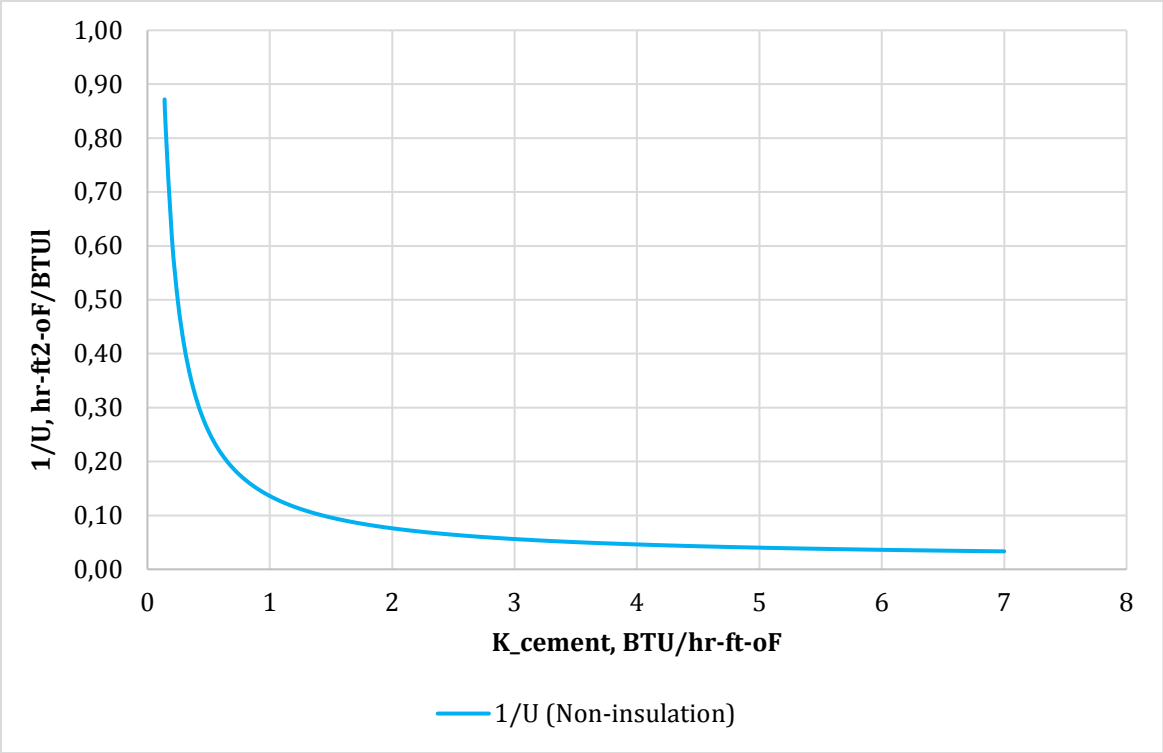
1,00
0,90
0,80
0,70
0,60
0,50
0,40
0,30
0,20
0,10
0,00
1/U, hr-ft2-oF/BTUl
0
1
2
3
4
5
6
7
8
K_cement, BTU/hr-ft-oF
1/U (Non-insulation)

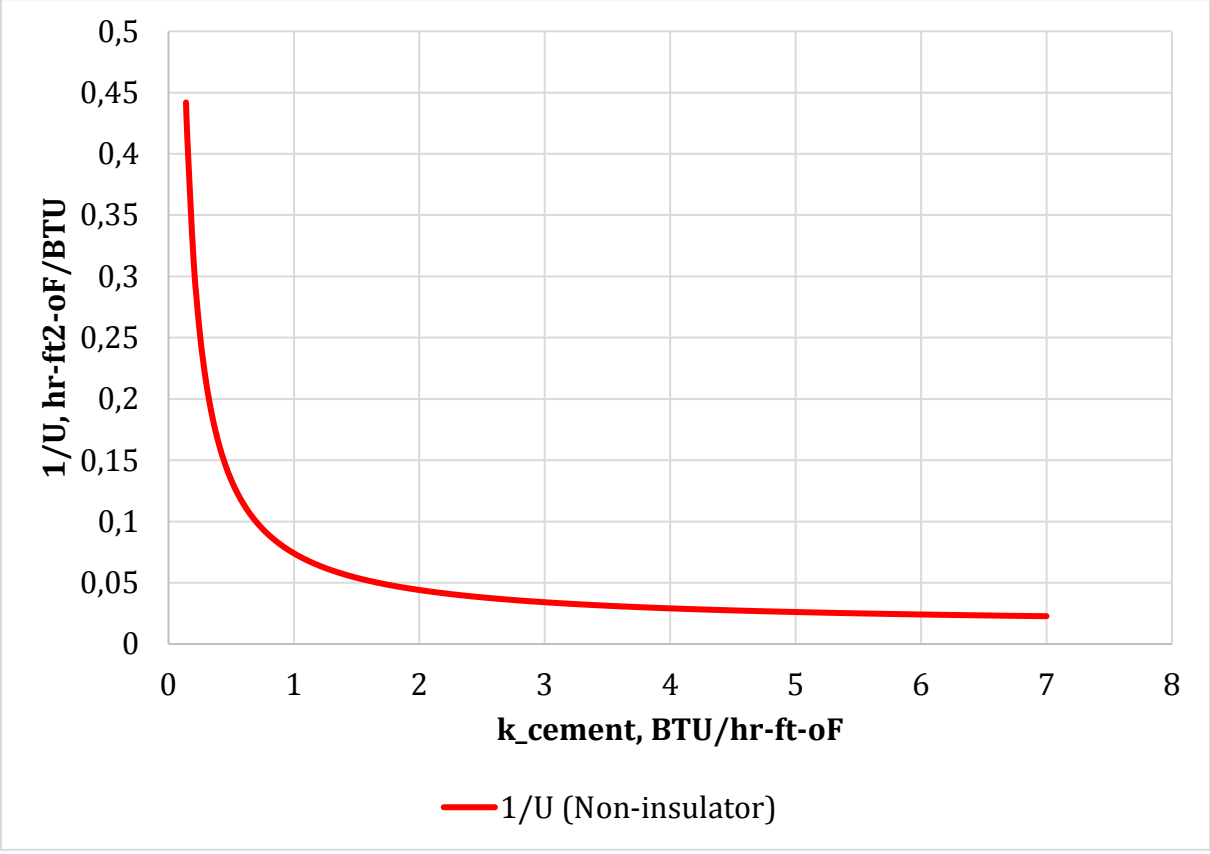
0,5
0,45
0,4
0,35
0,3
0,25
0,2
0,15
0,1
0,05
0
1/U, hr-ft2-oF/BTU
0
1
2
3
4
5
6
7
8
k_cement, BTU/hr-ft-oF
1/U (Non-insulator)